THE STATISTICAL PHYSICS OF THE 1-D TO 2-D CROSSOVER USING TRANSFER FUNCTION TECHNIQUES

by

ANDREW M. CAVE

A thesis submitted to
The University of Birmingham
for the degree of
DOCTOR OF PHILOSOPHY

School of Physics and Astronomy
The University of Birmingham

September 2015

Abstract

We develop a novel technique that allows us to directly probe the thermodynamics of the two dimensional limit of the nearest neighbour square lattice clock model. It is a process that uses exact diagonalisation techniques through the use of transfer functions. It is conceptually easy to understand as an extension of the transfer matrices used to solve the 1-D Ising model and other similar Hamiltonians. This transfer function technique is applied to a set of 1-D spiral geometries with increasing radius N. In the limit $N \to \infty$ the spiral becomes the square lattice and our results are interpreted with respect to this limit. We present convincing evidence that the two transitions that are exhibited in the $p > 4$ clock model have singular behaviour and above a certain temperature between the transitions convergently behave like the plane rotator model.

Acknowledgements

Over the course of this PhD there have been numerous people that have helped it towards its finish line and I would like to particularly express my gratitude towards that important group.

First I would like to thank my supervisor Martin with his very open door policy for helping students. I would like to thank my colleagues and friends who have watched at least some of this journey: Jon, Greg, Filippo, Andy, Kevin, Max, Arvid, Matt, Max, Andy, Austin, David and Ehren. Special thanks go to Richard and Amy who have undoubtedly passed through the same insanity I have and Matt who undoubtedly will. I would also in particular like to thank Greg, Matt and Jon for proof reading and providing important viva practice.

I would like to thank my wonderful parents and my grandmother who believed in me when I couldn't and have continuously provided love and support even when I didn't know I needed it. I would like to thank my twin Chris who's complementary journey has inspired me to finish and for always being on the end of a phone even when he's over five hundred miles away. I would like to thank my brother Richard, my sister-in-law Constance and my niece Charlotte for providing a world outside of physics to be able to step in and out of so easily. I would like to thank Gabi for having such a listening heart and Polly and her family: Laura, Simon, Alison, Archie and Lottie who know and understand such a large part of this journey very intimately.

I would like to thank my friends who have provided a listening ear to endless ranting: Felix, Claire, Lucy, Beth, Dave, Farah, Andy, Joe, John, Tanya, Neil, Tania, Mary, Christa, Ridhi, Josie, Jorine, Sharon and especially Hannah who understands.

I would like to thank my friends that I have made from both the Birmingham and Reading dance scenes who have welcomed me with open arms and have provided such a necessary perpendicular space to anything I've ever tried before. Thank you Martyn, Suzanne, Carola, Ian, Pam, Jack, James, Kim, Vasi, Jagoda, Jennifer, Luke, Lauren, Elliott, Emma, Laura,

Kayleigh, Jenn, Michael, Jon, Tom, Adam, Anne, Sarah, Sina, Peter, Alex, Marie and countless more.

Thank you to Quintessa who provided such a stimulating working environment for three months, in particular David, Peter and Jackie.

And last but by no means least thank you to Alexandra Jo who joined me on this journey at the steepest part whose seemingly bottomless care, hugs, support and cups of tea have provided that extra push over the Sisyphean edge.

To my parents and grandmother

Contents

List of Figures

List of Tables

Chapter 1

INTRODUCTION

Before commencing on any investigation of this size a section is required to provide the context with which the study falls within. This is to act as a starting point for those unfamiliar with the subject so that the argument that runs through the investigation can be followed throughout; this includes those without extensive prior knowledge of condensed matter systems. This requires significant prerequisite knowledge.

The focus of this investigation is on phase transitions within two dimensional magnets and comes after much important work in the area over a period of fifty years. Extensive research on the particular models studied here have included analytical results [1]-[12] that originate from field theoretic [1]-[6] and renormalisation group analysis [10] with numerical results on finite systems to enforce these conclusions [18]-[22]. There have been complementary experimental results performed on liquid helium films, thought to exhibit similar behaviour to the models we study [13]-[16]. These results are to be reviewed in this section, but first a thorough revision of basic condensed matter and statistical physics results is required.

The beginning of this introduction starts with the notion that accessible condensed matter systems are those with very high levels of symmetry that originates from the atomic lattice.

The crux of condensed matter systems which provide the rich range of different phenomena that can be seen experimentally stems from the behaviour of the electrons within the

lattice. A large section here will be devoted to building up some of these phenomena from the free electron model. The introduction begins at the hydrogen atom and its orbital structure which will include the Hund's rules that arise from crystal fields and a relativistic approach. Once the focus turns to electrons within the lattice it will be seen that the electrons form a band structure, this arises from the fact that with no interactions the electron has a lower energy state through delocalising across the system. This naturally will pass onto the single site Hubbard model where there exists a simple on-site interaction term between electrons. Though conceptually easy to understand, this is a nontrivial model which has a whole wealth of phases and is the nexus towards many complex models. The focus here will be on magnetism and there will be a derivation of the antiferromagnetic Heisenberg model in the limit of a large repulsive interaction. The Hubbard model is an exemplary starting point for any theoretical model to be built from physical systems, though with any physical example the model is far more complex with many electrons per site but it begins with considering the hopping and on-site repulsion energy scales. The section moves to classical magnetism and some examples of ground state Heisenberg Hamiltonians for simple lattices through exact diagonalisation, uniting what has been reviewed on both the lattice and magnetism.

After extensive reviews of magnetic ground states the section will move to a discussion of the effect of temperature on the system. There will be a review of standard statistical physics derivations that arise from the probabilistic nature of the canonical ensemble, which will include the physical definitions of some key thermodynamic quantities: free energy, correlation length, entropy and specific heat. These quantities provide significant singular behaviour in the region of critical points and after some discussion on them the section will move to discussing phase transitions.

We first introduce phase transitions through Landau's formulation, which is a mean field theory approach. It presents us with qualitative understanding of phase transitions and symmetries within the system relating to critical exponents. Once we state where it breaks down, the notion of renormalisation group theory is presented and we give a very

simple example of the analysis using the 1-D Ising model. This introduces the concept of universality and critical points. We move onto the existence of phase transitions in low dimensions and find that 2-D is critical.

Once normal phase transitions are discussed we move onto transitions influenced by topological charges, which includes a discussion of superfluid helium. We present the key results that occur from the Kosterlitz-Thouless transition, one which is based on the unbinding of vortices. We also review much of the numerical literature on clock model and plane rotator results.

After extensive background on the physics we discuss the mathematical concept of duality and apply it to condensed matter systems.

This investigation is split up into three parts. In chapter 1 we review the basic condensed matter background required to comprehend the further sections. In chapter 2 we present a derivation of the transfer function technique that we eventually use on the spiral systems and in chapter 3 we present our results.

1.1 Building the Bravais Lattice

The systems that are dealt with in solid state physics tend to be in environments that respect the symmetries of different point groups to greater or lesser degrees. There is a certain amount of translational symmetry which is exploited both experimentally and in theoretical calculations; within the point group there is a varying degree of rotational and reflective symmetry. The understanding in this section will begin in the way lattices are built; starting with the primitive unit cell which are tessellated using lattice vectors. Simple examples will be given in 2-D before moving onto more physically realistic 3-D examples. There will be discussion on the reciprocal lattice.

1.1.1 The Unit Cell

The unit cell and the lattice vectors are the building blocks that create the Bravais lattice. The unit cell present the basic elements, that when tessellated using the lattice vectors create the lattice, which spans the space. The simplest example is the linear chain, seen in figure 1.1 . Starting from one unit cell, a lattice vector provides the position of all other unit cells as integer amounts of the initial vector. In the case of the linear chain, the position of all other unit cells can be provided as

$$\mathbf{v} = na\hat{\mathbf{x}}. \tag{1.1.1}$$

From this simple definition we can say that there is a large amount of translational symmetry; each unit cell is equivalent to every other unit cell.

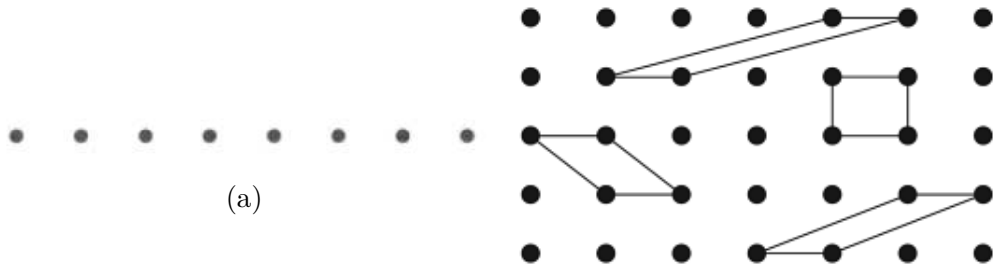

(a) (b)

Figure 1.1: The linear chain shown in (a) [33] and the square lattice in (b) with different possible unit cells [32]

In figure 1.1 we provide a 2-D square lattice with many possible unit cells. The number of lattice vectors required to tessellate the unit cell over the whole lattice is the dimension of the lattice. With a 3-D lattice all points can be described by the position vector $\mathbf{v}$:

$$\mathbf{v} = n_1\mathbf{a}_1 + n_2\mathbf{a}_2 + n_3\mathbf{a}_3, \tag{1.1.2}$$

where n_i are integers and the lattice vectors $\mathbf{a}_i$ are not in general orthonormal. In figure 1.2 we illustrate two well known cubic lattices: face centred cubic (fcc) and body centred cubic

(bcc) with their conventionally used lattice vectors.

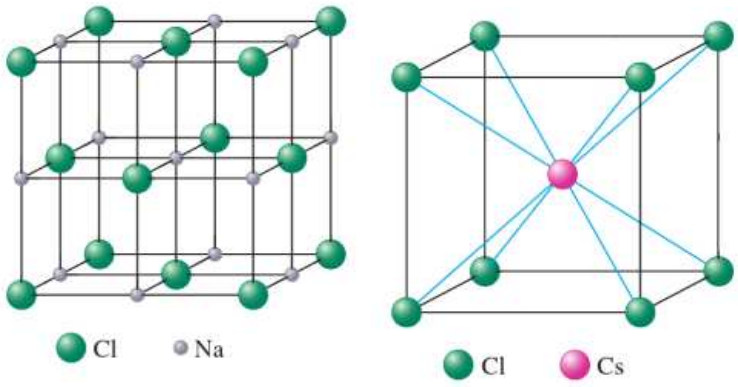

(a) Structure of $NaCl$ both atoms form inter-penetrating fcc lattices

(b) Structure of $CsCl$ which forms a bcc lattice

Figure 1.2: Examples of fcc (a) and bcc (b), both taken from [31]

1.1.2 The Reciprocal Lattice

The reciprocal lattice provides a neat analytical treatment of the periodicity inherent in lattice systems, it provides the building block of investigating the lattice experimentally as it is the Fourier transform of the real space lattice. Much of what we discuss here is found in [34].

The reciprocal lattice of a Bravais lattice made of points $\mathbf{R}$ is defined as the points $\mathbf{k}$ that satisfy

$$e^{i\mathbf{k}\cdot\mathbf{R}} = 1 \tag{1.1.3}$$

for every point within the Bravais lattice, which in turn creates another Bravais lattice and can be written as a linear combination of three lattice vectors $\mathbf{b}_i$:

$$\mathbf{k} = k_1\mathbf{b}_1 + k_2\mathbf{b}_2 + k_3\mathbf{b}_3, \tag{1.1.4}$$

where

$$\begin{aligned}\mathbf{b}_1 &= 2\pi\frac{\mathbf{a}_2 \wedge \mathbf{a}_3}{\mathbf{a}_1 \cdot (\mathbf{a}_2 \wedge \mathbf{a}_3)} \\ \mathbf{b}_2 &= 2\pi\frac{\mathbf{a}_3 \wedge \mathbf{a}_1}{\mathbf{a}_1 \cdot (\mathbf{a}_2 \wedge \mathbf{a}_3)} \\ \mathbf{b}_3 &= 2\pi\frac{\mathbf{a}_1 \wedge \mathbf{a}_2}{\mathbf{a}_1 \cdot (\mathbf{a}_2 \wedge \mathbf{a}_3)}.\end{aligned} \tag{1.1.5}$$

The simple cubic lattice has Cartesian vectors as its lattice vectors $\mathbf{a}_i = a\hat{\mathbf{x}}_i$, where a is some lattice constant, and from (1.1.5) its reciprocal lattice is another square lattice $\mathbf{b}_i = \frac{2\pi}{a}\hat{\mathbf{x}}_i$.

The face centred cubic lattice in figure 1.2a has a body centred cubic lattice as its reciprocal lattice and likewise the body centred cubic lattice has a face centred cubic lattice as its reciprocal lattice with lattice constant $\frac{4\pi}{a}$.

1.2 Magnetism

Magnetism is a vast subject to introduce, with plenty of different manifestations within condensed matter systems ranging from the quantum regime to the classical. A lot of the behaviour that is experimentally observable occurs due to the nature of the electrons within the lattice. After building some groundwork on electrons in a lattice we shall present a microscopic model for interacting electrons in a lattice, the Hubbard model that can lead to magnetic phenomena. This model has a whole wealth of physics embedded within it but we shall be dealing with simply one region of interest.

We start with a single hydrogen atom to present the idea of different orbital states that occur in the shells of the atom. This will lead naturally to Hund's rules and the effect of a symmetric crystal field on the electronic states.

Electrons in a lattice interact with a periodic potential, so it can be assumed that the actual state it takes can be somewhat periodic. We deal with the tight binding Hamiltonian which leads to the Fermi gas. We get there through a variational approach and see that the

lowest energy states are those that are delocalised across the system. This leads us nicely to band structure analysis, the structure factor and the effect of the lattice on the energy states of the system.

Up until then only non-interacting electrons are considered and electrons are highly interacting, and so we introduce a very simple two body interaction. This will be the single site Hubbard model which has such a wealth of different phenomena associated with it. We will focus on a single case of a large repulsive term which will lead us, through perturbation theory, to the Heisenberg model.

We then move to the crux of the investigation which is classical magnetism. We solve the Heisenberg model for many different systems and discuss the different types of order. Once we have put ourselves in good stead with a magnetism background and the ground state of the system we will be able to move onto the effect of temperature on magnetic systems and will start discussing basic thermodynamics before we move onto the effect of phase transitions, and how they are observed.

1.2.1 The Hydrogen Atom

The behaviour of electrons guides most of the phenomena experienced in condensed matter systems. Though the collective behaviour of many electrons within a periodic potential is the source of solid state physics, it is worth discussing a single electron in a hydrogen atom. We will see that the energy levels within the hydrogen atom split quite naturally into shells which fill up and behave as core electrons, and the open shell is what guides the physics.

Once we have introduced the shells within the atom, we discuss Hund's rules and their meanings, which brings us naturally onto the effect of the crystal.

There won't be any complex derivations, rather we will state the answer to a lot of the mathematics.

We begin with the single particle Hamiltonian of the hydrogen atom.

$$\left[-\frac{\hbar^2}{2m}\nabla^2 - \frac{e^2}{|\mathbf{r}|} - E\right]\psi(\mathbf{r}) = 0, \tag{1.2.1}$$

where m and e are the mass and the charge of the electron respectively. The solution to this Hamiltonian naturally separates into radial and angular wave functions. The radial part describes the energy of the electron and the angular part describe the angular momentum, providing three quantum numbers. The two quantum numbers that are associated with the angular momentum describes the total angular momentum and the amount in one direction. No more can be known as the angular momentum operators in different directions do not commute

$$[\mathbf{L}_i, \mathbf{L}_j] = i\hbar\epsilon_{ijk}\mathbf{L}_k, \tag{1.2.2}$$

yet the total angular momentum operator commutes with all directions

$$[L, \mathbf{L}_i] = 0, \tag{1.2.3}$$

where $L = \mathbf{L} \cdot \mathbf{L}$. The final wave function is of the form

$$\psi(\mathbf{r}) = R_{nl}(r)\, Y_{lm}(\theta, \phi), \tag{1.2.4}$$

where the quantum number n refers to the energy, l refers to the total angular momentum and follows the rule that $l < n$. Both of these numbers make up the electron shell, which are filled with electrons of different values of m that correspond to the amount of angular momentum in an arbitrary direction which follows that $-l < m < l$. Each configuration of n, m, l corresponds to a possible electron state and considering that there is also a spin degree of freedom, it allows two electrons per state.

The energy of each electron state is

$$E \sim -\frac{1}{n^2}, \tag{1.2.5}$$

which depends only on the principal quantum number n. The radial part of the wave function in turn depends on the n and l. It is of the form

$$R_{nl}(r) \sim r^l e^{-\frac{r}{n}} L_{n-l-1}^{2l+1}(r), \tag{1.2.6}$$

where L_{n-l-1}^{2l+1} are Laguerre polynomials. It should be noted that the exponential tail as seen in figure 1.3 is less aggressive in higher shells, noting that the electron cloud is more likely to be found further away from the atom in higher shells. This makes sense as it is higher in energy and so further away from the positive nucleus. As this is in polar coordinates, the radial probability is

$$P_{nl}(r) = r^2 |R_{nl}(r)|^2, \tag{1.2.7}$$

and some sample wave functions in different shells with their probabilities are:

$$\begin{aligned} R_{10} \sim & e^{-r} \\ R_{20} \sim & (2-r)\, e^{-\frac{r}{2}} \\ R_{30} \sim & \left(27 - 18r + 2r^2\right) e^{-\frac{r}{3}}, \end{aligned} \tag{1.2.8}$$

and those within the same shell

$$\begin{aligned} R_{30} \sim & \left(27 - 18r + 2r^2\right) e^{-\frac{r}{3}} \\ R_{31} \sim & (6-r)\, r e^{-\frac{r}{3}} \\ R_{32} \sim & r^2 e^{-\frac{r}{3}}. \end{aligned} \tag{1.2.9}$$

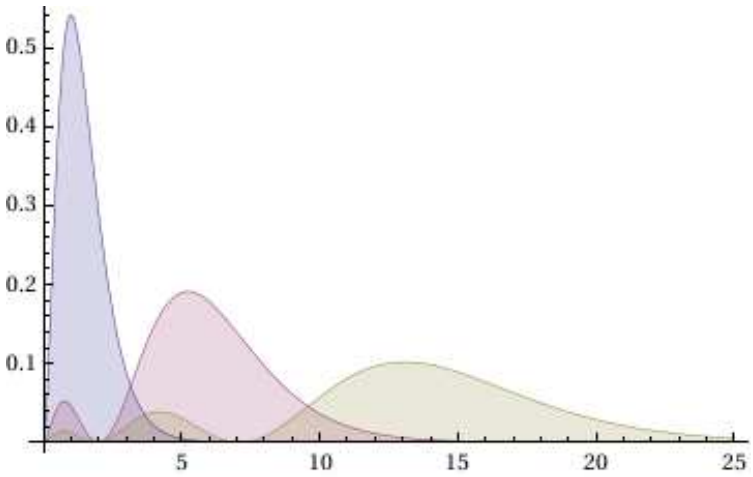

(a) The radial probabilities of the $1s$, $2s$ and $3s$ shells

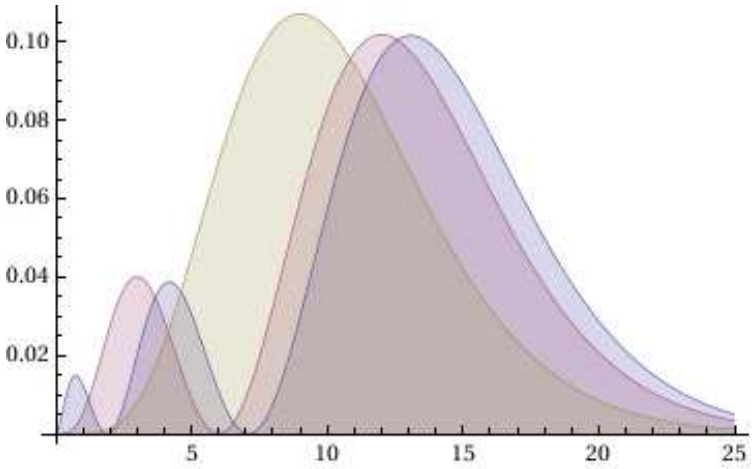

(b) The radial probabilities of the $3s$, $3p$ and $3d$ shell

Figure 1.3: Radial probabilities of some sample wave functions

It can be seen that between shells, there is a huge difference in the position of the electron. The lower the shell, the more localised is the electron and nearer the nucleus. Within the shell, it can be seen that those with lower total angular momentum are further away from the nucleus. The angular momentum states $l = 0, \cdots, 3$ are labeled s, p, d, f respectively and are usually prefixed with their principal quantum number n.

The angular part to the wave function Y_{lm} are spherical harmonics

$$Y_{lm} \sim e^{im\phi} P_{lm} \left(\cos \left(\theta \right) \right), \tag{1.2.10}$$

where P_{lm} are Legendre Polynomials. Some sample wave functions are

$$\begin{aligned} Y_{00} &\sim 1 \\ Y_{11} &\sim e^{i\phi} \sin(\theta) \\ Y_{10} &\sim -\cos(\theta) \\ Y_{22} &\sim e^{2i\phi} \sin^2(\theta) \\ Y_{21} &\sim e^{i\phi} \sin(\theta) \cos(\theta) \\ Y_{20} &\sim \left(3\cos^2(\theta) - 1\right). \end{aligned} \tag{1.2.11}$$

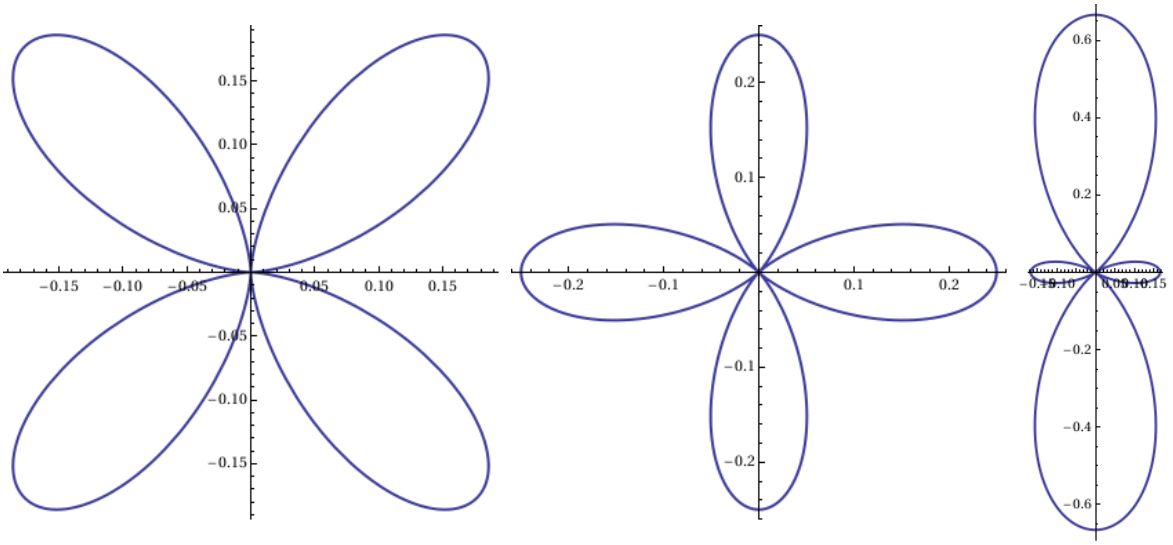

(a) (b) (c)

Figure 1.4: The angular probabilities Y_{21}, Y_{22} and Y_{20} in (a), (b) and (c) respectively of the $3d$ shell.

The shells with higher energy have more states as larger values of orbital angular momentum are available.

At the moment all states that have the same principal quantum number n are degenerate and so we must answer the question: what happens with elements that have more than one electron. It can be assumed that the states are very similar, despite the fact that electrons

interact with each other, the dominant energy is the attraction of the nucleus. The full answer lies with Hund's rules.

Hund's Rules and Crystal Field Effects.

Hund's rules describe a set of atomic interactions that lift the degeneracy that is apparent within the atom but it also competes with interactions within the lattice, one of them being the crystal field.

The first rule states that in an open shell, the total spin is maximal. This is due to the fact that the electron-electron interaction is minimal with an antisymmetric spatial wave function, which leads to a symmetric spin wave function.

The second rule states that the orbital angular momentum is maximised, subject to the Pauli exclusion principle. Depending on the system, this tends to be in direct competition with effects of the lattice, and much work is needed to understand which is the dominant energy scale.

The third rule originates from spin-orbit coupling, which states that for the first half of an open shell the spin must be anti-parallel to the orbital angular momentum and in the second half the spin is parallel. This leads to spin and angular momentum no longer being good quantum numbers, rather j is used which is the total angular momentum which corresponds to the operator $\mathbf{J} = \mathbf{L} + \mathbf{S}$ such that for the first half of the shell $j = |l - s|$ and the second half $j = |l + s|$. This observable still acts very much like orbital angular momentum, it splits into states that are varying degrees parallel to a direction labelled by j_z such that $|j_z| \leq j$.

These are all interactions that occur in free atoms, which are in a spherically symmetric environment. In lattices the environment is vastly different, we tend to deal with cubic symmetric environments, a potential that originates from the Pauli exclusion of the electron cloud that surrounds the atom. If we construct cubic symmetric wave functions from the spherically symmetric wave functions, then the orbital angular momentum quantum num-

ber m is not an appropriate quantum number and there is mixing between states. The states that we form break into irreducible representations that map onto each other under transformations of the point group. We give examples for p and d shells:

$$\begin{aligned} \frac{1}{\sqrt{2}}\left(Y_{11}+Y_{1\bar{1}}\right) &\sim \frac{x}{r} \\ \frac{1}{\sqrt{2}}\left(Y_{11}-Y_{1\bar{1}}\right) &\sim \frac{y}{r} \\ Y_{10} &\sim \frac{z}{r}. \end{aligned} \tag{1.2.12}$$

For the d-shell there are two irreducible representations that map onto each other under the cubic symmetry transformations, the first is the t_{2g} shell

$$\begin{aligned} \frac{1}{\sqrt{2}}\left(Y_{21}+Y_{2\bar{1}}\right) &\sim \frac{zx}{r^2} \\ \frac{1}{\sqrt{2}}\left(Y_{21}-Y_{2\bar{1}}\right) &\sim \frac{yz}{r^2} \\ \frac{1}{\sqrt{2}}\left(Y_{22}-Y_{2\bar{2}}\right) &\sim \frac{xy}{r^2}, \end{aligned} \tag{1.2.13}$$

and the second is the e_g

$$\begin{aligned} \frac{1}{\sqrt{2}}\left(Y_{22}+Y_{2\bar{2}}\right) &\sim \frac{x^2-y^2}{r^2} \\ Y_{20} &\sim \frac{3z^2-1}{r^2}. \end{aligned} \tag{1.2.14}$$

In a cubic lattice if the crystal field is dominant over the second Hund's rule, these are the states that are occupied. The degeneracy between the two representations is lifted when considering the effect of the electron states around the atom. Notice that the e_g states in a cubic lattice will point towards the sites that surround it and the t_{2g} points towards the unoccupied space. This splits the energies of the two shells depending on whether the states it points to are holes or electrons.

1.2.2 Chemical Bonding and Hopping

Here we shall begin dealing with the lattice, where we introduce a periodic $\frac{1}{r}$ potential to the Hamiltonian which will give us a kinetic energy term, hopping electrons between nearest neighbours. With no interaction between electrons this leads to delocalised states across the system, which amounts to an ideal Fermi gas. We see that the lattice is very important to the energy states and we start dealing with the structure factor which gives us the band structure of the system.

In a lattice electrons interact with more than just the one potential as we have been considering so far, they interact with a lattice of periodic potentials

$$\mathbf{H} = \frac{p^2}{2m} - e^2 \sum_i \frac{1}{|\mathbf{r} - R_i^{nuc}|}, \tag{1.2.15}$$

where R_i^{nuc} are the positions of the lattice sites.

We deal first simply with a linear chain of hydrogen atoms and we assume that the states of the system will form some linear combination of the single potential states on each atom

$$\psi = \sum_i u_i \psi_i, \tag{1.2.16}$$

where $\psi_i \sim e^{-|r - R_i^{nuc}|}$. As these are non orthogonal states we must solve [66]

$$\mathcal{H}_{ij} u_j = E O_{ij} u_j, \tag{1.2.17}$$

where $\mathbf{H}_{ij} = \langle \psi_i^\dagger | \mathbf{H} | \psi_j \rangle$ and $O_{ij} = \langle \psi_i | \psi_j \rangle$. We shall first solve this for the linear chain but we make the critical assumption that only wave functions that are associated with nearest neighbour sites have a non zero overlap:

$$O_{ij} = \delta_{ij} + \alpha \delta_{\langle ij \rangle}, \tag{1.2.18}$$

and similarly for the Hamiltonian

$$\mathcal{H}_{ij} = \epsilon\delta_{ij} - t\delta_{\langle ij\rangle}, \tag{1.2.19}$$

where ϵ is the on-site energy and t is the nearest neighbour hopping term.

It is easier to deal with states that are both local to each atom and orthogonal to each other, so we create Wannier States that satisfy

$$c_i c_j^\dagger|0\rangle = \delta_{ij}|0\rangle, \tag{1.2.20}$$

where $c_i^\dagger$ creates a Wannier State on site i. We can now write this Hamiltonian in second quantised form

$$\epsilon\sum_i c_i^\dagger c_i - t\sum_{\langle ij\rangle} c_i^\dagger c_j, \tag{1.2.21}$$

where we have renormalised ϵ and t according to the Wannier States.

This Hamiltonian is trivially solved using a Bloch Wave, and our first example will be a linear chain of N atoms:

$$c_k^\dagger = \frac{1}{\sqrt{N}}\sum_j e^{ikj} c_j^\dagger, \tag{1.2.22}$$

where $k \in \frac{2\pi n}{N}$, which diagonalises the Hamiltonian

$$\mathcal{H} = \sum_k \left[\epsilon - t\cos(k)\right] c_k^\dagger c_k, \tag{1.2.23}$$

and the cosine term originates from the structure factor

$$\gamma_k = \frac{1}{Z}\sum_{\langle 0n\rangle} e^{ikn}. \tag{1.2.24}$$

The eigenstates of this Hamiltonian are delocalised across the system with a certain phase on each site. Therefore in a lattice it can be assumed that the electron lowers its energy by delocalising whenever possible. Notice that in this case the lowest energy state is

the $k = 0$ state where the phase is the same across every site.

This is the standard case for all lattices with this model, that the diagonalised Hamiltonian is of the form

$$\mathcal{H} = \sum_k \gamma_k c_k^\dagger c_k, \tag{1.2.25}$$

where $\epsilon = 0$ is a standard simplification. We will list the structure factor for some well known lattices:

square lattice

$$\gamma_{\mathbf{k}} = \frac{1}{2}\left(\cos k_x + \cos k_y\right), \tag{1.2.26}$$

triangular lattice

$$\gamma_{\mathbf{k}} = \frac{1}{3}\left[\cos\left(k_x\right) + \cos\left(\frac{k_x + \sqrt{3}k_y}{2}\right) + \cos\left(\frac{k_x - \sqrt{3}k_y}{2}\right)\right], \tag{1.2.27}$$

body centred cubic lattice

$$\gamma_{\mathbf{k}} = \cos k_x \cos k_y \cos k_z, \tag{1.2.28}$$

and face centred cubic

$$\gamma_{\mathbf{k}} = \frac{1}{3}\left[\cos k_x \cos k_y + \cos k_y \cos k_z + \cos k_z \cos k_x\right]. \tag{1.2.29}$$

Thus far we have only discussed non interacting fermions. Electrons of course repel each other with a $\frac{1}{r}$ potential which if included would be a long range many-body interaction and would be very non-trivial to solve. The next section discusses the inclusion of this interaction in its simplest form which will lead to the Hubbard model.

1.2.3 The Hubbard Model

Thus far we have discussed only non-interacting electrons within a lattice, which leads simply to delocalised electrons across the whole system, best described using Bloch states. In most situations this is not a physical result and it is the many-body interactions that exist between electrons that give rise to magnetism and other interesting phenomena. This was first shown by *Heisenberg* [56]. We shall state the Hubbard model as a very simple many-body Hamiltonian between electrons and focus on the region that is of most interest to us: a dominant repulsive energy term. This will lead to the Heisenberg model. We shall then move onto the classical regime which is the crux of this investigation.

The easiest way to include a many-body term in the Hamiltonian with hydrogen atoms is to include an on-site repulsive term. We assume this to be the dominant interaction between two electrons as the potential behaves as $\frac{1}{r}$. With the kinetic energy term the Hamiltonian is

$$\mathcal{H} = -t \sum_{\sigma\langle ij\rangle} c^{\dagger}_{i\sigma} c_{j\sigma} + U \sum_{i} c^{\dagger}_{i\uparrow} c_{i\uparrow} c^{\dagger}_{i\downarrow} c_{i\downarrow}. \tag{1.2.30}$$

We are still dealing with one electron level per site, but we have included a spin label and note that the interaction term is only between two electrons on the same site that are anti-parallel due to Pauli exclusion. This is the single-band Hubbard model, which is easily extendable to many bands and other interactions. This is solvable using the Bethe Ansatz but it is far beyond the capabilities of this investigation and we shall focus simply on the trivial region $0 < t \ll U$.

In the case that $U = \infty$ the electrons are completely localised on a single atom with one atom per site and there is a large spin degeneracy. We take the case that $U \gg t$ and using perturbative approaches we reach the Heisenberg interaction.

Consider the Hamiltonian

$$\mathcal{H}_1 = U \sum_{\sigma i} c^\dagger_{i\uparrow} c_{i\uparrow} c^\dagger_{i\downarrow} c_{i\downarrow}, \tag{1.2.31}$$

with N sites and N electrons. The ground state has a high spin degeneracy with one electron per site. We consider the perturbation

$$\begin{aligned} \mathcal{H} =& \mathcal{H}_1 + \mathcal{H}_2 \\ \mathcal{H}_2 =& \frac{t}{2} \sum_{\langle ij \rangle \sigma} c^\dagger_{i\sigma} c_{j\sigma} + c^\dagger_{j\sigma} c_{i\sigma}. \end{aligned} \tag{1.2.32}$$

From perturbation theory it is known that the second order correction maps degenerate states onto each other, and the resulting matrix must be diagonalised

$$E_{n_1 n_2} = - \sum_{n' \neq n} \frac{\langle n_1 | \mathcal{H}_2 | n' \rangle \langle n' | \mathcal{H}_2 | n_2 \rangle}{E_{n'} - E_n}, \tag{1.2.33}$$

where n_1 and n_2 are states within the degenerate subspace which have energy E_n. This is the highest order that lifts the spin degeneracy. The only states that contribute to this energy are those that are one hop away from any ground state, which have a single doubly-occupied state across the whole system. Between any two ground states

$$E = -\frac{t^2}{U} \sum_{\langle ij \rangle} \sum_{\{|1\rangle\}} \sum_{\sigma, \sigma'} \langle \sigma_i \sigma_j | \left(c^\dagger_{i\sigma} c_{j\sigma} + c^\dagger_{j\sigma} c_{i\sigma} \right) |1\rangle \langle 1| \left(c^\dagger_{i\sigma'} c_{j\sigma'} + c^\dagger_{j\sigma'} c_{i\sigma'} \right) |\sigma'_i \sigma'_j \rangle, \tag{1.2.34}$$

where the state $|1\rangle$ is a state that is one hop away. This leads to an effective Hamiltonian that acts on the ground state sub-space:

$$H_{eff} = -\frac{t^2}{U} \sum_{\langle jj' \rangle \sigma} \sum_{\langle ii' \rangle \sigma'} c^\dagger_{j\sigma} c_{j'\sigma} c^\dagger_{i\sigma'} c_{i'\sigma'} \delta_{ij'} \delta_{i'j}. \tag{1.2.35}$$

This leads eventually to Hamiltonian

$$H_{eff} = J \sum_{\langle ij \rangle} \left[\hat{\mathbf{S}}_i \cdot \hat{\mathbf{S}}_j - \frac{1}{4} \right], \tag{1.2.36}$$

where $\hat{\mathbf{S}}$ are the spin operators, which in spin-half space amounts to the Pauli operators, and $J = \frac{4t^2}{U}$. This is the Heisenberg Hamiltonian. The spin operators satisfy an angular momentum style commutator

$$\left[\hat{S}_\alpha, \hat{S}_\beta \right] = i\epsilon_{\alpha\beta\gamma} \hat{S}_\gamma, \tag{1.2.37}$$

where again the total spin commutes with the spin component in any arbitrary direction, but as they do not commute with each other, just like the angular momentum operators only the total spin and the component in one direction is known. Each state is labelled as $|M, m\rangle$ such that

$$\begin{aligned} \hat{\mathbf{S}} \cdot \hat{\mathbf{S}} |M, m\rangle &= M |M, m\rangle \\ \hat{S}_z |M, m\rangle &= m |M, m\rangle, \end{aligned} \tag{1.2.38}$$

where $M = S(S+1)$ and $|m| \leq S$, where S is an integer or half-integer. By convention we label the M state by S. For an electron that is spin half there are two states $|\frac{1}{2}, \frac{1}{2}\rangle$, $|\frac{1}{2}, \frac{\bar{1}}{2}\rangle$.

With many spins, they can be added in different ways but in the cases that we deal with which are in the atom we already know from Hund's first rule that spins must add maximally.

The operators and their observables are of order S and so we normalise them $\tilde{\mathbf{S}} = \frac{1}{S}\hat{\mathbf{S}}$ and rewriting the commutator

$$\left[\tilde{S}_\alpha, \tilde{S}_\beta \right] = \frac{1}{S} i\epsilon \tilde{S}_\gamma, \tag{1.2.39}$$

which implies that in the limit of $S \to \infty$ the commutator between different components of

the spin go to zero. This is the classical regime, where it is possible to know the direction of the spin. The spins becomes a vector of fixed length. The magnetic state is thus found through minimisation of

$$\mathcal{H} = \frac{J}{2} \sum_{\langle ij \rangle} \mathbf{S}_i \cdot \mathbf{S}_j, \tag{1.2.40}$$

subject to the constraint $\mathbf{S_i} \cdot \mathbf{S}_i = S^2$. The normal procedure for solving this is to use the Fourier transform

$$\begin{aligned} \mathbf{S_k} &= \frac{1}{\sqrt{N}} \sum_j e^{i\mathbf{k}\cdot\mathbf{R}_j} \mathbf{S}_j \\ \mathbf{S_{-k}} &= \frac{1}{\sqrt{N}} \sum_j e^{-i\mathbf{k}\cdot\mathbf{R}_j} \mathbf{S}_j, \end{aligned} \tag{1.2.41}$$

which diagonalises the Hamiltonian

$$\mathcal{H} = \frac{JZ}{2} \sum_{\mathbf{k}} \gamma_{\mathbf{k}} \mathbf{S_k} \cdot \mathbf{S_{-k}}. \tag{1.2.42}$$

This complicates the spin constraint to

$$\sum_{\mathbf{kG}} S_{\mathbf{k}} \cdot S_{\mathbf{q-k+G}} = NS^2 \sum_G \delta_{\mathbf{qG}}, \tag{1.2.43}$$

where $\mathbf{G}$ are the lattice Bragg points that we explored earlier in the section on the reciprocal lattice. This very much limits the number of non zero $\mathbf{S_k}$ points.

In this magnetism section we have discussed the different important interactions that can lead to a magnetic interaction. We started with the hydrogen atom, first in free space considering the different states, then in a lattice where we notice that the electron is kinetic particle that delocalises across the whole system if it is allowed to. Then we notice that electrons interact and that we must at least include an on site repulsive term, leading to the single-band Hubbard model. We pick a certain regime of a dominant repulsive term

and note that at half filling we are able to get a model for the magnetism that is seen: the Heisenberg Hamiltonian. The minimisation in the classical regime is quite similar to the hopping Hamiltonian that we saw earlier.

1.3 Statistical Physics

Thus far we have dealt solely with ground state physics. Our investigation here discusses finite temperature phase transitions and so it is paramount that there exists an understanding of how a system reacts at a finite temperature. This requires a review of statistical physics starting from the microscopic interactions to macroscopic quantities; dealing with the approach of ensembles to find the equilibrium state and the role of the free energy within the system.

1.3.1 Thermodynamic equilibrium

Throughout the previous section a lot of the work was done at a microscopic level. In this section we deal with macroscopic quantities which occur through the average of microscopic states. In thermodynamic systems there are of order 10^{23} particles and it is naive to attempt to follow the motion of each particle and explore each possible state individually. Statistical physics is a means of understanding the macroscopic quantities and gain meaningful observables of a large interacting system without the need of understanding the motion of individual particles, and it does so through averaging over ensembles.

In the pursuit of these observables some clarity must be made on the terminology. A macrostate is described by experimentally accessible observables without any specific knowledge of the behaviour of individual particles. In contrast a microstate is the knowledge of the behaviour of individual particles. An ensemble is the set of possible microstates and their probabilities that make up a given macrostate. We shall discuss different types of ensembles that are appropriate to use at different times.

Our idea is to find the observables that occur at thermal equilibrium which we will see is closely linked to the statistical weight and the probabilities that are assigned to each microstate. It is assumed that all microstates that have the same energy are equally likely.

Once we discuss the partition function and ensemble averages we shall move onto the thermodynamic quantities that arise from the partition function and discuss their physical relevance.

1.3.2 The Gibbs Canonical Ensemble

The Gibbs canonical ensemble is the ensemble that we use throughout our investigation and so we shall discuss it in depth here.

Consider a system connected to a heat bath which is at a fixed temperature. Only heat is transferred between the connected systems, and so the system we consider has constant volume and particle number but the energy may fluctuate. We create an ensemble which lists all the possible microstates with their probabilities and group them with their associated macrostates labelled by parameters $\{\lambda\}$. We assume that degenerate microstates are equally probable, and assign a Boltzmann probability distribution to each microstate:

$$\begin{aligned} P\left(E_i\right) =& \frac{e^{-\beta E_i}}{\mathcal{Z}} \\ \mathcal{Z} =& \sum_i e^{-\beta E_i}, \end{aligned} \tag{1.3.1}$$

here $\beta = \frac{1}{T}$, $\mathcal{Z}$ is the partition function which is the sum over all possible microstates, and i labels the state which has energy E_i. We shall see that the partition function is an important quantity as it provides a lot of the thermodynamic quantities of the system.

If we know the probabilities of the system we are able to calculate macroscopic quantities of the system:

$$\langle O \rangle = \frac{\sum_i O_i e^{-\beta E_i}}{\mathcal{Z}}, \tag{1.3.2}$$

where O is some observable and O_i is its value in state i. One example of this is the mean energy

$$\begin{aligned} \langle E \rangle =& \frac{\sum_i E_i e^{-\beta E_i}}{Z} \\ =& -\frac{1}{Z}\frac{\partial Z}{\partial \beta}, \end{aligned} \tag{1.3.3}$$

and its variance

$$\begin{aligned} \langle E^2 \rangle - \langle E \rangle^2 =& \frac{1}{Z}\frac{\partial^2 Z}{\partial \beta^2} - \left(\frac{1}{Z}\frac{\partial Z}{\partial \beta}\right)^2 \\ =& \frac{\partial}{\partial \beta}\left(\frac{1}{Z}\frac{\partial Z}{\partial \beta}\right) \\ =& -\frac{\partial}{\partial \beta}\langle E \rangle, \end{aligned} \tag{1.3.4}$$

which is proportional to the specific heat at constant volume. The specific heat is an experimentally accessible quantity which measures the amount of energy required to change the temperature of the system, and here we have related the response of a system from an external parameter to fluctuations about some mean value. The specific heat is a key quantity in investigating phase transitions which we will see in later sections, and it is important as it has singular behaviour in critical regions.

An important quantity that we deal a lot with is the correlation length, which in magnetic systems arise from the correlation function

$$\langle \mathbf{S}_0 \cdot \mathbf{S}_n \rangle = \frac{\sum_i \mathbf{S}_0 \cdot \mathbf{S}_n e^{-\beta E_i}}{Z}, \tag{1.3.5}$$

where $\mathbf{S}_n$ is the spin at site n. The correlation length ζ is defined in the large $n \to \infty$ limit

$$\langle \mathbf{S}_0 \cdot \mathbf{S}_n \rangle \sim e^{-\frac{n}{\zeta}}, \tag{1.3.6}$$

which indicates how far correlations extend within the system, and is thus a quantity that can help determine the order of the system.

Another key quantity to discuss here is the Helmholtz free energy which is defined both statistically and using macroscopic quantities:

$$\begin{aligned} \mathcal{F} =& U - TS \\ =& -\frac{\log \mathcal{Z}}{\beta}, \end{aligned} \tag{1.3.7}$$

this is an important quantity because it is minimal at equilibrium if the system holds a constant volume and is at a constant temperature. This illustrates the non-trivial relationship between temperature and amount of disorder in a system. At low temperature the energy term dominates and so the equilibrium state is one with minimal energy. This tends to be an ordered state, which has very low entropy. As the temperature rises, the free energy is minimised by raising the entropy of the system. In increasing the entropy of the system, this will tend to increase the energy, and so there is a balance between the two. This is illustrative of the fact that a state at high temperature is disordered and a state at low temperature is ordered. This plays an important role later when we discuss phase transitions.

1.4 Phase Transitions

The statistical physics that has been covered was with the idea that all thermodynamic quantities were smooth, well defined functions, with no singular behaviour. Realistically, physical systems exist in the thermodynamic limit where the number of statistical particles diverges and it is possible for a system to undergo singularities in its macroscopic quantities. This is the study of phase transitions which exist between two states of different symmetries.

In this section we introduce the notion of phase transitions through Landau formulation, which is a mean-field approach. We find critical points and relate them to the divergences in thermodynamic quantities. We show that there is a degree of universality between systems that respect the same sort of symmetries and introduce the concept of critical exponents.

We move onto renormalisation group theory which uses the idea that critical fluctuations are key to a transition. We start with the method of decimation on the 1-D Ising chain to present an example of the analysis. From here we discuss flow diagrams and the existence of critical points, moving onto universality between models.

Once general information about phase transitions is presented we discuss their existence in systems with low dimensionality. Once an argument is given about the lack of phase transitions in 1-D, then we discuss the argument given be Mermin and Wagner about phase transitions in 2-D. This then leads us onto the Kosterlitz Thouless transition.

We present some experimental evidence of phase transitions in superfluid helium, relating that model onto the plane rotator model. Then we present some brief arguments about the existence of vortices and a phase transition that is topological in nature.

After these physical introductions we briefly introduce the mathematical concept of duality and its application to condensed matter systems.

1.4.1 Landau formulation

The theory and quantitative nature of phase transitions is very hard to calculate exactly. Landau theory [54] is a conceptually easy-to-understand process which qualitatively describes the behaviour of phase transitions using broken symmetry ideas to expand the free energy about the critical point. It is a mean-field approach which deals only with macroscopic quantities; there are inaccuracies associated with it but it is a very useful approach.

We shall introduce a power law expansion based on the order parameter of a system within the context of the spin systems that we have been dealing with. From there we follow the natural progression to phase transitions and the behaviour about the critical

point. We shall also show where the theory is invalid. We follow arguments provided by [55].

Generally as a system passes through a phase transition from a disordered state to an ordered state it reduces in the number of symmetries it respects. This tends to be characterised by an order parameter M, which behaves singularly at the critical point, taking a non-zero value below the transition and a zero value above. The order parameter is a macroscopic quantity and the mean-field assumption is that the fluctuations about the mean of this order parameter are negligible, implying that the free energy can be expressed around the critical region as a power law expansion in this order parameter

$$f(M,T) = f_0 + A(T)M^2 + b(T)M^3 + c(T)M^4 + \cdots - hM, \tag{1.4.1}$$

where A, B, C, h are functions of temperature.

Through knowledge of certain symmetries of the Hamiltonian we can eliminate some powers. We deal with spin systems, so our order parameter is the expectation value of the spin $M = \langle S \rangle$. Let us consider the Ising Hamiltonian with no magnetic field, which has the symmetry $s \to -s$, which implies that to preserve this symmetry there can only be even powers of the order parameter within the system:

$$f(M,T) = f_0 + A(T)M^2 + c(T)M^4 + \cdots, \tag{1.4.2}$$

which we now minimise with respect to the only parameter under our control, M. Above a phase transition the minimum must occur at $M = 0$, implying $A(T) > 0$. Below a phase transition the minimum occurs at $M \neq 0$, which requires $A(T) < 0$. It must be that $A = 0$ at the transition temperature, and assuming it is linear to first approximation in temperature $A(T) = a(T - T_c)$. We can see from figure 1.5 that decreasing the temperature through T_c continuously changes the global minimum of the free energy and so the order parameter moves from zero to a non zero value.

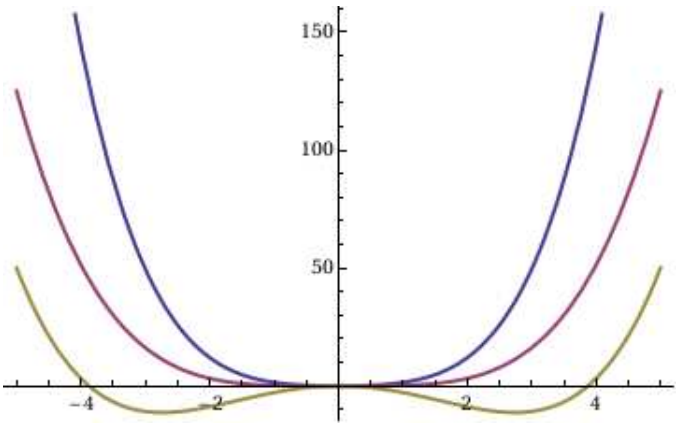

Figure 1.5: A mean-field approximation to a continuous phase transition.

$$M = \begin{cases} 0 & : T > T_c \\ \pm\sqrt{a\frac{|T-T_c|}{2c}} & : T < T_c \end{cases} \tag{1.4.3}$$

This is a second order transition as the order parameter increases smoothly from zero. The specific heat contains a discontinuity at the phase transition

$$C = \begin{cases} T\frac{\partial^2 f_0}{\partial T^2} & : T > T_c \\ T\frac{\partial^2 f_0}{\partial T^2} + \frac{2a^2 T}{c} & : T < T_c \end{cases} \tag{1.4.4}$$

Most second order phase transitions contain singularities in the specific heat at the critical region, implying that theory requires the fluctuations that it ignores, but qualitatively this discontinuity is also seen.

One is also able to describe first-order phase transitions using Landau theory, where the order parameter jumps discontinuously, which can be seen in solid to liquid transitions, where the order parameter is the density. Consider the possibility that the fourth-order term is negative, then we must include a positive sixth-order term so that the global minimum of the free energy does not occur at a divergent value of the order parameter:

$$f(M,T) = f_0 + a(T - T_0)M^2 + bM^4 + cM^6, \tag{1.4.5}$$

which has minima at

$$M = \begin{cases} 0 & : T > T_c \\ \pm\sqrt{\frac{-4b \pm \sqrt{16b^2 - 48ac}}{12c}} & : T < T_c \end{cases} \tag{1.4.6}$$

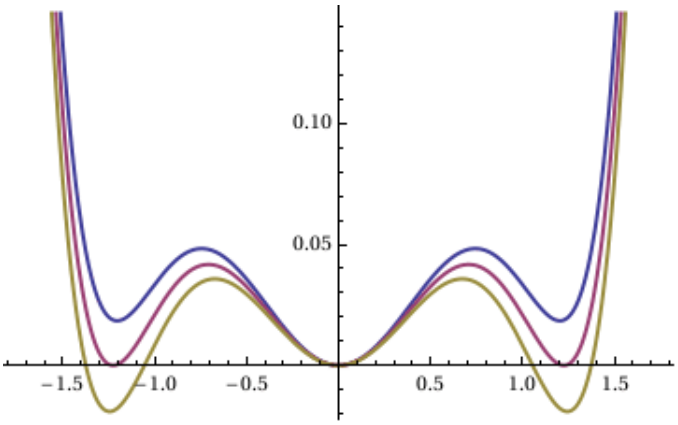

Figure 1.6: A mean-field approximation to a first order phase transition

This discontinuity can be seen in figure 1.6 where the global minima jumps. The transition temperature occurs at $T_c = T_0 + \frac{3b^2}{16ac}$, and the latent heat released at the transition temperature is $\Delta C = \frac{-3abT_c}{8c}$.

Landau's theory of phase transitions picks up a lot of the qualitative nature of critical points, both first and second order transitions provide approximate behaviour of macroscopic quantities. It should be noted that the Hamiltonian is not directly considered and so we have a very universal theory that gives the same results for Hamiltonians that share the same symmetry.

As this is a mean-field approach it does not consider fluctuations about the mean of the order parameter. This is an overly simple assumption as we shall see when we consider more sophisticated techniques to phase transitions. In fact at critical points fluctuations are important at every length scale, and it is known that the upper critical dimension for which this theory is valid is 4.

1.4.2 2-D Ising Model Results

There are very few exactly solvable models that exhibit phase transitions. The model that is most relevant to this investigation is the square-lattice Ising model, where the partition function was first found exactly by *Onsager* [42], and the transition temperature was found exactly by *Kramers* and *Wannier* [41]. Separate solutions were found by *Yang* [44] and *Lieb et al* [45].

The Ising model is a restricted nearest-neighbour ferromagnetic model which allows the spins to point in only two opposite directions, labelled by $\sigma_i = \pm 1$:

$$\mathcal{H} = -J \sum_{\langle ij \rangle} \sigma_i \sigma_j. \tag{1.4.7}$$

Exact results include the magnetisation, [42]

$$M = \left(1 - [\sinh 2\beta J]^{-4}\right)^{\frac{1}{8}}, \tag{1.4.8}$$

which around the transition temperature provides the critical exponent $\beta = \frac{1}{8}$. The specific heat has a logarithmic divergence

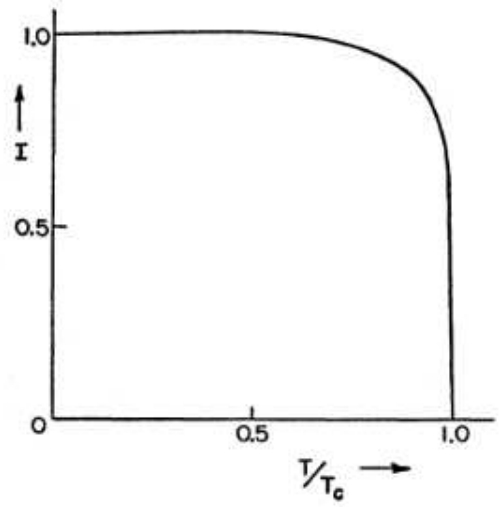

Figure 1.7: The magnetisation of the 2-D Ising model taken from [44]

$$C \sim \log |T - T_c|, \tag{1.4.9}$$

which implies that the critical exponent $\alpha = 0$ and that its first two derivatives behave as $\frac{1}{|T-T_c|}$ and $\frac{1}{|T-T_c|^2}$. The free energy can be expressed exactly [42]

$$-\beta f = \log 2 + \frac{1}{8\pi^2} \int_0^{2\pi} d\theta_1 d\theta_2 \log \left[\cosh^2 2\beta J - \sinh 2\beta J \left(\cos \theta_1 + \cos \theta_2 \right) \right], \tag{1.4.10}$$

and we plot the specific heat with our calculated specific heat, along with its first two derivatives in figures 1.8, 1.9 and 1.10. Note that the derivatives on the exact free energy have been performed numerically.

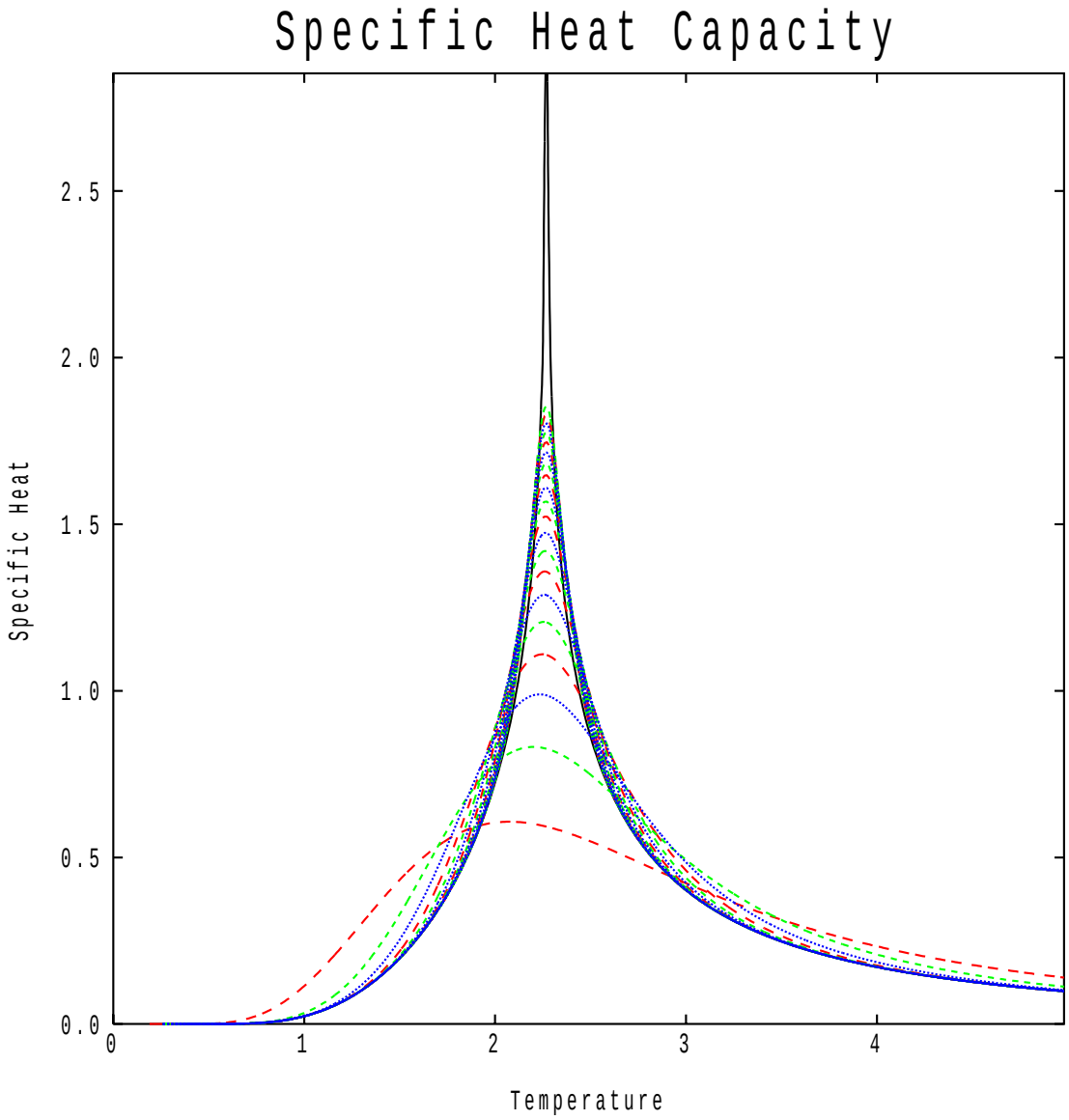

Figure 1.8: The exact specific heat of the 2-D Ising model overlaid with our results of the $J_1 - J_N$ model. The black curve is the exact result. The lowest curve is $J_1 - J_2$ and each higher curve is the next value of N up until the highest curve $J_1 - J_{21}$.

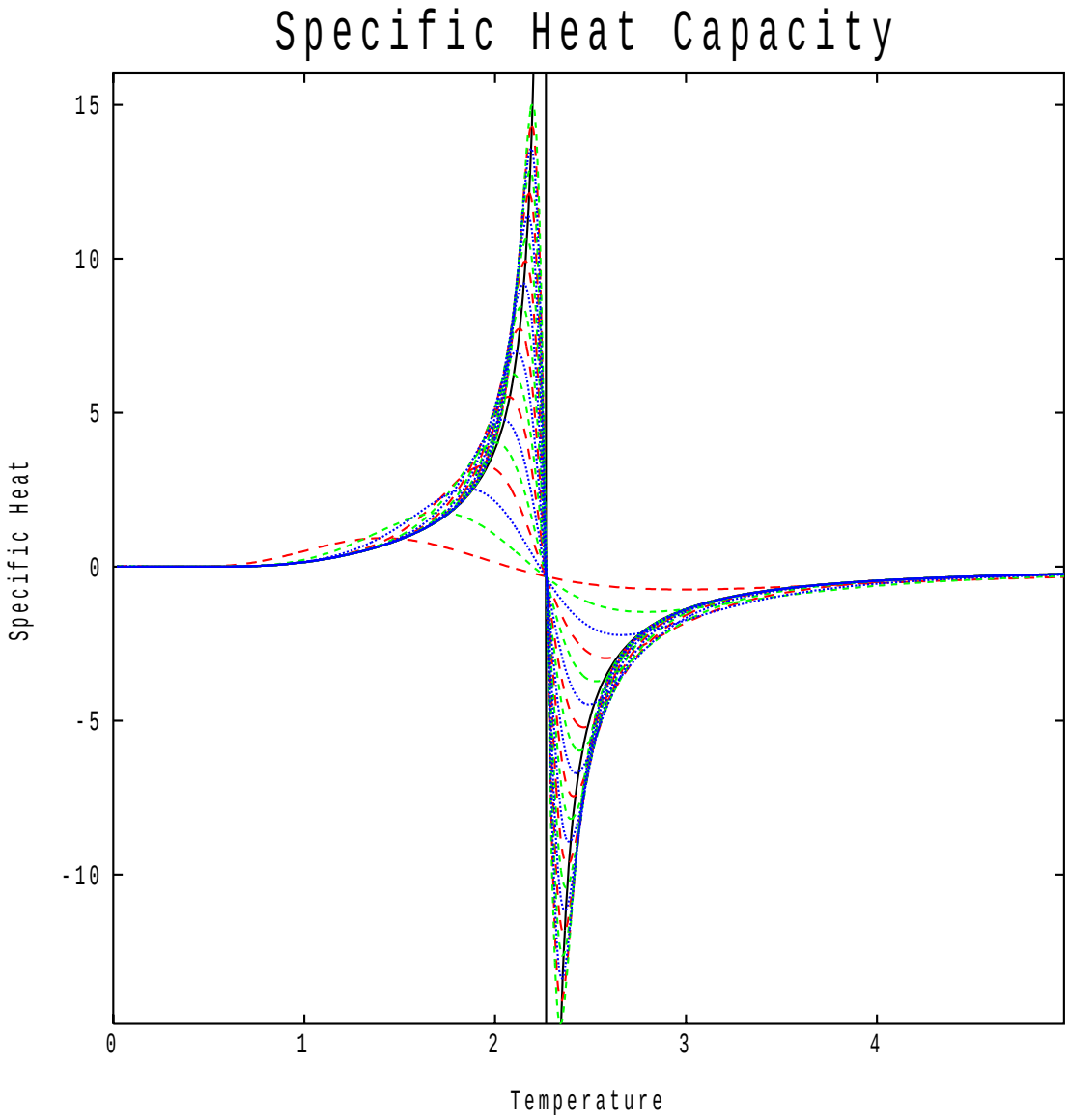

Figure 1.9: The first derivative of the 2-D Ising specific heat overlaid with our results. The curves correspond to the same models explained in figure 1.8.

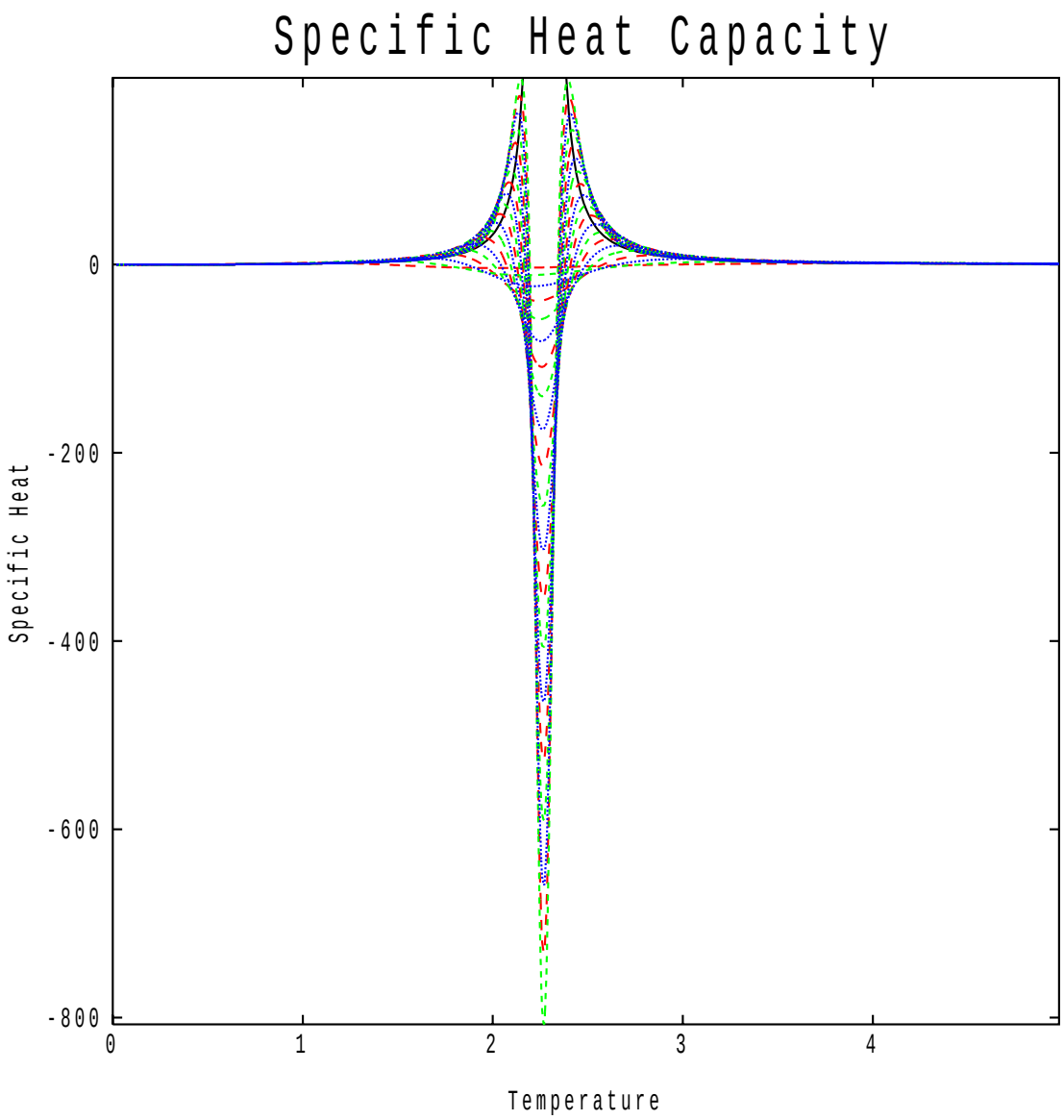

Figure 1.10: The second derivative of the 2-D Ising specific heat overlaid with our results. The curves correspond to the same models explained in figure 1.9.

1.4.3 Renormalisation Group

The Landau formulation is a mean-field theory that does not consider fluctuations about the transition to be key. As it turns out they are important at every length scale at a critical point. Renormalisation group theory attempts to consider fluctuations at all levels, and uses the idea that at critical points there is a degree of scale invariance in the spatial extent of fluctuations. At the outset it is a theory that considers the problem at every length scale giving an effective temperature and flow diagram; presenting the behaviour of thermodynamic quantities at critical points.

We very briefly outline an example of renormalisation group theory in the 1-D Ising chain. This presents the idea of flow diagrams and scale. We then discuss simple scaling examples and universality.

Coarse Graining and The Ising Model

At critical points the system has a certain scale invariance; the correlation length goes to infinity and if we do any coarse graining, each scale is statistically equivalent to the initial one. This we shall illustrate with the flow through parameter space and see that fixed points illustrate phase transitions. We shall start with coarse graining the Ising model and see that there are two fixed points, one at $T = 0$ and one at $T = \infty$. The arguments that we provide follow the discussion in [55].

We want to integrate out each length scales one at a time up to macroscopic lengths, so we do something called coarse graining, where a single spin represents a finite group of spins, we then require that the Hamiltonian and thus partition function remains invariant and re-describe these as function of the new spins. This is then repeated and the aim is to be able to understand how the couplings between spins change at each iteration of this process. This then provides the flow diagrams in parameter space and shows the critical regions.

We start with the 1-D Ising model, using a process called decimation

The Ising Chain

The Ising chain is known to exhibit no phase transitions, and so we shall hope that this process does not reveal any finite-temperature fixed point. The reduced Hamiltonian is

$$\mathcal{H} = K \sum_i \sigma_i \sigma_{i+1}, \tag{1.4.11}$$

where σ_i can take the values of ± 1 only. The coupling $K = -\beta J$ where J is the nearest neighbour coupling and we have simply included the temperature. We now coarse grain this model, by grouping the spins into collections of 2. We then take a single spin as the representation for that group and re-describe the Hamiltonian in terms of this spin. This process is illustrated in figure 1.11 and is called decimation. The idea of this process is to rewrite the partition function in terms of these new spins, and hope that it provides an easier sum than the initial problem.

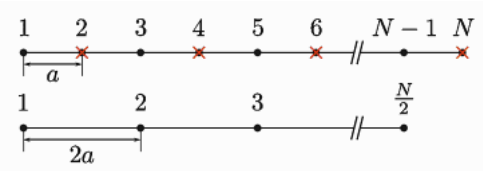

Figure 1.11: The decimation procedure on the linear chain. Figure is taken from [35]

$$\mathcal{Z} = \sum_{\{\sigma^0\}} \exp\left(K \sum_i \sigma_i^0 \sigma_{i+1}^0 \right), \tag{1.4.12}$$

where σ^i represents the number of iterations that have been performed. After the decimation the partition function must remain unchanged.

$$\mathcal{Z} = \sum_{\{\sigma^1\}} \exp\left(\mathcal{H}_1\right), \tag{1.4.13}$$

where $\exp(\mathcal{H}_1) = \sum'_{\sigma^0} \exp\left(K \sum_i \sigma_i^0 \sigma_{i+1}^0\right)$, where the primed sum is over only half the spins. This process is then iterated

$$\mathcal{Z} = \sum_{\{\sigma^i\}} \exp\left(\mathcal{H}_i\right), \tag{1.4.14}$$

where $\exp(\mathcal{H}_i) = \sum'_{\sigma^{i-1}} \exp\left(\mathcal{H}_{i-1}\right)$.

In general this process can over-complicate the Hamiltonian and require the computation of very difficult sums, but in this 1-D Ising case it can be shown that the iterated Hamiltonian has the form

$$\mathcal{H}_n = \sum_i a_n\left(\beta\right) + c_n\left(\beta\right)\sigma_i^n\sigma_{i+1}^n, \tag{1.4.15}$$

this provides important information about the physics of the system. The quantity c_n tells us the value of the new coupling, which in turn tells us the temperature of the new system. The idea is to find the flow of this coupling as the process is iterated. In this case the values of a_n and c_n are

$$\begin{aligned} a_n =& \frac{1}{2}\log\left(4\cosh 2c_{n-1}\right) \\ c_n =& \frac{1}{2}\log\left(\cosh 2c_{n-1}\right). \end{aligned} \tag{1.4.16}$$

After each iteration, at finite temperature the new block of spins do not look statistically similar to the previous as the process provides a new temperature each time. There are two fixed points at $\beta = 0$ and ∞, and we see from the flow diagram in figure 1.12 that $\beta = \infty$ is an unstable fixed point, and all temperatures flow towards $\beta = 0$. This tells us that even at very low temperatures the Ising chain is not in an ordered state, apart from the special case of $T = 0$. This is a result we will discover again in depth when we discuss finite energy domains.

The 1-D Ising model is a very special case where the renormalised Hamiltonian has the same form as the previous one. In general this is not the case and just one iteration can move into a high dimensional parameter space of couplings that are no longer between nearest

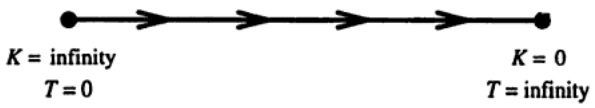

Figure 1.12: The renormalisation flow for the 1-D Ising model. Taken from [55]

neighbours nor simply quadratic interactions.

The idea of renormalisation group theory is to find points that are fixed within the parameter space, indicating that there is a degree of scale invariance as each iteration is statistically similar. These fixed points within parameter space correspond to the system's critical points, where it is undergoing a phase transition. Normally the non trivial fixed points are unstable and the flow on either side tends to either go to $T = 0$ or $T = \infty$ indicating vastly different physics on either side.

Within the vicinity of these critical points are regions where certain macroscopic quantities exhibit power law behaviour of the form $O \sim \left(\frac{T-T_c}{T_c}\right)^a$, where T_c is the temperature of the critical point and a is some positive number called the critical exponent. The remarkable finding with phase transitions is that between systems that do not appear to share any of the same properties, they exhibit exactly the same critical exponents around their phase transitions. This is the idea of universality between systems, which can be explained using renormalisation group theory. The critical exponents that are of interest to this investigation are those associated with the specific heat and correlation length

$$\begin{aligned} C &\sim \left(\frac{T-T_c}{T_c}\right)^{-\alpha} \\ \zeta &\sim \left(\frac{T-T_c}{T_c}\right)^{-\nu}, \end{aligned} \tag{1.4.17}$$

where for the 2-D Ising model $\alpha = 0$ and $\nu = 1$. The divergence in the specific heat is known to be a logarithmic divergence.

Here we have given a very brief overview of the idea of renormalisation group theory using the Ising model as an example. We have show one process of renormalisation: the

decimation technique, which works perfectly well in 1-D but becomes overly complicated in 2-D. The idea is to be able to find a process that will not be unusable. From renormalisation there comes the idea of universality, where many seemingly dissimilar systems exhibit the same power law expansion about critical points.

Still keeping with phase transitions we shall look into their existence in 1-D and 2-D systems, following the arguments made by Mermin and Wagner, and its application to isotropic systems.

1.4.4 Mermin-Wagner Theory and Domain Walls

In this subsection we discuss the existence of phase transitions in low dimensional systems. We find that in 1-D even models with discrete degrees of freedom, such as the Ising model, do not exhibit long range order at finite temperature. This is due to the finite energy of the excited states in the thermodynamic limit. Once we move to 2-D we see that the Ising model must have a phase transition and using an argument by Peierls we gain an approximate transition temperature. With isotropic spins the arguments are different and we must depend on the Mermin Wagner theorem to provide an answer of phase transitions in 2-D. Then we shall see what was provided to explain the existence of a transition in 2-D.

We again consider the Ising model in 1-D. We know from the renormalisation group analysis that there is no critical point, but let us discuss this with respect to the physics involved. A system in thermodynamic equilibrium minimises the free energy

$$F = E - TS. \tag{1.4.18}$$

At zero temperature the minimum free energy occurs in the ground state: $F = E_0$. Excitations are domain walls as seen in figure 1.13, one domain wall being the lowest lying excitation. This costs $2J$ in energy, and in a periodic system has an entropy $\log N$ associated with it; N are the number of sites in the system. Considering only the lowest excitations

at low energy the free energy is

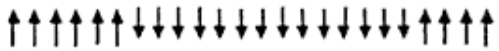

Figure 1.13: An example of two domain walls in the ferromagnetic Ising chain. Taken from [36]

$$F = E_0 + 2J - T \log N, \tag{1.4.19}$$

and in the thermodynamic limit $N \to \infty$ this is a lower free energy at all finite temperatures than the one associated with the ground state. This is a disordered state as the order parameter $\langle \sigma_i \rangle = 0$. At all finite temperatures the Ising chain is a disordered system, and any phase transition must occur at zero temperature. This is in agreement with the renormalisation group flow that was discussed earlier and was an argument initially provided by *Ising* [39].

Let us discuss the effect of domains in 2-D, where we follow the arguments provided by *Peierls* [40].

Again at zero temperature the minimum free energy occurs in the ground state. The excitations that will eradicate the long range order are domain walls that extend across the length of the system. We depict these boundaries in figure 1.14. They have energy $E = 2LJ$ where L is the length of the domain wall. The argument that *Peierls* provides over-counts the number of possible boundary configurations and the entropy associated with such a state is 2^L which means that the change in free energy is

$$F = E_0 + 2LJ - TL \log 2. \tag{1.4.20}$$

Once $2J - T \log 2 < 0$ then the domain walls are favourable and the system is in a disordered state, below this temperature, the ordered state is preferable. This gives a temperature $T_c = 2.885J$, close to the exact solution found by *Kramers* and *Wannier* $T_c = 2.269J$ [41].

Thus far we have dealt with the existence of phase transitions with discrete degrees of

freedom. This investigation is based on the plane rotator model, an isotropic spin model. The Mermin-Wagner theory [7] of long range order applies here, and using the Heisenberg model we see that in any system with fewer than 3 dimensions the order parameter $M = \langle S \rangle = 0$ at any finite temperature. This is done first by assuming long range order at finite temperature and calculating the size of the fluctuations. The inconsistency comes about when we note that the fluctuations diverge, implying that there is no macroscopic moment. This does not imply a disordered state down to zero temperature, and we shall see when we discuss the X-Y model that at low temperature the system contains quasi-long range order.

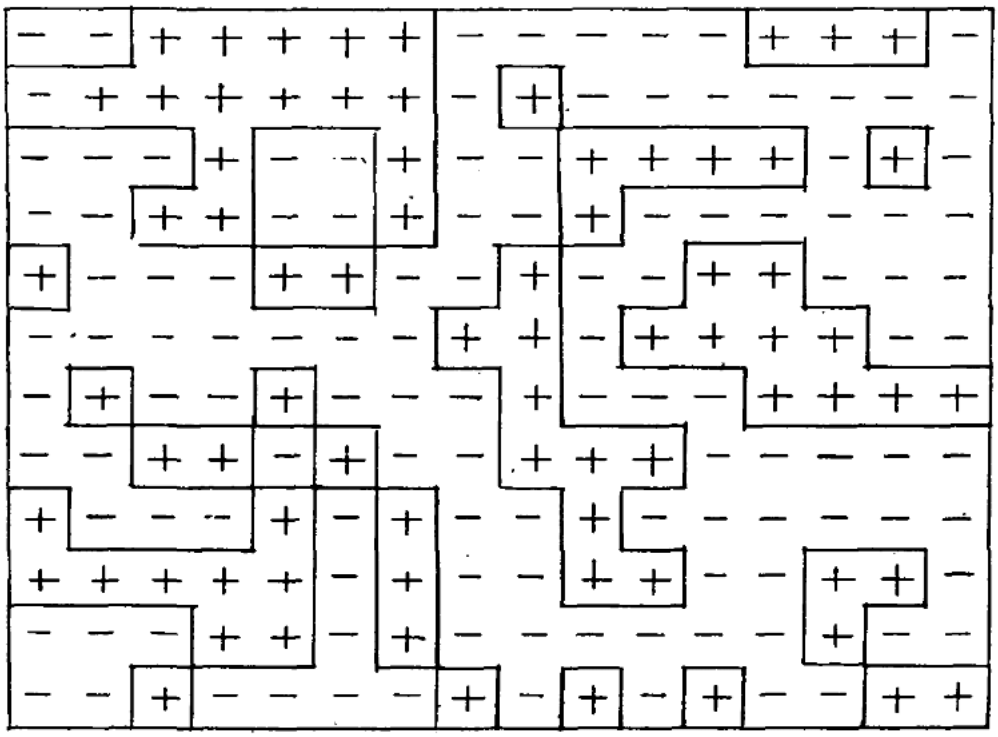

Figure 1.14: Domain wall excitations in the Ising model taken from [40]

The ferromagnetic Heisenberg model can be expressed in terms of the Holstein-Primakoff bosons [67]; assuming that there is long range order along the $\hat{z}$ direction, and that the quartic terms are negligible the Hamiltonian is

$$
\begin{aligned}
\mathcal{H} =& - J \sum_{\langle ij \rangle} \mathbf{S}_i \cdot \mathbf{S}_j \\
S^z =& S - b^\dagger b \\
S^+ =& b\sqrt{2S} \\
S^- =& b^\dagger \sqrt{2S} \\
S^x =& \frac{1}{2}\left(S^+ + S^-\right) \\
S^y =& \frac{1}{2i}\left(S^+ - S^-\right) \\
\mathcal{H} =& - \frac{JS^2 ZN}{2} + \frac{JS}{2} \sum_{ij} \left(b_i^\dagger - b_j^\dagger\right)\left(b_i - b_j\right) + O\left(1\right),
\end{aligned}
\tag{1.4.21}
$$

where we are using the limit $S \to \infty$ and Z is the coordination number of the lattice. The aim is to find the order parameter, assuming it is ordered along the $\hat{z}$ direction

$$
\langle S^z \rangle = S - \langle b^\dagger b \rangle, \tag{1.4.22}
$$

this thermodynamic average is best understood using the eigenfunctions of the Hamiltonian, which are the Bloch states.

$$
b_{\mathbf{k}}^\dagger = \sum_{\mathbf{R}_j} e^{i\mathbf{R}_j \cdot \mathbf{k}} b_j^\dagger. \tag{1.4.23}
$$

These diagonalise the Hamiltonian and provides the energy spectrum

$$
\mathcal{H} = -JSZ \sum_k b_k^\dagger b_k \left(1 - \gamma_k\right), \tag{1.4.24}
$$

where γ_k is the structure factor as we saw in section 1.2.2 and we have ignored the constant term. The order parameter is best understood in terms of the eigenfunctions

$$
\langle S^z \rangle = S - \sum_{k,k'} \langle b_k^\dagger b_{k'} \rangle. \tag{1.4.25}
$$

This simplifies to the Bose function $\langle b_k^\dagger b_{k'} \rangle = \delta_{kk'} n\left(E_k\right)$,

$$\sum_k \langle b_k^\dagger b_k \rangle \propto \frac{1}{(2\pi)^d} \int \frac{k^{d-1} dk}{\exp\left(\beta JSZ\left[1-\gamma_k\right]\right)-1}. \tag{1.4.26}$$

Singular contributions of this integral occur at the $k \to 0$ limit and we see in one dimension ($d = 1$) where the structure factor can be approximated as $\gamma_k = \cos k \approx 1 - k^2$, that the integral is

$$\langle b_k^\dagger b_k \rangle \sim \int \frac{dk}{k^2}, \tag{1.4.27}$$

which is divergent at the origin, indicating that the fluctuations at any finite temperature destroy the long range order. In two dimensions the structure factor at the origin is approximated as $\gamma_k \approx 1 - k_x^2 - k_y^2$, and the integral is again divergent, though only logarithmically at the origin

$$\langle b_k^\dagger b_k \rangle \sim \int \frac{k dk}{k^2}. \tag{1.4.28}$$

In three dimensions, it is not divergent, and so it is possible for the model to exhibit long range order at low temperature. This is the essence of the Mermin-Wagner argument, and similar discussions can be made with X-Y model; isotropic spins systems do not exhibit long range order in a system with fewer dimensions than three.

There are very interesting consequences that arise from this theory. One dimension is a very special case where it is known that there cannot exist any ordered state at any finite temperature. In two dimensions there must also exist a phase transition, despite there being clearly no long range order. This was shown by *Fröhlich* and *Spencer* [8], [9] who conclude that at low temperature the plane rotator model exhibits power law correlations and exponential correlations at high temperature. A resolution to this apparent paradox has been provided in work by *Kosterlitz* and *Thouless* [1],[2] and *Berezinskii* [3], [4]. Before we discuss the Kosterlitz-Thouless transition in detail we must formally introduce the clock

model and an overview of the literature.

1.5 The Clock Model

The investigation here is based on the nearest neighbour two dimensional clock model, which is very closely related to the plane rotator. We shall discuss the current situation in the literature, including well known renormalisation results on the model and subsequent numerical simulations on finite sized systems. We shall then briefly give an overview of how our results sit with the literature.

The ferromagnetic clock model Hamiltonian on the square lattice between nearest neighbours with one continuous spin degree of freedom ϕ_i is

$$\mathcal{H} = -J \sum_{\langle ij \rangle} \cos\left(\phi_i - \phi_j\right) - \sum_i \sum_p h_p \cos\left(p\phi_i\right), \tag{1.5.1}$$

where there is a nearest neighbour ferromagnetic interaction and an on-site crystal field interaction. This model has been studied extensively in the literature and of particular note are the well-known renormalisation results [10]. In this investigation we only take the case where a single crystal field interaction is positive infinite and all other are zero. This greatly simplifies (1.5.1) to spins with discrete degrees of freedom $n_i \in 0, \cdots, p-1$.

$$\mathcal{H} = -\sum_{\langle ij \rangle} \cos \frac{2\pi}{p} \left(n_i - n_j\right), \tag{1.5.2}$$

where we have normalised the interaction coupling to $J = 1$. We have included in figure 1.15 two examples of spins that have an infinite crystal field interaction in the form of the on-site term from 1.5.1.

The main analytic results that we will review on the clock model in (1.5.1) come from the seminal paper by *José et al* [10], which uses a renormalisation approach to both the plane rotator and clock model using Migdal techniques on a square lattice [46]-[49], an

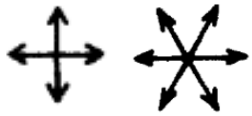

(a) (b)

Figure 1.15: Two examples of spins that are restricted to point only along the clock directions for $p = 4$ (a) and $p = 6$ (b). Taken from [10]

approximate method that uses a decimation procure not unlike that which was introduced in section 1.4.3. The results here were for $p = 1$ to 4 and $p = 6$. We plot the main phase diagrams found for $p = 4$, $p = 6$ model.

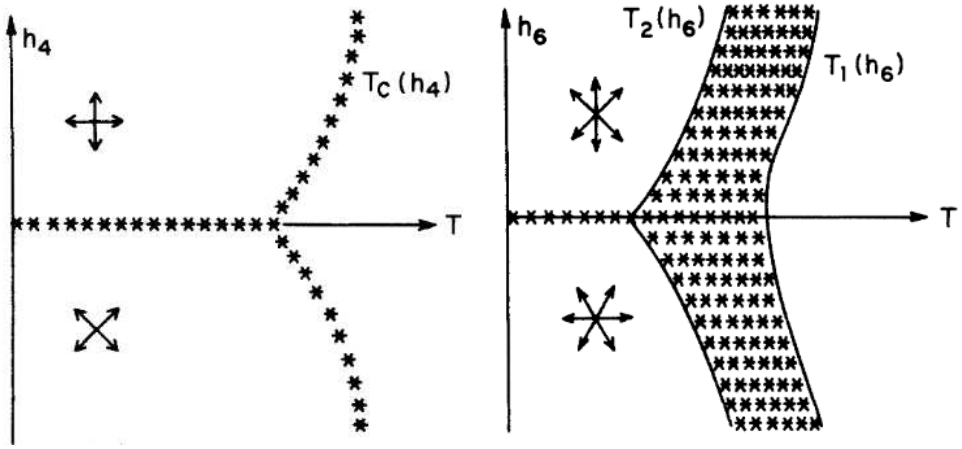

(a) (b)

Figure 1.16: The main $h_p - T$ phase diagram results for the $p = 4$ (a) and $p = 6$ (b) model from [10]. The asterisk denote critical points/ regions.

We see from the figure that for the $p = 6$ model there exist two transitions at finite temperature up to infinitesimal h_6. Another key result from this work are the eigenvalues of the crystal field λ_p, which determine the relevance of the field in the renormalisation. In the case $\lambda > 0$ it is relevant, $\lambda < 0$ irrelevant, and in the long range fluctuation limit equivalent to the plane rotator model. We plot this result in figure 1.17 and see that at finite temperature the eigenvalue for the $p = 6$ model is less than zero, indicating that above this temperature h_6 is irrelevant and can be used to model the plane rotator system.

There is a lot of literature on the clock model that is numerical Monte Carlo simulations

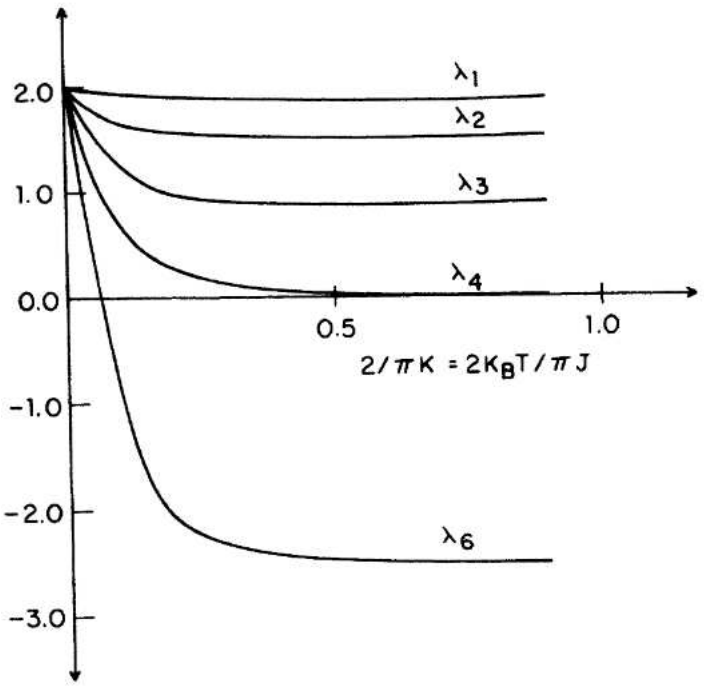

Figure 1.17: The eigenvalues for the renormalisation theory for the crystal field λ_p. Notice that only $\lambda_6 < 0$. Taken from [10]

on finite sized, periodic systems. There is some discrepancy between results of different investigations but all agree that there exist two phase transitions in the $p > 4$ model. It must be noted that *Ortiz et al* [50] find a duality mapping much like the Ising model discussed later in section 1.7 that maps the two transitions in the $p > 4$ model onto each other, concluding that both must be a Kosterlitz-Thouless transition, one between a long range ordered state and a critical region and another between a critical region and a paramagnetic state.

Monte Carlo work on the plane rotator model by *Tobochnik et al* [18] determine a Kosterlitz-Thouless transition at $T_c = 0.89$ [1] but find a sharp specific heat anomaly significantly above the transition temperature at $T = 1.02$. The Monte Carlo investigation presented position of vortices in one of the finite sized systems at different temperatures above and below the transition temperature, as we show in figure 1.18.

Lapilli et al [25] argue that, despite conclusions made by *Jose et al*, that the clock model becomes thermodynamically indistinguishable from the plane rotator below the Kosterlitz-

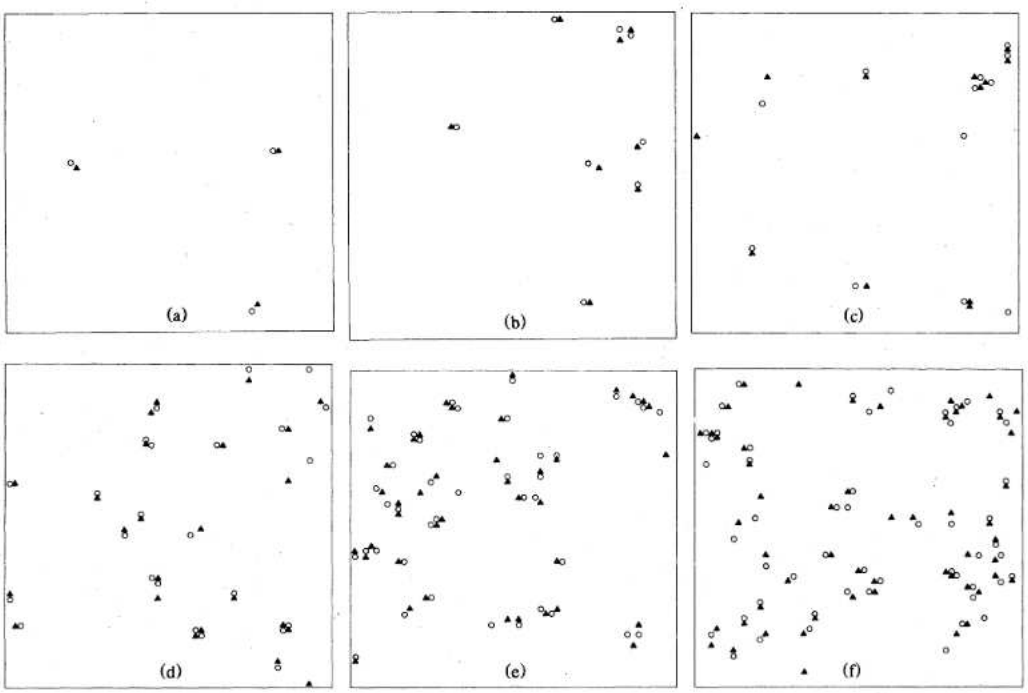

Figure 1.18: The position of vortices in Monte Carlo data taken from [18]. The system has 3600 spins with empty circles as positive vortices and filled triangles as negative vortices. Figures (a)-(f) are at temperatures $T = 0.8$, $T = 0.85$, $T = 0.9$, $T = 0.95$, $T = 1.00$, $T = 1.05$ respectively, where the predicted transition temperature is between (b) and (c) and the specific heat anomaly occurs between (e) and (f)

Thouless transition temperature only for models $p > 7$ and that for $p < 7$ the high temperature transition is not of Kosterlitz-Thouless type. They conclude that at a temperature T_{eu} all $p > 4$ models are indistinguishable from the plane rotator and that for $p < 7$ this is at a temperature greater than the transition temperature. We show their main results in figure 1.19.

Other Monte Carlo data exists on different p state clock models which we summarise in table 1.1.

There also exists a Fisher Zero approach to the $p = 6$ state clock model [30]. The numerical investigation exploits an analytic method to predict standard phase transitions developed by *Yang*, *Lee* and *Fisher* [51]-[53] that we review in section 2.4. The investigators conclude that the $p = 6$ state clock model is not of Kosterlitz Thouless type, agreeing with the results found by *Lapilli et al* [25]. They conclude that the specific heat peak above the

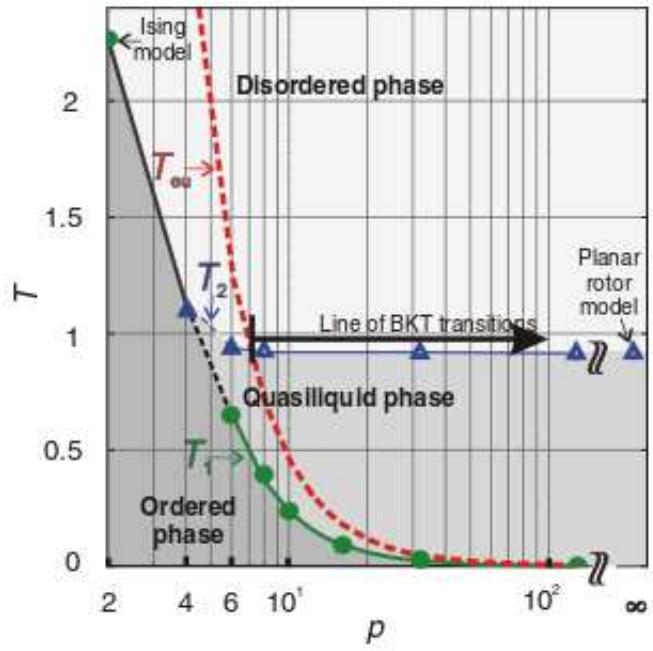

Figure 1.19: The temperature for different p models found by *Lapilli et al* [25] where there is thermodynamic convergence between the clock model and plane rotator. The convergence for $p < 6$ is higher than its high temperature transition temperature and is thus argued not to be of Kosterlitz Thouless type.

author	p	T_{KT}
Okabe et al [26]	6	0.9
	8	0.8936
	12	0.8937
Challa et al [24]	6	0.92
Yamagata et al [28]	6	0.9
Tobochnik [29]	5	1.1

Table 1.1: Key Monte Carlo investigations for the high temperature transition for different p state clock models

Kosterlitz Thouless temperature does diverge in the thermodynamic limit

There appears to be much discrepancy within the literature. It appears from *Jose et al* results [10] that above $p = 6$ the crystal field becomes irrelevant and the clock model is indistinguishable from the plane rotator, and that according to *Ortiz et al* there is a duality that maps the two clock transitions onto each other [50]. The numerical simulations present different results for systems that should have the same Kosterlitz-Thouless transition at high

temperature. There are also results suggesting that some clock models do not exhibit the same type of transition.

In this investigation, which uses exact transfer function techniques and is in the thermodynamic limit, we shall argue that for all $p > 4$ clock models there exist two transitions that exhibit the same behaviour, and that above the lower temperature transition there exists power law convergence between the clock models and the plane rotator. We shall provide an overview of the Kosterlitz-Thouless transition and its experimental realisation in the superfluid phase of liquid helium, but first we shall show the equivalence between the Ising model and the $p = 4$ model.

1.5.1 The $p = 4$ model

A lot of the Ising model plots that we calculate actually uses the $p = 4$ model, which is identical to the Ising, but with a rescaled temperature. We shall very briefly show the relationship between the Ising model and the $p = 4$ model.

The $p = 4$ nearest neighbour Hamiltonian is

$$\mathcal{H} = -\sum_{\langle ij \rangle} \cos \frac{\pi}{2} \left(n_i - n_j \right), \tag{1.5.3}$$

where the spins are able to point along $\pm\hat{\mathbf{x}}$ and $\pm\hat{\mathbf{y}}$ direction. This can be rewritten as two Ising variables σ, τ

$$\mathbf{S}_i = \sigma_i \frac{\hat{\mathbf{x}}}{\sqrt{2}} + \tau_i \frac{\hat{\mathbf{y}}}{\sqrt{2}}, \tag{1.5.4}$$

which is the same problem, rotated by $\frac{\pi}{4}$. The Hamiltonian which is the dot product between nearest neighbours is thus

$$\mathcal{H} = \sum_{\langle ij \rangle} \sigma_i \sigma_j + \tau_i \tau_j, \tag{1.5.5}$$

and so the partition function is

$$\begin{aligned} \mathcal{Z} &= \sum_{\{\sigma,\tau\}} \exp\left(\beta \sum_{\langle ij\rangle} \sigma_i\sigma_j + \tau_i\tau_j\right), \\ \mathcal{Z} &= \sum_{\{\sigma\}} \exp\left(\beta \sum_{\langle ij\rangle} \sigma_i\sigma_j\right) \sum_{\{\tau\}} \exp\left(\beta \sum_{\langle ij\rangle} \tau_i\tau_j\right), \\ \mathcal{Z} &= \left(\mathcal{Z}_{\text{Ising}}\right)^2, \end{aligned} \tag{1.5.6}$$

and so the free energy is

$$\mathcal{F} = -2T \log \mathcal{Z}_{\text{Ising}}, \tag{1.5.7}$$

where the temperature has scaled from the Ising model by 2. The transition temperature is thus half that of the $p = 2$ model.

1.6 The Kosterlitz-Thouless Transition

The Kosterlitz-Thouless transition [1]-[4] provides an answer to this seeming paradox of isotropic spins that exhibit no long range order but still undergo a phase transition, through a continuum limit of the plane rotator model. There are plenty of applications to this limit, one of which is the model for superfluid helium and its superfluid transition. We will very briefly review the main experiments performed on liquid helium and the model that describes the Bose-Einstein condensate.

Liquid helium has a unique property that at atmospheric pressure, it does not solidify and remains a liquid to zero temperature. Instead it passes through a transition in which it becomes a Bose-Einstein condensate at $T_c = 2.18K$ referred to the lambda transition. The condensate exhibits superfluidity in which a macroscopic quantity of the liquid sits in the ground state of the system with zero viscosity. The fluid is incompressible and is described

using a two fluid model. The density is split into two parts, the superfluid component ρ_s and the normal liquid component ρ_n both of which depend on temperature

$$\rho_{\text{Tot}} = \rho_n(T) + \rho_s(T), \tag{1.6.1}$$

and it is found that the temperature dependence of the densities satisfy:

$$\begin{aligned} \lim_{T\to 0} \frac{\rho_s}{\rho_{Tot}} &= 1, \\ \lim_{T\to T_c^-} \frac{\rho_s}{\rho_{Tot}} &= 0, \end{aligned} \tag{1.6.2}$$

and above the transition $\rho_s = 0$, and so acts as an order parameter for the transition. In three dimensions the superfluid density exhibits a continuous phase transition, and the bulk material can be seen to exhibit a transition in the specific heat. In two dimensions the measurements are much harder as there is no bulk material and standard thermodynamic quantities are not accessible. Instead the fluid is placed in a porous material either Vycor or Mylar and resonated. The amount of fluid that vibrates with the substrate changes as a function of temperature, and so the period of oscillation changes. This is what is measured, and work by *Bishop et al* provides archetypal results for the period of oscillation as seen in figure 1.20 [13].

To explain the link between the superfluid and the plane rotator model we first describe the condensate as a complex wave function

$$\psi(\mathbf{x}) = \rho^{\frac{1}{2}} e^{i\phi(\mathbf{x})}, \tag{1.6.3}$$

where ρ is the total density of the fluid, and as helium is an incompressible fluid all the physics lies within the phase of the wave function.

One takes the Gross-Pitaevskii equation to describe the ground state of identical bosons, which has a wave function that is a product of many single particle wave functions described

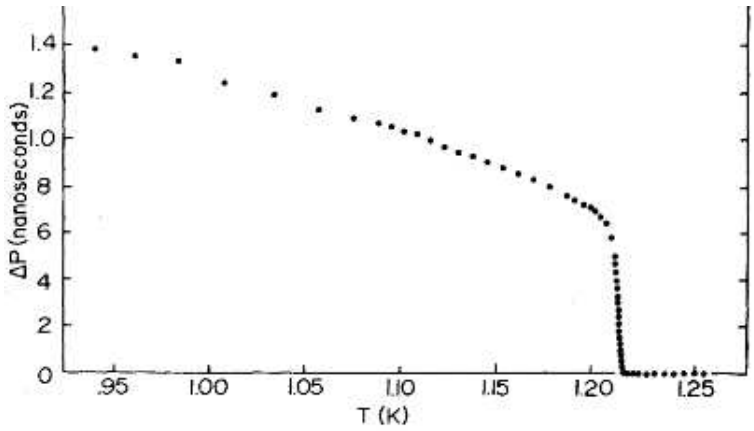

Figure 1.20: The phase transition seen in the superfluid density of helium-4 in Mylar. Figure is taken from [13]

by

$$\begin{aligned} \Psi\left(\mathbf{r}_1, \cdots, \mathbf{r}_N\right) &= \psi\left(\mathbf{r}_1\right) \cdots \psi\left(\mathbf{r}_N\right) \\ \mathcal{H} = \left(\nabla^2 + V\left(\mathbf{r}\right) + g|\psi\left(\mathbf{r}\right)|^2\right) \psi\left(\mathbf{r}\right) &= \mu\psi\left(\mathbf{r}\right), \end{aligned} \tag{1.6.4}$$

Substituting the condensate wave function and recognising that ρ is constant implies that the Hamiltonian is

$$H = \int \left(\nabla\phi\right)^2 dx. \tag{1.6.5}$$

and the velocity of the fluid, related to the current operator

$$\begin{aligned} \mathbf{j} =& i\left(\psi\nabla\psi^* - \psi^*\nabla\psi\right), \\ \mathbf{v} =& \frac{\mathbf{j}}{\rho} \\ \sim& \nabla\phi, \end{aligned} \tag{1.6.6}$$

which implies an irrotational velocity field $\nabla \wedge \mathbf{v} = 0$. This is only the case with a simply connected space but if there is a region that is not simply connected, as ϕ can be discontinuous,

then it follows that the loop integral about the region can be non zero

$$\oint d\mathbf{x} \cdot \mathbf{v} = 2\pi n, \tag{1.6.7}$$

where n is some integer.

This model is very much intricately linked to the magnetic plane rotator Hamiltonian on a discrete lattice

$$\mathcal{H} = -J \sum_{\langle ij \rangle} \cos\left(\theta_i - \theta_j\right). \tag{1.6.8}$$

Assuming small variations in θ between sites, which one can make at low temperature, one can expand the cosine term to its quadratic representative.

$$\mathcal{H} = J \sum_{\langle ij \rangle} \left(\theta_i - \theta_j\right)^2, \tag{1.6.9}$$

and taking the continuum limit

$$\mathcal{H} = J \int \left(\nabla\theta\left(\mathbf{x}\right)\right)^2 d\mathbf{x}. \tag{1.6.10}$$

This is the same model seen in liquid helium, including the angular nature of the field $\theta\left(x\right)$. One can solve the thermodynamics of this model, calculating the partition function

$$\mathcal{Z} = \int \mathcal{D}\theta\left[\mathbf{x}\right] e^{-J\beta \int (\nabla\theta)^2 d\mathbf{x}}, \tag{1.6.11}$$

which provides critical behaviour all the way up to $T = \infty$, as can be seen from the correlation function

$$\langle \cos\left(\theta_0 - \theta_m\right) \rangle \sim \left(\frac{1}{|m|}\right)^{\eta}, \tag{1.6.12}$$

where $\eta = \frac{1}{2\pi\beta J}$. This is critical behaviour and implies a quasi long range ordered state for

all temperatures. This is an unphysical result. It is known experimentally that liquid helium exhibits a transition between a superfluid and a normal liquid state, and it is in fact proven by *Fröhlich* and *Spencer* [8], [9] that at low temperature for the discrete lattice system the plane rotator has power law correlations, whereas at high temperature the correlations are exponential.

Arguments first provided by *Beresinskii* [3], [4], then *Kosterlitz* and *Thouless* [1], [2] discuss the existence of vortices in these models and their role in providing a phase transition. Let us first consider the energy and entropy balance of a single vortex within a square, periodic lattice centred at the origin as shown in figure 1.21. If vortices are thermodynamically favourable then the system is in a disordered state.

$$\mathbf{S}_i = \left(-\frac{y_i}{r_i^2}, \frac{x_i}{r_i^2} \right), \tag{1.6.13}$$

where x, y are the coordinates of the spin which are distance r_i from the origin. In the continuum limit the energy density is $(\nabla\theta)^2 = \frac{1}{r^2}$, thus the energy:

$$\begin{aligned} U =& \pi J \int_a^L \frac{r dr}{r^2} \\ =& \pi J \log\left(\frac{L}{a}\right), \end{aligned} \tag{1.6.14}$$

where L is the radius of the system and a is the short length scale cutoff normally defined by the lattice spacing. There are $\left(\frac{L^2}{a^2}\right)$ possible vortex configurations, implying that the free energy of a vortex is

$$\begin{aligned} F =& U - TS \\ =& (\pi J - 2T) \log\left(\frac{L}{a}\right). \end{aligned} \tag{1.6.15}$$

A vortex is thermodynamically favourable above a temperature $T_c = \frac{J\pi}{2}$. This is the

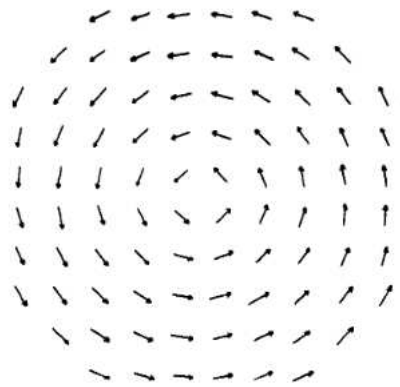

Figure 1.21: An isolated vortex in the plane rotator model taken from [1]

qualitative argument given that the plane rotator model has a phase transition associated with topological charges. The behaviour of vortices and their interaction with each other is very similar in which Coulombic charges behave in 2-D.

This field θ is not continuous and can have a discontinuity of $2n\pi$. About a vortex, the loop integral is

$$\oint \nabla\theta \cdot d\mathbf{l} = 2\pi n. \tag{1.6.16}$$

Instead of dealing with θ one deals with $u = \nabla\theta$ which is well defined everywhere apart from the vortex core, where it is singular. To agree with equation (1.6.16) it must satisfy

$$\nabla \wedge \mathbf{u} = 2\pi \sum_i n_i \delta\left(\mathbf{r} - \mathbf{r}_i\right), \tag{1.6.17}$$

where $\mathbf{r}_i$ are the position of the vortices and n_i is the number of times the angle winds around the vortex.

We are able to split up the field $\mathbf{u}$ into two parts, a background contribution that is smooth and is not associated with vortices and a second term that is.

$$\mathbf{u} = \nabla\phi - \nabla \wedge \left(\hat{z}\psi\right), \tag{1.6.18}$$

where ϕ is a continuous scalar quantity and ψ must satisfy

$$\nabla^2\psi = 2\pi \sum_i n_i \delta\left(\mathbf{r} - \mathbf{r}_i\right), \tag{1.6.19}$$

which implies that ψ is the Green's function for the Laplace equation in 2-D, which is

$$\psi = \sum_i n_i \log\left(|\mathbf{r} - \mathbf{r}_j|\right), \tag{1.6.20}$$

and so the energy of the configuration is

$$\begin{aligned} \mathcal{H} =& \frac{J}{2}\int d^2x \mathbf{u}\cdot\mathbf{u} \\ =& \frac{J}{2}\int d^2x \left[(\nabla\phi)^2 - 2\nabla\phi\cdot\nabla\wedge(\hat{z}\psi) + (\nabla\wedge(\hat{z}\psi))^2\right]. \end{aligned} \tag{1.6.21}$$

The second term has a zero contribution if $\phi \to 0$ on the boundary and the last term simplifies to $(\nabla\psi)^2$, which after integration by parts leads to

$$\mathcal{H} = \frac{J}{2}\int d^2x \left[(\nabla\phi)^2 + \psi\nabla^2\psi\right], \tag{1.6.22}$$

as long as the charge neutrality is conserved $\sum_j n_j = 0$. The first term is the normal spin wave contribution found earlier, the final term has the contribution to the energy as

$$J\pi \sum_{ij} n_i n_j \log\left(|\mathbf{r}_i - \mathbf{r}_j|\right), \tag{1.6.23}$$

which diverges at $i = j$, and so there must be some core energy

$$H_{\text{vort}} = \sum_i E_{\text{core}} + J\pi \sum_{i\neq j} n_i n_j \log\left(|\mathbf{r}_i - \mathbf{r}_j|\right). \tag{1.6.24}$$

This along with the spin wave contribution from $(\nabla\phi)^2$ is the Hamiltonian that is solved by *Kosterlitz* and *Thouless* [1], [2] where we simply quote the key behaviour of the correlation

length and the free energy, both of which have essential singularities. This implies that all derivatives of the free energy and thus the thermodynamic behaviour are not power law expandable about the critical point and that there is no sharp behaviour, as is standard in a phase transition:

$$\begin{aligned} \zeta \sim & e^{\frac{b}{(T-T_c)^{\frac{1}{2}}}} \\ F \sim & \zeta^{-2}. \end{aligned} \tag{1.6.25}$$

Any inverse plot of a thermodynamic function would go to zero very smoothly at the critical point along with all its derivatives. This implies that the transition is not one which happens collectively as is standard, rather it is simply two vortices unbinding.

The order parameter that is used is the superfluid density in liquid helium, or equivalently the helicity modulus in the plane rotator model, which is equivalent to the leading order cost in the free energy to place a single spiral across the system. The prediction is that at the transition temperature, there exists a universal jump in the order parameter, which can be seen in figure 1.22.

$$\frac{\rho_s\left(T_c^-\right)}{T_c} = \text{constant}. \tag{1.6.26}$$

Much like the clock model there is plenty of numerical analysis and Monte Carlo data on the plane rotator model. We have already mentioned the seminal work by *Tobochnik* and *Chester* [18] who find a large specific heat anomaly above the proposed Kosterlitz Thouless transition temperature. Numerical work performed on finite systems by *Van Himbergen* and *Chakravarty* [22] find the same anomaly and propose that the height of the peak saturates and does not diverge in the thermodynamic limit, which we show in figure 1.23.

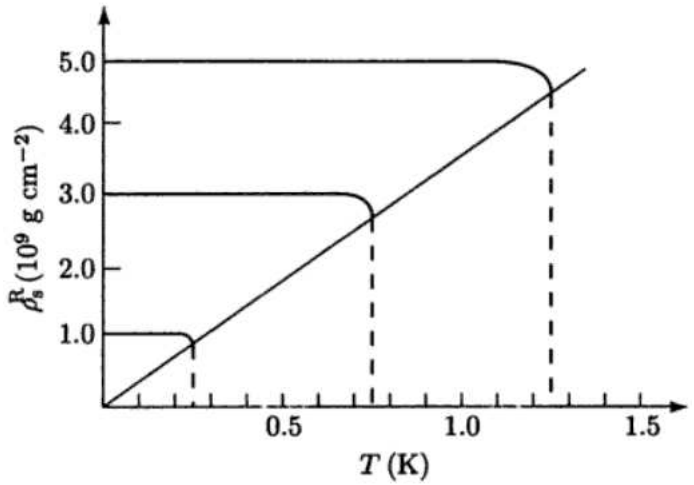

Figure 1.22: The predicted discontinuity in the superfluid density from field theoretic results. Taken from [38]

Monte Carlo investigations by *Gupta et al* find the specific heat anomaly [19], where they fit to both a second order phase transition and a Kosterlitz Thouless transition where they acknowledge that the differentiating between the two type of transitions on finite sized numerical data is difficult. There also exists data at infinite temperature by *Ben-Av* and *Solomon* who restrict large spin flips so that there is zero vorticity within the system and find that correlations are still power law. Thus they conclude that vorticity is paramount to the phase transition.

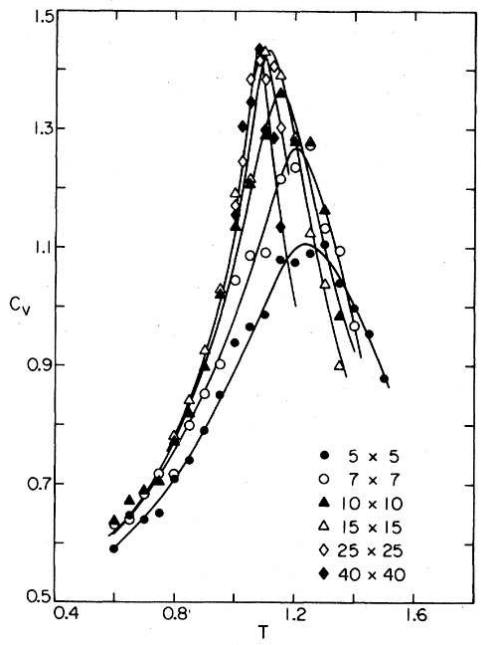

(a)

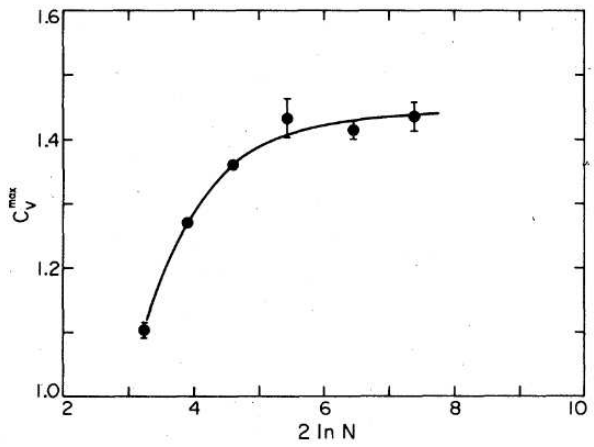

(b)

Figure 1.23: The Monte Carlo results of the specific heat as a function of temperature (a), and the size of the peak as a function of the system size in (b), from [22] who conclude that the specific heat does not diverge in the thermodynamic limit.

1.7 Duality Transformation

We find in this investigation that with the correlation functions we calculate, their representation in the Fourier spin space is rather illuminating. We find that the high temperature limit is best represented using Fourier spin space, and real spin space for the low temper-

ature limit. It is then worth discussing how high temperature can map exactly onto low temperature in certain spin models. These use duality transformations. We shall formally introduce the duality transform through a Fourier series approach and then use the Ising model as an example.

A lot of this section follows the arguments provided by an appendix in the paper by *Fröhlich* and *Spencer* [8],[9] on the high temperature and low temperature results on the plane rotator model and the arguments provided by *Kadanoff* in his textbook on statistical physics [36].

With duality, one must describe a dual lattice, where there are quantities that exist on the direct lattice, on the bonds between sites and on the dual lattice. If the direct lattice is a square lattice and describes quantities with sites (j,k) then its dual is also a square lattice defined by sites $\left(j+\frac{1}{2},k+\frac{1}{2}\right)$ and its bonds between sites are $\left(j+\frac{1}{2},k\right)$ and $\left(j,k+\frac{1}{2}\right)$. This is illustrated in figure 1.24. We define quantities on the bonds and the sites $\rho_{j+\frac{1}{2},k}=\phi_{j+1,k}-\phi_{j,k}$ and $\eta_{j,k+\frac{1}{2}}=\phi_{j,k+1}-\phi_{j,k}$ where ρ has been defined on the x bond and η on the y bond. We intend that the quantities on the sites ϕ obey a certain periodicity:

Figure 1.24: The dual lattice of the square lattice. The filled sites are the direct lattice, the unfilled sites its dual and the triangular sites are the bonds. Taken from [37]

$$\begin{aligned} C_{j+\frac{1}{2},k+\frac{1}{2}} =& \rho_{j+\frac{1}{2},k}-\rho_{j+\frac{1}{2},k+1}+\eta_{j+1,k+\frac{1}{2}}-\eta_{j,k+\frac{1}{2}} \\ =& 0\,(\text{mod } p)\,, \end{aligned} \tag{1.7.1}$$

so that about a closed loop the quantities must add to $0\,(\text{mod } p)$. Notice that the quantity

$C_{j+\frac{1}{2},k+\frac{1}{2}}$ is defined on the dual lattice.

Consider translationally invariant couplings $K_x(\rho)$, $K_y(\eta)$ that depend on the difference between the quantities on the site. The partition function of such a coupling is:

$$Z = \mathrm{Tr}_\phi \prod_{j,k=1}^{L} \exp\left\{K_x\left[\rho_{j+\frac{1}{2},k}\right] + K_y\left[\eta_{j,k+\frac{1}{2}}\right]\right\}. \tag{1.7.2}$$

To turn the trace over the ϕ variables into traces over the bond variables one must make sure the quantity C is conserved, and so we multiply the partition function by the factor

$$\Delta_{j+\frac{1}{2},k+\frac{1}{2}} = \frac{1}{p}\sum_{\psi=1}^{p} \exp\left[\frac{2\pi i \psi_{j+\frac{1}{2},k+\frac{1}{2}} C_{j+\frac{1}{2},k+\frac{1}{2}}}{p}\right], \tag{1.7.3}$$

implying that the partition function is now a trace over the ρ and η variables

$$Z = \mathrm{Tr}_\rho \mathrm{Tr}_\eta \prod_{j,k=1}^{L} \exp\left\{K_x\left[\rho_{j+\frac{1}{2},k}\right] + K_y\left[\eta_{j,k+\frac{1}{2}}\right]\right\} \Delta_{j+\frac{1}{2},k+\frac{1}{2}}. \tag{1.7.4}$$

The sum over each bond variable can act as a Fourier series

$$\sum_{\rho}^{p} e^{K_x\left[\rho_{j+\frac{1}{2},k}\right]} \exp\left\{\frac{2\pi i \rho_{j+\frac{1}{2},k}\left[\psi_{j+\frac{1}{2},k+\frac{1}{2}} - \psi_{j+\frac{1}{2},k-\frac{1}{2}}\right]}{p}\right\} = \exp\left\{\tilde{K}_y\left[\psi_{j+\frac{1}{2},k+\frac{1}{2}} - \psi_{j+\frac{1}{2},k-\frac{1}{2}}\right]\right\}, \tag{1.7.5}$$

and so the x coupling has been mapped onto the y coupling. This implies that the partition function can be rewritten in terms of the new variables ψ with dual coupling $\tilde{K}$, defined on the dual lattice

$$Z = \mathrm{Tr}_\psi \prod_{j,k=1}^{L} \exp\left\{\tilde{K}_y\left[\psi_{j+\frac{1}{2},k+\frac{1}{2}} - \psi_{j+\frac{1}{2},k-\frac{1}{2}}\right] + \tilde{K}_x\left[\psi_{j+\frac{1}{2},k+\frac{1}{2}} - \psi_{j-\frac{1}{2},k+\frac{1}{2}}\right]\right\}. \tag{1.7.6}$$

We shall present a translationally invariant example in the Ising model where the reduced

Hamiltonian is

$$\mathcal{H} = \frac{K}{2} \sum_{\langle j,k \rangle} \cos \pi \left(\phi_{j+1,k} - \phi_{j,k} \right) + \cos \pi \left(\phi_{j,k+1} - \phi_{j,k} \right). \tag{1.7.7}$$

From the Fourier series (1.7.5) we can see that

$$e^{-2\tilde{K}} = \tanh K, \tag{1.7.8}$$

where $\tilde{K}$ is the dual coupling associated with the dual lattice. We are able to write the partition function in terms of two different variables that correspond to the direct lattice and the dual lattice, which have exactly the same coupling form. However, as $K \to \infty$ it corresponds to $\tilde{K} \to 0$ and vice versa, thus we have successfully related the high and low temperature physics. The point at which $\tilde{K} = K$ at some finite temperature is the transition temperature between the ferromagnetic phase and paramagnetic phase. This occurs at $T_c \approx 2.269J$ where J is the original coupling strength.

In the results that we use, we Fourier transform the spin variable in certain correlation functions. What we find eventually is that in the clock model there is a subtle relationship between the high and low temperature.

Chapter 2

THE TRANSFER FUNCTION APPROACH

The technique that is introduced and presented in this section exploits the idea that regardless of system size, the spin models that are investigated are exactly solvable in 1-D. An infinite spiral geometry can be equated to the models studied in 2-D, its size characterised by the number of sites in one revolution and in the limit that the size is infinite the geometry is the 2-D square lattice. Exact thermodynamics are accessible in the 1-D system and conclusions are drawn by investigating trends for increasing system size where 2-D behaviour is then deduced. This 1-D to 2-D crossover technique provides an alternative method of study to the 2-D limit of inaccessible thermodynamics.

The details of the transfer function technique are provided in this section. The 1-D Ising chain, an established context of the use of transfer matrices [55] mark this section's introduction, where a review of its well known results are presented. Once transfer matrices are introduced it is applied to the clock models that feature predominantly in this investigation and important thermodynamic quantities such as the free energy, correlation length and order parameters are calculated. Throughout, there are points of discussion on the complexities inherent in the technique, including the issue of 1-D observables that must have a meaningful representation in 2-D.

It is worth noting that the mathematics behind these transfer functions are worth investigating in their own right, there is an interesting gauge symmetry which has yet to be

fully exploited and also the eigenvalue structure provides key thermodynamic information, including points of criticality in the 2-D limit. This is explored here in this section but an in depth investigation is required for a thorough understanding.

2.1 The 1-D Ising Chain

The Ising chain is an archetypal, fully solved system with which to introduce transfer functions. Here the thermodynamics are obtained analytically, making it easy to review the concept behind the technique. Once models with higher complexity are introduced, the understanding developed in this section is easily transferable to the technique used throughout this investigation. Though there are plenty of quantities that are available in this model, the two key observables that are relevant to the investigation are exhibited here: the free energy and the correlation length.

Transfer matrices as a technique presents the normally impossible task of calculating the partition function of a system in a matrix format and its thermodynamics are fully described within the eigenvalues of this matrix. The process involves exploiting the local, translationally invariant interactions that the system must have and recognising that the partition function can be expressed iteratively. It is a powerful technique that can be implemented on a variety of systems, such as those investigated here.

2.1.1 Free Energy

In this section the free energy, and in subsequent sections, the correlation length of the Ising chain is calculated to a high level of detail so that the understanding gained here is transferable to the technique developed in later sections for the clock model on the spiral geometry. It is important to realise that the requirements for transfer matrices to be applicable is that all interactions must be purely local and contain a translational symmetry. Here the system is shown to meet these requirements and it is understood that the locality of the

interactions imply a finite transfer matrix and the translational invariance implies that the partition function is an iterative application of such a matrix. The Hamiltonian of the 1-D ferromagnetic Ising model was introduced in section 1.4.3

$$\mathcal{H} = -\sum_i \sigma_i \sigma_{i+1}, \tag{2.1.1}$$

where the spin variables σ can take the values of ± 1 only, which can correspond to a spin restricted to pointing only up or down. This Hamiltonian is clearly local and translationally symmetric; all interactions are between nearest neighbours only. The translational symmetry is exploited once the partition function is introduced and split into natural segments:

$$z = \sum_{\{\sigma\}} e^{-\beta \mathcal{H}}, \tag{2.1.2}$$

split into purely local and translationally invariant parts, it can be seen that there is an iterative operator application:

$$\begin{aligned} z &= \cdots \sum_{\sigma_2} e^{\beta \sigma_2 \sigma_3} \sum_{\sigma_1} e^{\beta \sigma_1 \sigma_2} \\ f_i(\sigma_i) &= \sum_{\sigma_{i-1}} e^{\beta \sigma_{i-1} \sigma_i} f_{i-1}(\sigma_{i-1}), \end{aligned} \tag{2.1.3}$$

where $f_1 = 1$. Here the contribution to the partition function of each spin is calculated one at a time in one direction, it can also be calculated in the other direction:

$$f_{i-1}^{\dagger}(\sigma_{i-1}) = \sum_{\sigma_i} e^{\beta \sigma_i \sigma_{i-1}} f_i^{\dagger}(\sigma_i), \tag{2.1.4}$$

where $f_N^{\dagger} = 1$ and N is the size of the chain. Here the notation for the complex conjugate of f has been used, rather than a separate function, these two functions eventually become the left and right eigenvectors of a Hermitian matrix.

In matrix format

$$\begin{aligned} \mathbf{f}_i &= \mathbf{T} \cdot \mathbf{f}_{i-1} \\ \begin{pmatrix} f_i\left(+1\right) \\ f_i\left(-1,\right) \end{pmatrix} &= \begin{pmatrix} e^{\beta} & e^{-\beta} \\ e^{-\beta} & e^{\beta} \end{pmatrix} \begin{pmatrix} f_{i-1}\left(+1\right) \\ f_{i-1}\left(-1\right) \end{pmatrix}. \end{aligned} \tag{2.1.5}$$

The partition function for N particles is the overlap

$$z = \mathbf{f}_N^{\dagger} \cdot \mathbf{T}^N \cdot \mathbf{f}_1, \tag{2.1.6}$$

which is the trace of the matrix $\mathbf{T}^N$

$$Tr\left(\mathbf{T}^N\right) = \lambda_+^N \left(1 + \frac{\lambda_-^N}{\lambda_+^N}\right), \tag{2.1.7}$$

where $\lambda_{\pm}$ are the eigenvalues of the transfer matrix, such that $\lambda_+ > \lambda_-$. Simply by exploiting the locality and translational invariance, the partition function is an eigenvalue problem of a 2×2 matrix.

Physically relevant systems are those that are in the thermodynamic limit, which in this case is the limit that $N \to \infty$. From (2.1.7) it can be seen that only the largest eigenvalue is relevant to the thermodynamics

$$z = \lim_{N \to \infty} \lambda_+^N, \tag{2.1.8}$$

and so the free energy per spin is

$$\frac{F}{N} = -\frac{1}{\beta} \log\left(\lambda_+\right). \tag{2.1.9}$$

It is now natural to associate the partition function z with λ_+ as opposed to λ_+^N. In the context of the Ising chain this is

$$z = 2\cosh(\beta), \tag{2.1.10}$$

the free energy

$$\frac{F}{N} = -\frac{1}{\beta}\log(z), \tag{2.1.11}$$

and the vectors from (2.1.3) and (2.1.4) must tend to the corresponding left and right eigenvectors $\mathbf{f}$ and $\mathbf{f}^{\dagger}$.

2.1.2 Correlation Length

The application of transfer matrices is not limited to the partition function, this section shows that attainable quantities are not restricted simply to derivatives of the free energy, they in fact extend to any thermodynamic observable that can be split into purely local parts. These examples include certain correlation functions and by extension the correlation length. Introduced here will be a detailed discussion of calculating such quantities which will be a basis for the understanding of the same quantities in the spiral geometry.

It is the translational invariance and locality of interactions within the Hamiltonian that allows the partition function to be split up into purely local parts to be solved using transfer matrices. If an observable can also be split up in a similar fashion then that too is calculable. The thermodynamic average of any quantity is

$$\langle G(\sigma_n \cdots \sigma_m)\rangle = \frac{\sum_{\{\sigma\}} G(\sigma_n \cdots \sigma_m)\, e^{-\beta\mathcal{H}}}{\sum_{\{\sigma\}} e^{-\beta\mathcal{H}}}. \tag{2.1.12}$$

If the observable can be split into a product of single-variable functions

$$G(\sigma_n \cdots \sigma_m) = \prod_{i=n}^{m} G_i(\sigma_i), \tag{2.1.13}$$

then the numerator of the thermodynamic average can be split in the same way the partition function is split.

$$\sum_{\sigma_m} f^{\dagger}(\sigma_m)\, e^{\beta\sigma_{m+1}\sigma_m} G_m(\sigma_m) \cdots \sum_{\sigma_n} G_n(\sigma_n)\, e^{\beta\sigma_{n+1}\sigma_n} f(\sigma_n), \tag{2.1.14}$$

where we have used the previous definitions for f and $f^{\dagger}$ from section 2.1.1 . In matrix format

$$\langle G \rangle = \frac{\mathbf{f}^{\dagger} \cdot \mathbf{G}_m \cdots \mathbf{G}_n \cdot \mathbf{f}}{z^{m-n}}, \tag{2.1.15}$$

where $\mathbf{G}_i \cdot \mathbf{f} = \sum_{\sigma_i} G_i(\sigma_i)\, f(\sigma_i)\, e^{\beta\sigma_i\sigma_{i+1}}$. From these results the observable does not need to be translationally invariant, though it does make calculation a lot easier and from here only translationally invariant observables will be used where the local functions $G_i = G_j$ for all i and j.

Correlation functions are such examples of solvable averages, and one function in particular is dealt with

$$\langle \sigma_1 \sigma_m \rangle = \frac{\sum_{\{\sigma\}} \sigma_1 \sigma_m e^{-\beta\mathcal{H}}}{\sum_{\{\sigma\}} e^{-\beta\mathcal{H}}}, \tag{2.1.16}$$

and in matrix format

$$\langle \sigma_1 \sigma_m \rangle = \frac{\mathbf{f}^{\dagger} \cdot \tilde{\mathbf{T}} \cdot \mathbf{T} \cdots \mathbf{T} \cdot \tilde{\mathbf{T}} \cdot \mathbf{f}}{z^m}, \tag{2.1.17}$$

where $\tilde{\mathbf{T}} \cdot \mathbf{f} = \sum_{\sigma_i} \sigma_i f(\sigma_i)\, e^{\beta\sigma_i\sigma_{i+1}}$ and $\mathbf{T} \cdot \mathbf{f} = \sum_{\sigma_i} f(\sigma_i)\, e^{\beta\sigma_i\sigma_{i+1}}$. There are m applications of $\mathbf{T}$ between the matrices $\tilde{\mathbf{T}}$.

This correlation function also provides access to the correlation length, which is defined in the limit $m \to \infty$. This is a significant quantity to the results and plays a pivotal role in determining the validity of any extrapolation to 2-D in the spiral geometry. Here the details of the calculation for the 1-D Ising chain will be presented as a preliminary discussion to the calculations for the clock model on the spiral geometry.

The correlation length ζ is defined as:

$$\langle \sigma_1 \sigma_m \rangle \sim \lim_{m \to \infty} e^{-\frac{m}{\zeta}}, \tag{2.1.18}$$

assuming that both σ_1 and σ_m are within the bulk of the system. From this limit, just as in equations (2.1.7) and (2.1.8) where a repeated application of the transfer matrix tended to one of its eigenvalues the numerator of the correlation length must tend likewise but to one which is in a different subspace and to understand this an aside must be made on the different symmetries within a Hamiltonian.

Symmetries within a Hamiltonian.

Understanding the symmetries of a system provides a natural grouping of its eigenvectors into non-overlapping subspaces that are differentiated by their behaviour under such transformations. The eigenvectors associated with the partition function and correlation length are examples of eigenvectors that belong to two different subspaces. This aside shows that the matrix $\tilde{\mathbf{T}}$ projects the eigenvector associated with the partition function onto a vector within a different subspace, and so repeated application of the Hamiltonian will provide a different eigenvector.

A matrix $\mathcal{H}$ is considered symmetric under a unitary transformation $\mathcal{U}$ if their commutator is zero : $[\mathcal{U}, \mathcal{H}] = 0$.

The eigenvectors $\mathbf{g}$ of $\mathcal{U}$ tend to form degenerate subspaces and it follows that each eigenvector $\mathbf{f}$ of $\mathcal{H}$ is represented only by eigenvectors $\mathbf{g}$ in the same subspace.

In the context of this system the Hamiltonian, and by extension the transfer matrix, respect the symmetry $\{\sigma\} \to \{-\sigma\}$. Any application of the transfer matrix onto a vector that has an overlap with only one subspace of degenerate eigenvectors of this symmetry does not change the subspace it overlaps with. From equation (2.1.3) the first vector the transfer matrix is applied to is $f_1 = 1$, which is indeed invariant under this symmetry and

any number of applications of the transfer matrix can only project the vector within the subspace; the final eigenvector associated with the partition function obeys this symmetry.

The operator $\tilde{\mathbf{T}}$ from equation (2.1.17) is antisymmetric under the transformation $\{\sigma\} \rightarrow \{-\sigma\}$ and projects any vector away from this subspace onto one which is antisymmetric: $f(\sigma) = -f(-\sigma)$, which has no overlap with the eigenvector associated with the partition function. Any repeated application of the transfer matrix preserves the antisymmetry of this vector and so the eigenvalue associated with the correlation length is indeed the largest eigenvalue within this antisymmetric subspace.

The Ising chain is a simple example and these statements are best illustrated within the context that this example provides. Using the matrix form presented in equation (2.1.5) the symmetry transformation that represents $\{\sigma\} \rightarrow \{-\sigma\}$ is

$$\mathcal{U} = \begin{pmatrix} 0 & 1 \\ 1 & 0 \end{pmatrix}, \tag{2.1.19}$$

which does indeed leave the transfer matrix in (2.1.5) unchanged. The two eigenvectors of this matrix correspond to two different eigenvalues and as such the two subgspaces of degenerate eigenvalues are both of size one. In larger systems such as those investigated in later sections, there are large subspaces of degenerate eigenvectors and so for the consideration of these larger systems the term subgspace will still be used to refer to the group of degenerate eigenvectors, despite that degeneracy being one.

The symmetric subgspace has the partition function eigenvalue associated with it: $\lambda_+ = 2\cosh(\beta)$ and indeed the initial vector for the partition function $f(\sigma) = 1$ is in this symmetric subspace; repeated application of the transfer matrix must tend towards the highest eigenvalue within this subspace. The antisymmetric subspace has the eigenvalue $\lambda_- = 2\sinh(\beta)$ associated with it and the application of the matrix $\tilde{\mathbf{T}}$ which is antisymmetric under the symmetry transformation: $\left\{\tilde{\mathbf{T}}, \mathcal{U}\right\} = 0$ on a symmetric eigenvector projects it onto the an-

tisymmetric subspace and thus has zero overlap with the symmetric subspace. Any further application of the transfer matrix does not change the subspace that the vector overlaps with and so must tend towards the antisymmetric eigenvector.

The correlation length therefore must be associated with the eigenvalue $\lambda_- = 2\sinh(\beta)$ and in full is

$$\frac{1}{\zeta} = \log\left(\frac{\cosh(\beta)}{\sinh(\beta)}\right). \tag{2.1.20}$$

.

2.1.3 A Summary of the Ising Chain

The intention of this section was to provide an understanding of the use of transfer matrices to solve a common and completely analytical model as a basis for further understanding of the models investigated in subsequent sections. Though these models have a higher complexity, the partition function and correlation length are found in the same simplistic way; both are the highest eigenvalues of different subspaces of a symmetry transformation, where the subspaces in these cases are larger than one. Further discussion will focus on the issues with more complex models and the intention of investigating the 2-D limit. The concept that is key to this section and further sections is that the thermodynamics of all the models investigated arise from the eigenvalues of the transfer matrix.

The macroscopic quantities that are deduced from these eigenvalues play an important role in the classification of phase transitions in the 2-D limit. The partition function provides access to specific heat quantities, which can provide clear singular behaviour in the vicinity of a transition. The eigenfunction associated with the partition function provides conditional probabilities of spin alignment, where the behaviour of different states can be determined. Once a correlation length that has an analogue in 2-D is found it can provide clear evidence of 2-D behaviour and an understanding of the universality class of the transitions. These,

and further results that are exhibited later stem from the mathematics discussed here and in the subsequent section.

2.2 The Transfer Function Technique on the Spiral Geometry

The Ising model served as an introductory section to the transfer function approach to thermodynamics; through exploiting certain symmetries, important observables are obtained. The mathematics developed in that section provide the basis of the understanding in this section; much of it extends to the Hamiltonians investigated and as such the previous section will be used as a reference. Much like the Ising model the focus here is on two main thermodynamic quantities, the partition function and correlation length, and there is also discussion on the partition function eigenvector and the local spin configuration.

The motivation for this investigation arise from the 2-D plane rotator and 2-D clock model. Both models are inaccessible thermodynamically and much work in the literature is based on either analytically or numerically solvable models that are extendable to 2-D. This section begins with these two models and formally introduces the method to which it is studied. An example in the form of the $J_1 - J_2$ Ising model presents the mathematical extension of the previous section. Throughout, the issues that arise from these Hamiltonians are tackled as they are of a higher complexity than the Ising chain.

2.2.1 The Hamiltonian and the Spiral Geometry

The technique that is the focus of this section corresponds to a spiral geometry of a 1-D clock model. The 2-D limit is a spiral with an infinite radius and though all calculations are performed with finite radii it will be part of the investigation to explore what 2-D characteristics are present in these 1-D calculations. The fundamental mathematics has been presented in the previous section, and so the main discussion arises from the complexity of

these Hamiltonians and the implications of choosing this geometry.

The 2-D model that is the motivation of this study is the clock model. It is a 2-D classical spin model with spins that point only within the plane, which can be defined by a single angle θ

$$\begin{aligned}\mathcal{H} &= -\sum_{\langle i,j\rangle} \mathbf{S}_i \cdot \mathbf{S}_j \\ &= -\sum_{\langle i,j\rangle} \cos\left(\theta_j - \theta_i\right).\end{aligned} \tag{2.2.1}$$

The clock model restricts these to discrete spins that are part of the set $\theta = \frac{2\pi n}{p}$ where $n \in \{0 \cdots p-1\}$ and p characterises the number of ticks within the model: $p = 2$ corresponds to Ising spins. No attempt is made to solve the thermodynamics of this model directly as it is beyond the capabilities of this investigation; there are very few exactly solvable 2-D spin models. Instead, the complexity of the system is lowered to a 1-D model that is easily extendable to 2-D. Consider the set of clock Hamiltonians:

$$\begin{aligned}\mathcal{H} &= \sum_i \mathbf{S}_i \cdot \mathbf{S}_{i+1} + \mathbf{S}_i \cdot \mathbf{S}_{i+N} \\ &= \sum_i \cos\left(\theta_{i+1} - \theta_i\right) + \cos\left(\theta_{i+N} - \theta_i\right).\end{aligned} \tag{2.2.2}$$

These Hamiltonians correspond to a spiral geometry that is illustrated in figure 2.1. Each spin shares a bond with four neighbouring spins: $i \pm 1$ and $i \pm N$. As these are the only bonds that exist in the model we denote it as the $J_1 - J_N$ model, and in the limit that $N \to \infty$ the spiral tends to the 2-D square lattice. This limit is investigated through grouping models with the same clock tick and analysing trends that are universal within the group.

These models are clearly only 1-D in the range of finite N, and as such from section 1.4.4, there can be no finite temperature phase transition as low energy domain fluctuations are

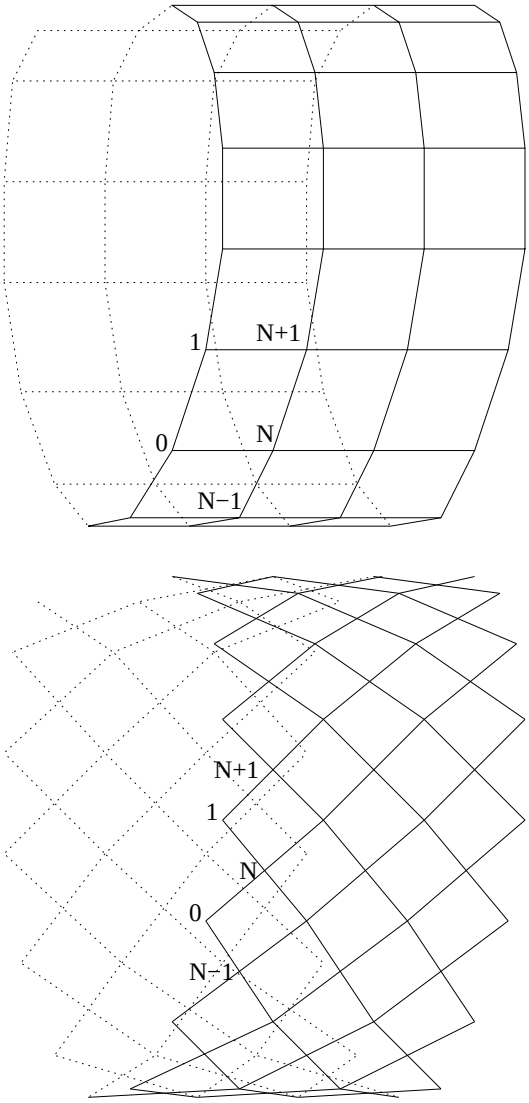

Figure 2.1: The spiral geometry for the $J_1 - J_N$ (ontop) and $J_N - J_{N-1}$ (below) models, taken from [58]

entropically preferable. Indeed, the focus of this investigation is on traits that imply phase transitions in the 2-D limit. The range of N is very much dependent on the number of clock ticks, analytically there is no limit but computationally the matrix to be diagonalised scales as p^N. For Ising spins the largest model that can be computed within a sensible time frame is the $J_1 - J_{26}$ model. For more clock ticks this corresponds to $J_1 - J_{12}$ for $p = 5$; $J_1 - J_{11}$ for $p = 6$; $J_1 - J_{10}$ for $p = 7$; $J_1 - J_9$ for $p = 8, 9$.

It is possible to reduce the matrix by a factor of p by exploiting the global symmetry

of the Hamiltonian $\{\theta\} \to \{\theta + \zeta\}$, where ζ is an arbitrary clock tick. It implies that the absolute angle of each spin is irrelevant, only the angle between neighbouring spins affects the thermodynamics. Mathematically this corresponds to a change of basis: $\phi_i = \theta_{i+1} - \theta_i$, which transforms the Hamiltonian from the fixed basis of θ to the floating basis of ϕ which have the same properties as θ

$$\mathcal{H} = -\sum_i \cos(\phi_i) + \cos(\phi_i + \cdots + \phi_{i+N-1}). \tag{2.2.3}$$

This Hamiltonian is thermodynamically equivalent to (2.2.2) but the number of spins is reduced by one, simplifying the calculation. Throughout this section there will only be reference to the fixed basis θ as it is easier conceptually, but all calculations are performed using the floating basis ϕ.

It is useful as a comparison to solve another set of models that correspond to the same limit

$$\begin{aligned}\mathcal{H} &= \sum_i \mathbf{S}_i \cdot \mathbf{S}_{i+N} + \mathbf{S}_i \cdot \mathbf{S}_{i+N+1} \\ &= \sum_i \cos(\theta_{i+N} - \theta_i) + \cos(\theta_{i+N+1} - \theta_i),\end{aligned} \tag{2.2.4}$$

which in the $N \to \infty$ limit is the square lattice geometry but rotated by 45° as seen in figure 2.1. Again as there are only bonds between site i and sites $i \pm N$, $i \pm N - 1$ we denote this the $J_{N-1} - J_N$ model. It costs the same amount of computation time to solve $J_1 - J_N$ models as it does to solve $J_{N-1} - J_N$ but the radius of the spiral is larger for the $J_{N-1} - J_N$ models as its circumference is $N\sqrt{2}$ rather than N.

The Transfer Function and Probabilities

The solution of the partition function works in much the same way as the Ising model, as again the Hamiltonian is purely local and translationally invariant, it is covered briefly here with another example that uses Ising spins, the $J_1 - J_2$ model which shows how the

matrix application works. There are interesting features of this transfer matrix, that include the inner product with which it is Hermitian to and the choice that exists for the local Hamiltonian. These are worth investigating in their own right but are not pursued further in this study.

The partition function of a system with Hamiltonian $\mathcal{H}$ and angles $\{\theta\}$ is

$$z = \sum_{\{\theta\}} e^{-\beta\mathcal{H}(\{\theta\})}, \tag{2.2.5}$$

and much like the Ising model in equation (2.1.3) the spiral clock model can be split up

$$\begin{aligned} f_i\left(\theta_i, \cdots, \theta_{i+N}\right) &= \sum_{\theta_{i-1}} e^{-\beta\mathcal{H}(\theta_{i-1}, \cdots, \theta_{i+N})} f_{i-1}\left(\theta_{i-1}, \cdots, \theta_{i-1+N}\right), \\ f_{i-1}^{\dagger}\left(\theta_{i-1}, \cdots, \theta_{i+N-1}\right) &= \sum_{\theta_{i+N}} e^{-\beta\mathcal{H}(\theta_{i-1}, \cdots, \theta_{i+N})} f_i^{\dagger}\left(\theta_i, \cdots, \theta_{i+N}\right), \end{aligned} \tag{2.2.6}$$

where

$$\begin{aligned} \mathcal{H}\left(\theta_{i-1}, \cdots, \theta_{i+N}\right) = &- \cos\left(\theta_{i+N} - \theta_i\right) \\ &- \frac{1}{2}\left[\cos\left(\theta_{i+1} - \theta_i\right) + \cos\left(\theta_{i+N} - \theta_{i+N-1}\right)\right] + 2, \end{aligned} \tag{2.2.7}$$

and $f_1 = 1$. The constant is introduced so that the lowest energy state is zero, which simplifies forthcoming calculations with the partition function. Once the thermodynamic limit is taken, where the spiral becomes infinitely long the partition function becomes the largest eigenvalue of the transfer matrix, which can be found computationally and exactly as a function of β:

$$\begin{aligned} z f\left(\theta_i, \cdots, \theta_{i+N}\right) &= \sum_{\theta_{i-1}} e^{-\beta\mathcal{H}(\theta_{i-1}, \cdots, \theta_{i+N})} f\left(\theta_{i-1}, \cdots, \theta_{i-1+N}\right) \\ z f^{\dagger}\left(\theta_{i-1}, \cdots, \theta_{i+N-1}\right) &= \sum_{\theta_{i+N}} e^{-\beta\mathcal{H}(\theta_{i-1}, \cdots, \theta_{i+N})} f^{\dagger}\left(\theta_i, \cdots, \theta_{i+N}\right), \end{aligned} \tag{2.2.8}$$

where f and $f^\dagger$ are the right and left eigenvectors of the transfer function respectively. The same technique used for the Ising model is just as applicable here as the Hamiltonian in (2.2.2) contains purely local interactions which are translationally invariant.

This at the moment is abstract formulation and it is best understood through example, the best example for this is the $J_1 - J_2$ Ising model.

$$\mathcal{H} = -\sum_{\sigma_i} \sigma_i \sigma_{i+1} + \sigma_i \sigma_{i+2}, \tag{2.2.9}$$

which amounts to solving

$$z f(\sigma_2, \sigma_3) = \sum_{\sigma_1} e^{\beta \mathcal{H}(\sigma_1, \sigma_2, \sigma_3)} f(\sigma_1, \sigma_2), \tag{2.2.10}$$

where $\mathcal{H}(\sigma_1, \sigma_2, \sigma_3) = -\frac{1}{2}(\sigma_1\sigma_2 + \sigma_2\sigma_3) - \sigma_1\sigma_3 + 2$, and in matrix format:

$$\begin{pmatrix} 1 & e^{-3\beta} & 0 & 0 \\ 0 & 0 & e^{-2\beta} & e^{-3\beta} \\ e^{-3\beta} & e^{-2\beta} & 0 & 0 \\ 0 & 0 & e^{-3\beta} & 1 \end{pmatrix} \overbrace{\begin{pmatrix} f(\uparrow,\uparrow) \\ f(\downarrow,\uparrow) \\ f(\uparrow,\downarrow) \\ f(\downarrow,\downarrow) \end{pmatrix}}^{f(\sigma_1,\sigma_2)} = z \overbrace{\begin{pmatrix} f(\uparrow,\uparrow) \\ f(\downarrow,\uparrow) \\ f(\uparrow,\downarrow) \\ f(\downarrow,\downarrow) \end{pmatrix}}^{f(\sigma_2,\sigma_3)}. \tag{2.2.11}$$

The first thing to notice is that the transfer matrix is not Hermitian under the standard overlap

$$(f, g) = \sum_{\sigma_1, \sigma_2} f(\sigma_1, \sigma_2)\, g(\sigma_1, \sigma_2), \tag{2.2.12}$$

implying that the eigenvectors need not be orthogonal. It is however, Hermitian with respect to the overlap

$$(f, g) = \sum_{\sigma_1, \sigma_2} f(\sigma_1, \sigma_2)\, g(\sigma_2, \sigma_1), \tag{2.2.13}$$

as long as the transfer matrix respects the symmetry $(\sigma_1, \sigma_2, \sigma_3) \to (\sigma_3, \sigma_2, \sigma_1)$. This extends to models for any N, the transfer matrix is Hermitian with respect to the overlap

$$(f, g) = \sum_{\{\theta\}} f\left(\theta_i, \cdots, \theta_{i+N}\right) g\left(\theta_{i+N}, \cdots, \theta_i\right), \tag{2.2.14}$$

if it respects the symmetry $\{\theta_i, \cdots, \theta_{i+N}\} \to \{\theta_{i+N}, \cdots \theta_i\}$.

This indeed implies the relationship between the right and left eigenvectors of the transfer matrix f and $f^\dagger$ that

$$f^\dagger\left(\theta_i, \cdots, \theta_{i+N}\right) = f\left(\theta_{i+N}, \cdots, \theta_i\right), \tag{2.2.15}$$

implying that the probability of any spin configuration $\left(\tilde{\theta}_i, \cdots, \tilde{\theta}_{i+N}\right)$ is

$$P\left(\tilde{\theta}_i, \cdots, \tilde{\theta}_{i+N}\right) = f\left(\tilde{\theta}_{i+N}, \cdots, \tilde{\theta}_i\right) f\left(\tilde{\theta}_i, \cdots, \tilde{\theta}_{i+N}\right), \tag{2.2.16}$$

and for spins that are further than N apart

$$P\left(\tilde{\theta}_i, \cdots, \tilde{\theta}_{i+N+m}\right) = f\left(\tilde{\theta}_{i+N+m}, \cdots, \tilde{\theta}_{i+m}\right) T_{i+m-1} \cdots T_i f\left(\tilde{\theta}_i, \cdots, \tilde{\theta}_{i+N}\right), \tag{2.2.17}$$

where $T_i = e^{-\beta \mathcal{H}\left(\tilde{\theta}_i, \cdots, \tilde{\theta}_{i+N+1}\right)}$, using the previous definition for $\mathcal{H}\left(\theta_i, \cdots, \theta_{i+N}\right)$ from (2.2.7).

These probabilities are used to probe the behaviour of the state, which is investigated using conditional probabilities; given that a spin is pointing in a certain direction, the probabilities of a spin halfway around the spiral pointing along different clock ticks are found.

Fourier spin space is also used to probe the behaviour of the state and the following is also calculated:

$$\tilde{f}\left(k_i, \cdots, k_{i+N-1}\right) = \frac{1}{\sqrt{p^N}} \sum_{\{\theta\}} e^{i\left(k_i \theta_i + \cdots + k_{i+N-1} \theta_{i+N-1}\right)} f\left(\theta_i, \cdots, \theta_{i+N-1}\right). \tag{2.2.18}$$

As this is a unitary transformation the overlap is preserved

$$\sum_{\{\theta\}} f\left(\theta_i, \cdots, \theta_{i+N-1}\right) g\left(\theta_{i+N-1}, \cdots, \theta_i\right) = \sum_{\{k\}} \tilde{f}\left(k_i, \cdots, k_{i+N-1}\right) \tilde{g}\left(k_{i+N-1}, \cdots, k_i\right). \quad (2.2.19)$$

Discussion Points on the Transfer Function

The transfer function approach developed here is a version with higher complexity of the Ising model developed previously. The principal is much the same but the matrices are much larger and Hermitian with respect to an unusual overlap.

It should be noted that the local Hamiltonian introduced in (2.2.7) is used because it is invariant under the transformation $(\theta_i, \cdots, \theta_{i+N}) \rightarrow (\theta_{i+N}, \cdots, \theta_i)$. This symmetry is not unique to this local Hamiltonian, there are other ways to split the Hamiltonian into local parts. Another example is:

$$\begin{aligned} \mathcal{H}\left(\theta_i, \cdots, \theta_{i+N+1}\right) = &- \frac{1}{N}\left[\cos\left(\theta_{i+1} - \theta_i\right) + \cdots + \cos\left(\theta_{i+N+1} - \theta_{i+N}\right)\right] \\ &- \cos\left(\theta_{i+N+1} - \theta_i\right). \end{aligned} \quad (2.2.20)$$

This yields a different transfer matrix, but must provide the same partition function as the choice of the local Hamiltonian cannot affect the thermodynamics. This amounts to a gauge symmetry and understanding the most natural gauge for this transfer function is beyond the scope of this investigation but worth studying in its own right.

Another valid discussion point centres on the difference between 1-D and 2-D quantities. The crossover between 1-D and 2-D requires that any quantity calculated on this spiral geometry to be relevant must have a meaningful analogue in 2-D. This is the focus of the next section in the discussion of the correlation length.

The Correlation length

The basis of calculating the correlation length was introduced in section 2.1.2 in the form of the Ising chain and with the clock model on the spiral geometry the concept is identical but with some complexities: It is the highest eigenvalue associated with a different symmetry subspace of eigenvectors of the transfer matrix to that of the partition function. Once introduced the complexities are discussed and a simple example is given to show that they are indeed of a different symmetry subspace. The correlation length that is calculated is strictly a 1-D observable and has no meaningful representation in 2-D and so some space is dedicated to finding an observable that does correspond to the 2-D correlation length once the limit $N \to \infty$ is taken.

The correlation function that is the extension to the function introduced in (2.1.16) is

$$\begin{aligned} \langle \mathbf{S}_0 \cdot \mathbf{S}_i \rangle =& \langle \cos\left(\theta_i - \theta_0\right) \rangle \\ =& \Re \langle e^{i(\theta_i - \theta_0)} \rangle. \end{aligned} \tag{2.2.21}$$

This can be split up in operator form

$$\langle e^{i(\theta_i - \theta_0)} \rangle = \frac{\mathbf{f}^\dagger \cdot \tilde{\mathbf{T}}^\dagger \cdot \mathbf{T} \cdots \mathbf{T} \cdot \tilde{\mathbf{T}} \cdot \mathbf{f}}{z^m}, \tag{2.2.22}$$

where $\tilde{\mathbf{T}} \cdot \mathbf{f} = \sum_{\theta_i} e^{i\theta_i - \beta \mathcal{H}(\theta_i, \cdots, \theta_{i+N})} f\left(\theta_i, \cdots, \theta_{i+N-1}\right)$.

The Hamiltonian and thus the transfer matrix once again respects the symmetry $\{\sigma\} \to \{-\sigma\}$ and the eigenvector of the partition function is again in the subspace of eigenvectors of the transfer matrix that is symmetric under the transformation. The operator $\tilde{\mathbf{T}}$ does not respect this symmetry and so projects the eigenvector onto a different subspace, one which has a zero overlap with the initial subspace. The eigenvalue associated with the correlation function is the highest eigenvalue within the second subspace. With the complications of an unusual overlap and a larger subspace, this is best illustrated via example. The simplest

example to use is the $J_1 - J_2$ Ising model introduced in (2.2.9), where the matrix $\tilde{\mathbf{T}}$ is

$$\tilde{\mathbf{T}} = \begin{pmatrix} 1 & -e^{-3\beta} & 0 & 0 \\ 0 & 0 & e^{-2\beta} & -e^{-3\beta} \\ e^{-3\beta} & -e^{-2\beta} & 0 & 0 \\ 0 & 0 & e^{-3\beta} & -1 \end{pmatrix}, \tag{2.2.23}$$

and the Hamiltonian is invariant under the symmetry transformation

$$\tilde{\mathbf{U}} = \begin{pmatrix} 0 & 0 & 0 & 1 \\ 0 & 0 & 1 & 0 \\ 0 & 1 & 0 & 0 \\ 1 & 0 & 0 & 0 \end{pmatrix}, \tag{2.2.24}$$

which amounts to $\{\sigma\} \to \{-\sigma\}$. It has two subspaces of the same size with eigenvalues ± 1. The eigenvector of $\tilde{\mathbf{T}}$ $f(\sigma_1, \sigma_2)$ has an overlap only with the subspace associated with the eigenvalue 1 and so must be of the form (a, b, b, a). The transfer matrix $\tilde{\mathbf{T}}$ projects the eigenvector onto the -1 subspace

$$\tilde{\mathbf{T}} \cdot \mathbf{f} = \begin{pmatrix} a - e^{-3\beta} b \\ e^{-2\beta} b - e^{-3\beta} a \\ e^{-3\beta} a - e^{-2\beta} b \\ e^{-3\beta} b - a \end{pmatrix}, \tag{2.2.25}$$

which is antisymmetric and thus has no overlap with the eigenvector $f(\sigma_i, \sigma_{i+1})$ and so the correlation length is the highest eigenvalue of the partition function that is within the antisymmetric subspace, exactly the same principle as the Ising chain, despite the fact that it is a system with higher complexity. The same principle extends to the clock model but there are more eigenvalues associated with the symmetry transformation $\{\theta\} \to \{-\theta\}$.

There exists a more natural representation for the correlation length in the form of its

representation in Fourier space. The transfer matrix in Fourier space is

$$T^{k_i,\cdots,k_{i+N-1}}_{k'_{i+1},\cdots,k'_{i+N}} = \frac{1}{p^{N-1}} \sum_{\theta_i,\cdots,\theta_{i+N}} e^{-i\left(k'_N\theta_{i+N}+\cdots+k'_{i+1}\theta_{i+1}\right)} T_{\theta_i,\cdots,\theta_{i+N}} e^{i(k_i\theta_i+\cdots+k_{i+N-1}\theta_{i+N-1})}, \quad (2.2.26)$$

where $T_{\{\theta\}} = e^{-\beta\mathcal{H}(\{\theta\})}$. The transfer matrix associated with the correlation function

$$\begin{aligned}\tilde{T}^{k_i,\cdots,k_{i+N-1}}_{k'_{i+1},\cdots,k'_{i+N}} =& \sum_{\theta_i,\cdots,\theta_{i+N}} e^{i\theta_i} e^{-i\left(k'_N\theta_{i+N}+\cdots+k'_{i+1}\theta_{i+1}\right)} T_{\theta_i,\cdots,\theta_{i+N}} e^{i(k_i\theta_i+\cdots+k_{i+N-1}\theta_{i+N-1})} \\ =& T^{k_i+1,\cdots,k_{i+N-1}}_{k'_{i+1},\cdots,k'_{i+N}}.\end{aligned} \quad (2.2.27)$$

The correlation length calculated here describes the long range decay of the correlation function $\langle \mathbf{S}_0 \cdot \mathbf{S}_i \rangle$. It does not consider the site $i+N$ to be nearest neighbours to site i, and as such describes the decay of correlations along a 1-D chain. It provides no use in the large N limit, instead the correlation length must describe the decay of correlations radially outwards from an arbitrary spin in this limit.

A more meaningful correlation length is one associated with the correlation function $\langle \mathbf{S}_0 \cdot \mathbf{S}_{Nm} \rangle$ which does treat the sites i and $i+N$ as nearest neighbours. This describes the decay of correlations in the direction of sites i, $i+mN$. In the limit $N \to \infty$ this direction is radially outwards from the initial spin and so this becomes the 2-D correlation length.

The 1-D correlation function calculated above has an oscillatory nature at short range where the correlations are affected by the relative position of spins around the spiral. At larger distances the amplitude of oscillations decrease as the relative positions have less of an effect, and at long range, $i \to \infty$, the amplitude of the oscillations tend to zero. At this range the decay in correlations are a result of only the lateral movement away from the initial spin, which is the decay that is associated with the 1-D correlation length. The relationship between the correlation length associated with $\langle \mathbf{S}_0 \cdot \mathbf{S}_i \rangle$ and $\langle \mathbf{S}_0 \cdot \mathbf{S}_{Ni} \rangle$ is

$$\zeta_{\text{2-D}} = \frac{\zeta_{\text{1-D}}}{N}, \tag{2.2.28}$$

there is periodicity in only one direction and if this periodicity does not affect the correlations, then the system is indistinguishable to one that is infinite in both directions. There is therefore a criterion for when the system is exhibiting 2-D behaviour: $\langle \mathbf{S}_0 \cdot \mathbf{S}_i \rangle = \langle \mathbf{S}_0 \cdot \mathbf{S}_{Ni} \rangle$ for $i < \frac{N}{2}$. This criterion is expected to be met at high temperature where the system is disordered.

Final remarks

This section has seen the introduction of the transfer function technique on the spiral geometry of the clock model. It was developed with reference to the transfer matrix approach to the 1-D Ising chain and it can be seen that it is indeed an extension of this approach; all the important thermodynamics are eigenvalues of a transfer matrix that arises from the locality of interactions in the Hamiltonian and their translational invariance.

There are some hidden complexities within this extension, each of which are worth separate investigations that go further than the current study. There exists an unusual overlap that provides an Hermitian transfer matrix and a gauge invariance in the choice of local Hamiltonian.

The spiral geometry introduced here is used as it provides easier calculations and allows larger values of N. It is spiral as there is only one site per unit cell, the transfer matrix moves along one spin at a time rather than a cylindrical geometry which transfers N sites at a time.

The technique that has been developed corresponds to the clock model only where the partition function is reduced to an eigenvalue problem. The plane rotator model, where the spins are isotropic can be reduced similarly but with some extra complexity. This will not be explored here, rather complementary work developed by *Robson et al* [58] is referenced where the partition function is presented in full. It is simply noted here that the plane rotator

model requires the equivalent analysis on an integral rather than a discrete summation

$$z f\left(\phi_{i+1}, \cdots \phi_{i+N}\right) = \frac{1}{2\pi} \int_0^{2\pi} \mathrm{d}\phi \; e^{-\beta \mathcal{H}_{i,i+N}} f\left(\phi_i, \cdots, \phi_{i+N-1}\right). \tag{2.2.29}$$

The next discussion in this section on the partition function and the transfer function approach is focused on the application of the of the partition function in providing derivatives of the free energy. Recognising results that originate in the perturbation theory normally seen in quantum mechanics it is possible to calculate the first derivative of the free energy exactly, which provides a higher accuracy for higher numerical derivatives.

Thus far there has been discussion about the eigenvalues of the transfer matrix that provide the main thermodynamics of the system, but it is possible for them to indicate points of criticality within the system. This is to be the final part of the discussion prior to introducing the results which extends the Fisher Zero approach to phase transitions.

2.3 Exact First Derivatives

The observables that are useful for this investigation are those that are known to provide clear behaviour around critical points. These tend to be first or second derivatives of the free energy with respect to some parameter, for example the energy and specific heat:

$$\text{Energy: } E = -\frac{\partial \log\left(z\right)}{\partial \beta};$$
$$\text{Specific Heat: } \frac{C}{k_B} = -\beta^2 \frac{\partial^2 \log\left(z\right)}{\partial \beta^2}.$$

These derivatives can be found numerically, but it shall be seen that from well known analytic results of perturbation theory that the first derivative can be found exactly. First the process of calculating the numerical derivative is showed.

The Taylor's expansion for a function $f(x)$

$$f(x^* + h) = f(x^*) + h\frac{\partial f}{\partial x}\bigg|_{x=x^*} + \frac{h^2}{2!}\frac{\partial^2 f}{\partial x^2}\bigg|_{x=x^*} + \cdots, \tag{2.3.1}$$

and in matrix format for even derivatives:

$$\frac{1}{2}\begin{pmatrix} f(x^*+h) + f(x^*-h) - 2f(x^*) \\ f(x^*+2h) + f(x^*-2h) - 2f(x^*) \\ f(x^*+3h) + f(x^*-3h) - 2f(x^*) \\ \vdots \end{pmatrix} = \begin{pmatrix} \frac{1}{2!} & \frac{1}{4!} & \frac{1}{6!} & \cdots \\ \frac{2^2}{2!} & \frac{2^4}{4!} & \frac{2^6}{6!} & \cdots \\ \frac{3^2}{2!} & \frac{3^4}{4!} & \frac{3^6}{6!} & \cdots \\ \vdots & \vdots & \vdots & \ddots \end{pmatrix} \begin{pmatrix} h^2\frac{\partial^2 f}{\partial x^2} \\ h^4\frac{\partial^4 f}{\partial x^4} \\ h^6\frac{\partial^6 f}{\partial x^6} \\ \vdots \end{pmatrix},$$

and for odd:

$$\frac{1}{2}\begin{pmatrix} f(x^*+h) - f(x^*-h) \\ f(x^*+2h) - f(x^*-2h) \\ f(x^*+3h) - f(x^*-3h) \\ \vdots \end{pmatrix} = \begin{pmatrix} 1 & \frac{1}{3!} & \frac{1}{5!} & \cdots \\ 2 & \frac{2^3}{3!} & \frac{2^5}{5!} & \cdots \\ 3 & \frac{3^3}{3!} & \frac{3^5}{5!} & \cdots \\ \vdots & \vdots & \vdots & \ddots \end{pmatrix} \begin{pmatrix} h\frac{\partial f}{\partial x} \\ h^3\frac{\partial^3 f}{\partial x^3} \\ h^5\frac{\partial^5 f}{\partial x^5} \\ \vdots \end{pmatrix},$$

which is terminated depending on the accuracy required. The standard in this investigation is eight points around $f(x^*)$ so that the first two derivatives are known to $O(h^6)$. In this case $h = 0.01$ so the derivatives are known to an accuracy of 10^{-12}

Now consider a perturbation in the transfer matrix with respect to some parameter p

$$T(p + \delta p) = T(p) + \delta p\frac{\partial T}{\partial p} + \frac{(\delta p)^2}{2}\frac{\partial^2 T}{\partial p^2} + \ldots, \tag{2.3.2}$$

where its eigenvalues are equally perturbed

$$z(p + \delta p) = z(p) + \delta p\frac{\partial z}{\partial p} + \frac{(\delta p)^2}{2}\frac{\partial^2 z}{\partial p^2} + \ldots. \tag{2.3.3}$$

From non-degenerate perturbation theory the eigenvalue must behave as

$$\begin{aligned} z\left(p+\delta p\right) =& z\left(p\right)+\delta p\langle 0|\frac{\partial T}{\partial p}|0\rangle+\frac{\left(\delta p\right)^{2}}{2}\sum_{n\neq 0}\frac{\langle 0|\frac{\partial T}{\partial p}|n\rangle\langle n|\frac{\partial T}{\partial p}|0\rangle}{z_{n}-z_{0}} \\ &+\frac{\left(\delta p\right)^{2}}{2}\langle 0|\frac{\partial^{2}T}{\partial p^{2}}|0\rangle+\ldots, \end{aligned} \tag{2.3.4}$$

where $|n\rangle$ is the eigenvector associated with eigenvalue $z_n\left(p\right)$ From this result

$$\begin{aligned} \frac{\partial z}{\partial p} =& \langle 0|\frac{\partial T}{\partial p}|0\rangle \\ =& f^{\dagger}\frac{\partial T}{\partial p}f, \end{aligned} \tag{2.3.5}$$

which is a simple overlap, therefore the first derivative of the free energy with respect to any parameter is accessible. In the case of $p=\beta$

$$\frac{\partial T}{\partial \beta}=-\mathcal{H}e^{-\beta\mathcal{H}}, \tag{2.3.6}$$

which provides the energy exactly. The first numerical derivative of this quantity provides the second derivative of the free energy which can be found to $O\left(10^{-14}\right)$

2.4 Fisher Zeros and Criticality

This section discusses the use of the eigenvalue structure of the transfer matrix in not only determining the main thermodynamics of the system but also providing information on the points of criticality and the existence of phase transitions. This method is built on the method developed by Fisher and provides the backdrop of this section [52], [53].

Fisher's method treats the temperature as a complex variable and finds the zeros of the partition function within the complex plane; a phase transition is characterised as a zero on the real line. The partition function is solved numerically in finite 0-D systems, and via finite size scaling one attempts to find the position of the zeros in the 2-D limit. This

technique is appropriate for only 0-D to 2-D; In the spiral technique used here the position of the zeros in the complex plane are not dependent on the size of the spiral.

In this section an extension to Fisher Zeros is developed which is appropriate for the 1-D to 2-D crossover. It amounts to associating phase transitions not with zeros of the partition function but with degeneracy of eigenvalues within the transfer function. This is a novel technique and it is used to illustrate the different states explored when a spin spiral is introduced into the system. Here there will be a review of Fisher Zeros with a very simple partition function example, then the extension is introduced but the context in terms of spin spirals will be covered in the results section of this investigation.

2.4.1 A Toy Partition Function

The methodology of Fisher zeros can be quite mathematically taxing, so this outline will be as brief and comprehensible as possible. The partition function of even the simplest models with a phase transition is complex, so a toy partition function is provided which in the infinite limit has a first order phase transition, though it will have no real physical bearing. Once introduced it will be seen that it is not applicable to the spiral technique and in the following section the extension is produced.

The outline given here follows closely with the argument given by M.E Fisher in (reference lectures on theoretical physics Volume VII C). First it should be recognised that any finite partition function is a function solely of $z = \exp(-\beta)$, and can be expressed as a polynomial of z. This polynomial is characterised by its roots.

$$\mathcal{Z}(z) = \prod_i (z - z_i), \tag{2.4.1}$$

where z_i are the roots. The partition function of a finite system is smooth and positive definite for all real β, so any roots must be complex. The quantity that has physical

significance is the free energy, proportional to $\log \mathcal{Z}$

$$\log\left(\mathcal{Z}\right) = \sum_i \log\left(z - z_i\right). \tag{2.4.2}$$

A phase transition is defined as any non analytic point of the free energy for any positive and real beta. Here we confirm a well known result, a finite system can not undergo a phase transition as the roots of the partition function are complex; phase transitions can only exist in the thermodynamic limit.

To illustrate critical points in the thermodynamic limit and the process of Fisher Zeros we introduce here a toy partition function. Investigations into Fisher Zeros in the literature tend to be numerical in type and use finite size scaling to predict the infinite limit. Consider the partition function of a system with N particles

$$\mathcal{Z} = 2e^{NK(\beta)} \cosh\left[\frac{1}{2} N\epsilon\left(\beta - \beta_c\right)\right], \tag{2.4.3}$$

which has zeros at

$$\beta_j = \beta_c \pm \left(2j+1\right)\pi \frac{i}{N\epsilon}, \tag{2.4.4}$$

and so the free energy

$$-\beta F = K\left(\beta\right) + \frac{1}{N}\sum_j \log\left(\epsilon\beta - \epsilon\beta_j - \frac{\left(2j+1\right)\pi i}{N}\right), \tag{2.4.5}$$

and in the thermodynamic limit $N \to \infty$ this becomes the integral

$$-\beta F = \frac{1}{2\pi}\int_{-\infty}^{\infty} \log\left[\epsilon\left(\beta - \beta_c\right) + i\theta\right] \mathrm{d}\theta, \tag{2.4.6}$$

and the energy is

$$U\left(\beta\right) = -K'\left(\beta\right) + \frac{1}{2\pi i}\int_{-\infty}^{\infty} \frac{\epsilon}{\theta - i\epsilon\left(\beta - \beta_c\right)}, \tag{2.4.7}$$

where the contribution from the integral changes by ϵ at $\beta = \beta_c$, clearly a first order phase transition.

Turning to the partition function of the systems that are used, it shall be seen that Fisher Zeros are not applicable; their position in the complex plane are not dependant on the size of the system, and so do not converge to the real line, even though most of the results here will indicate the existence of two transitions. To illustrate this the $J_1 - J_2$ and $J_2 - J_3$ Ising model is to be used which is known to have a transition temperature in the 2-D limit. This amounts to finding the position of the root of the highest eigenvalue of the transfer matrix.

The transfer matrix of the $J_1 - J_2$ Ising model in the floating basis introduced in section 2.2.1 is

$$T = \begin{pmatrix} 1 & x \\ x & x^2 \end{pmatrix}, \tag{2.4.8}$$

where $x = \exp(-\beta)$, which has the characteristic polynomial

$$\epsilon \left[\epsilon - \left(x^2 + 1 \right) \right] = 0, \tag{2.4.9}$$

where the highest eigenvalue is zero in the case that $x^2 + 1 = 0$.

For the $J_2 - J_3$ model the transfer matrix

$$T = \begin{pmatrix} 1 & x^3 & 0 & 0 \\ 0 & 0 & x^4 & x \\ x^3 & x^2 & 0 & 0 \\ 0 & 0 & x & x^2 \end{pmatrix}. \tag{2.4.10}$$

The eigenvalue is zero at $x^4 = 1$, providing poles on the unit circle. This is the case for larger Ising systems, where the Fisher Zeros populate only the unit circle; even though it is known to have a transition, the root of the partition function does not tend to the transition

temperature; an extension is required.

2.4.2 Degeneracy in the Transfer matrix

The extension, much like all the important thermodynamics of the spiral system lies within the eigenvalue structure of the transfer matrix. Here it will be shown that points of criticality imply a degeneracy in the highest eigenvalue of the transfer matrix. The approach used here is only on well behaved transfer matrices as only finite spirals are considered but in the limit that $N \to \infty$ the degeneracy is achieved. The formulation is shown here and its application to the results is discussed in further sections.

Consider the polynomial

$$p\left(z,\beta\right) = \prod_i \left(z - z_i\right), \tag{2.4.11}$$

where z_i are the eigenvalues of a transfer matrix, which depend solely on β. The roots of this polynomial are the places of interest, and the highest root is the partition function. We explore the behaviour of the system at singular points in thermodynamic quantities in the context of this polynomial. Differentiating once provides the energy

$$\begin{aligned} \frac{\mathrm{d}p}{\mathrm{d}\beta} - \frac{\partial p}{\partial \beta} =& p' \frac{\partial z}{\partial \beta} \\ U =& \frac{1}{z}\frac{\partial z}{\partial \beta} \\ =& \frac{1}{p'z}\left[\frac{\mathrm{d}p}{\mathrm{d}\beta} - \frac{\partial p}{\partial \beta}\right], \end{aligned} \tag{2.4.12}$$

which must be evaluated at the highest eigenvalue z_j, which corresponds to $p = 0$.

Differentiating a second time

$$\frac{1}{2}\left[\frac{\mathrm{d}^2 p}{\mathrm{d}\beta^2} - \frac{\partial^2 p}{\partial \beta^2}\right] = p' \frac{\partial^2 z}{\partial \beta^2} + p'' \left(\frac{\partial z}{\partial \beta}\right)^2, \tag{2.4.13}$$

and so the specific heat is

$$\begin{aligned}\frac{C}{\beta^2} =& \frac{\partial U}{\partial \beta} \\ =& -\left(\frac{1}{zp'}\right)^2 \left(\frac{\mathrm{d}p}{\mathrm{d}\beta} - \frac{\partial p}{\partial \beta}\right)^2 \\ &+ \frac{1}{p'z}\left(\frac{1}{2}\left[\frac{\mathrm{d}^2 p}{\mathrm{d}\beta^2} - \frac{\partial^2 p}{\partial \beta^2}\right] - \frac{p''}{(p')^2}\left[\frac{\mathrm{d}p}{\mathrm{d}\beta} - \frac{\partial p}{\partial \beta}\right]\right).\end{aligned} \tag{2.4.14}$$

We see the effect of Fisher Zeros on the specific heat with both $\frac{1}{Z}$ and $\frac{1}{Z^2}$ contributions. We also see that it is singular in the case $p' = 0$, and with the condition that corresponds to $p = 0$, the singular behaviour occurs when $p(z)$ has a multiple root at its highest zero. This degeneracy in the eigenvalue spectrum is a phase transition.

Chapter 3

RESULTS

We have established from the chapter 2 that the spiral geometry and the transfer function approach gives us access to the eigenvalues of the transfer matrix for a model with arbitrary sized radius. These eigenvalues are obtained through repeated application of the transfer matrix to an arbitrary starting vector with the desired symmetry. Thus we can calculate subject to numerical limitations any derivative of the free energy and have access to correlation functions and correlation lengths. This gives us a vast amount of quantities to calculate, and truly the problem is no longer how to calculate but what to calculate.

We wish to gain as much insight as possible into the 2-D limit of the system and this is the criterion to the observables we calculate and present. We require quantities with clear 2-D analogues that are well defined in the $N \to \infty$ limit. From the quantities calculated on our 1-D system we expect them to have echoes of 2-D phenomena and the task at hand is to spot these. We seek mainly the critical phenomena experienced around phase transitions.

There are limitations to the technique that we have developed and this plays a crucial role in the finite size scaling of the results. The computation time for a system with p clock ticks and N system size scales as p^N. This exponential wall is the main limiting factor to calculations. For an Ising $p = 2$ model results can go as far as $N \sim 26$, for $p = 5$, $N \sim 12$ and $p = 9$, $N \sim 9$. Smaller clock ticks may seem an intelligent choice, but the phenomena that we see in our results are better separated at high clock ticks. There is a clear pay off

between higher N and clearer phenomena. We tend to settle on the $p = 7$ model although we do present results for clock ticks $p = 5 \ldots 9$ in the appendices C-E.

Before we discuss the results in detail we must first properly introduce the aims to the section with the context of how the results will meet these aims. This will give us a guide on how the section will be structured and presented. There are other questions that have been answered along the way and we will address them once the main layout is introduced.

Investigations into systems with inaccessible exact thermodynamics tend only to find the broad, qualitative properties. This is normally the case with most 2-D systems and even though we have exact thermodynamics for our 1-D systems we can answer very little about their 2-D limit. We do have some access to the singular behaviour associated with phase transitions, but our evidence for these is convincing rather than proof. Once phase transitions are established we will attempt to classify the different phases and seek out possible critical exponents of the transitions.

Our results must justify the use of these 1-D systems as representatives of the correct 2-D limit. Where we can, we compare our results to well known 2-D behaviour, either via exactly solved 2-D models or seeking 2-D behaviour in our calculated quantities extrapolated to the $N = \infty$ limit. The 2-D Ising model has a well known transition temperature and we are able to compare the $p = 2$ and $p = 4$ models in our spiral system to known 2-D Ising model results; we prefix any clock model $p > 4$ results with comparisons between our Ising model calculations and the known results. Where appropriate we present a polynomial extrapolation of our results, showing the $N = \infty$ limit. We fit results to a Lagrange polynomial in $\frac{1}{N}$, and use the value of the intercept for the quantity at the 2-D limit. This is not expected to exhibit singular behaviour but it is able to emphasise 2-D properties qualitatively. All deductions about the 2-D limit from our calculations rely on this justification and we emphasise this in the way we structure our results.

We show our most crucial results first, those that present the most convincing evidence of the existence of phase transitions and those that show that our clock models do not require

long range effects to describe phase transitions. The correlation length provides both kinds of evidence and also labels one of the transitions with possible critical exponents. The specific heat also shows two phase transitions in the form of diverging anomalies. Once convinced of the existence of phase transitions we present results that investigate the phases between transitions. The conditional probabilities between two spins give us information about the direction the spins are pointing relative to one another; it tells us about the magnetic state of the different phases. The analogue in Fourier spin space is used to emphasise the similarity between the two transitions and show that at low temperature the spins are best described in a real space representation and that at high temperature, the reciprocal space. We suggest order parameters from the helical stiffness, highlighting the difference between the two bonds with respect to this. The difference gives two quantities for the helical stiffness and we use these as two possible order parameters for both transitions. After our main set of results we address other discoveries that provide insight into the systems that we use and more general thermodynamic behaviour.

These interesting phenomena do not directly contribute to the bulk of the results outlined above but are interesting within their own right. We discovered these following reviews of the literature surrounding phase transitions and also complementary work done on the plane rotator spiral system by *Robson et al* [58]. There exists a theory detailed by Fisher that allows determination of phase transitions in the 2-D limit of 0-D systems. This theory treats temperature as a complex variable and tracks the roots of the partition function with increasing system size. A phase transition is found if finite sized scaling suggests the existence of a root on the real line in the 2-D limit. We find a comparable criterion in the 2-D limit of 1-D systems, that degenerate behaviour of the eigenvalues of the partition function indicate phase transitions. This is explored here with respect to increasing the number of spin spirals in the system at a fixed temperature. Comparisons between the results found in this piece and results on the plane rotator suggest a thermodynamic convergence between clock and plane rotator systems above the low temperature transition; we use a high temperature

expansion to quantify the convergence and confirm that the high temperature transition is universal for all $p > 4$ up to $p = \infty$. These phenomena provide plenty of areas of further research once we obtain the basic thermodynamic properties of the system.

It is important to dedicate some space to the way our results are presented. We plot results with increasing N on top of each other to draw attention to trends. The curves start with the $J_1 - J_2$ model and increase up to the appropriate limit. Where appropriate we plot with the polynomial extrapolation to deduce any singular behaviour. The Ising model is consistently used as a check against known results, as outlined above. Most clock model results will use the $p = 7$ model, other results can be found in the appendix, but we find traits which are universal for all clock models.

3.1 Correlation Length

The main validity for using these 1-D systems as representations of the 2-D limit originate from our correlation length results and it is for this reason amongst others that the correlation length is one of the most crucial quantities that we calculate. Our results on finite radii show qualitatively 2-D behaviour giving us reason to believe that there are no infinite range phenomena that directly affect the physics of 2-D systems. We take temperature derivatives and see that these give results that indicate possible universality classes. We present these first due to both the insight it provides and its starkness.

It is established from earlier sections that we have access to the correlation length of the system exactly (2.1.16) and (2.2.22). The quantity that will correspond to the correlation length in the 2-D limit was discussed in section 2.2 where we use equation (2.2.28)

The Ising model will be used as the context of our results. Once we establish a useful correlation length we will find that it provides the correct correlation length for the Ising model in the 2-D limit, both by finding a good estimate for the transition temperature and a correct range for the critical exponent ν. This will then serve as a basis of comparison for

the clock model which we will see show very similar results.

We plot the correlation length first as an indication that we have 2-D behaviour, then we plot its derivatives with respect to temperature to pick out the critical exponents.

3.1.1 Correlation length Results

We plot first the inverse correlation length for the Ising model for increasing N in figure 3.1a. This presents a direct comparison between our method in 1-D to the well known results in 2-D. Our extrapolation presents correct 2-D behaviour as it is finite above the transition and zero below. It is convincing that our results do have 2-D echoes and that there is no long range behaviour key to the physics of the system that we have missed in using our 1-D systems.

We plot the results for the clock model in figure 3.1b and note the similar traits between the clock and the Ising model. The extrapolation in both cases give believable 2-D behaviour, remaining zero below a transition temperature. We recognise a pattern for increasing N in both correlation lengths and predict that any models with higher values of N will have a correlation length that falls within the white space between what is plotted and the extrapolation. This again implies that there are no longer range effects that are key to the transitions.

Note that for both of these systems there is a convergence of the correlation length at high temperature, and that for increasing N the temperature range of convergence is closer to the transition temperature.

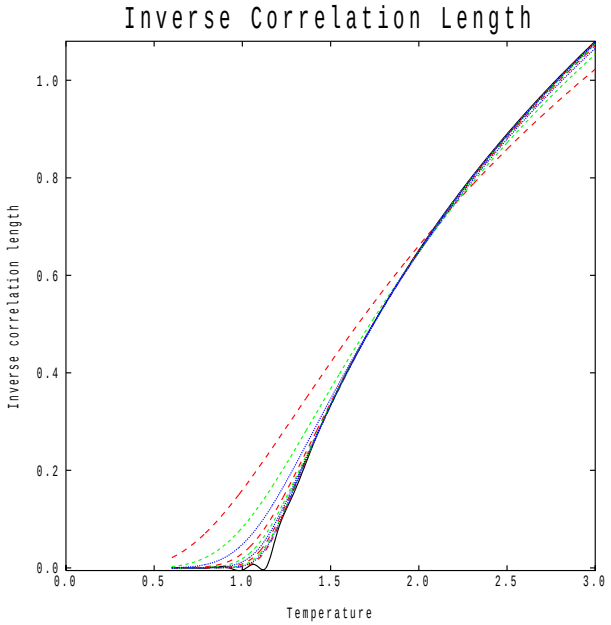

(a)

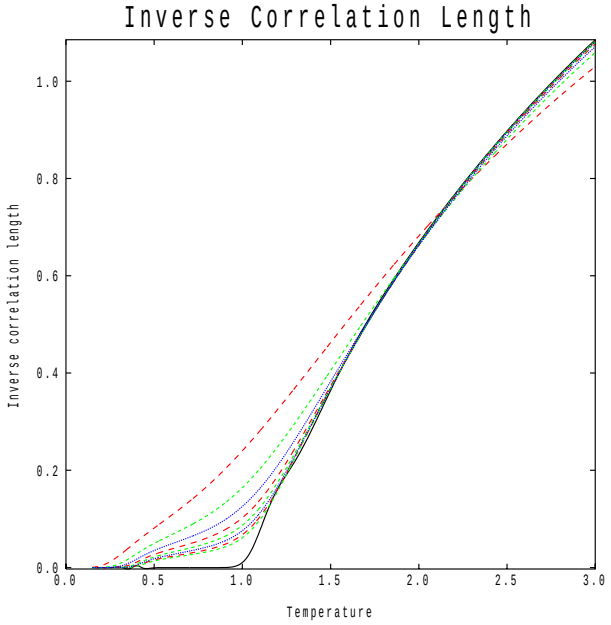

(b)

Figure 3.1: The inverse correlation length for the $p = 4$ (a) and $p = 7$ (b) model. Both are plotted with the extrapolation (black solid line). The low temperature for the $p = 4$ is not shown as at low temperature the difference between eigenvalues is smaller than computational accuracy. As N increases the curves converge and get closer to the extrapolation. The $J_1 - J_2$ models are the high red curve and they go up to $J_1 - J_{11}$ for $p = 4$ and $J_1 - J_9$ for $p = 7$.

3.1.2 Correlation Length Derivatives

We appear to have the correct 2-D behaviour for the clock model and so we turn our attention to the critical exponent of the correlation length. These exponents are key to determining the universality class of the phase transition and describe the behaviour of the system within the vicinity of the critical temperature. The correlation length behaves as:

$$\zeta^{-1} \sim (T - T_c)^{\nu} \, \theta \, (T - T_c) \, , \tag{3.1.1}$$

if the critical exponent lies between n and $n+1$ then in the $(n+1)$th derivative there should be a non zero term at the critical point proportional to

$$(T - T_c)^{\nu-(n+1)} \, \theta \, (T - T_c) \, , \tag{3.1.2}$$

which will show up as a divergence for a general ν at $T = T_c$, and any further derivative will contain a stronger divergence. In the special case where ν is an integer, there will be a derivative which appears as a step function, and thus the next derivative will appear as a delta function. This is the case in the Ising model where $\nu = 1$, and our results show quantities that are diverging in the limit of $N \to \infty$. The derivatives with respect to temperature present a range for the critical exponent ν

We use the Ising model as an example again as the quantity $\nu = 1$ in 2-D. The first derivative is seen in figure 3.2a, and the second in figure 3.2b . We see a curve diverging to a singularity in the second derivative, where we expect a delta function to be and can only assume that this will be a delta function singularity. Again this picks up the correct 2-D behaviour.

We plot the first derivative of the clock model in figure 3.3a,and the second in figure 3.3b. In the second derivative we see a divergence at the transition not unlike the divergence in figure3.2b. This puts the value of the critical exponent between 0 and 1.

A small decreasing anomaly also appears at low temperature, we will see that this occurs

at the same temperature of another transition, but in the infinite limit this should go to zero as the system is ordered at that temperature.

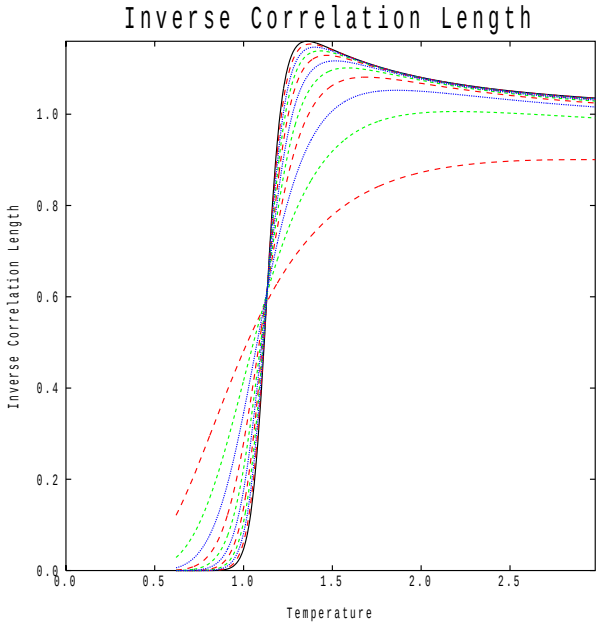

(a)

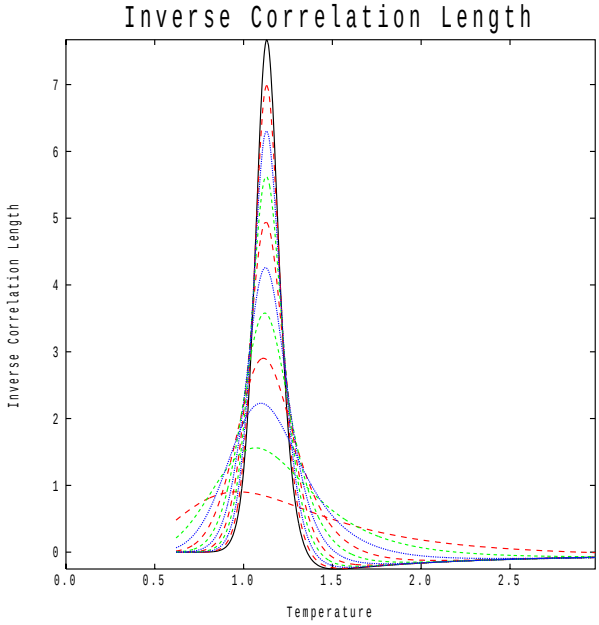

(b)

Figure 3.2: The first two derivatives of the inverse correlation length with respect to temperature of the $p = 4$ model, plotted with the extrapolation (black solid curve). The curves get closer to the extrapolation with increasing N, the red lowest red curve is the $J_1 - J_2$ model and they go up to $J_1 - J_{11}$.

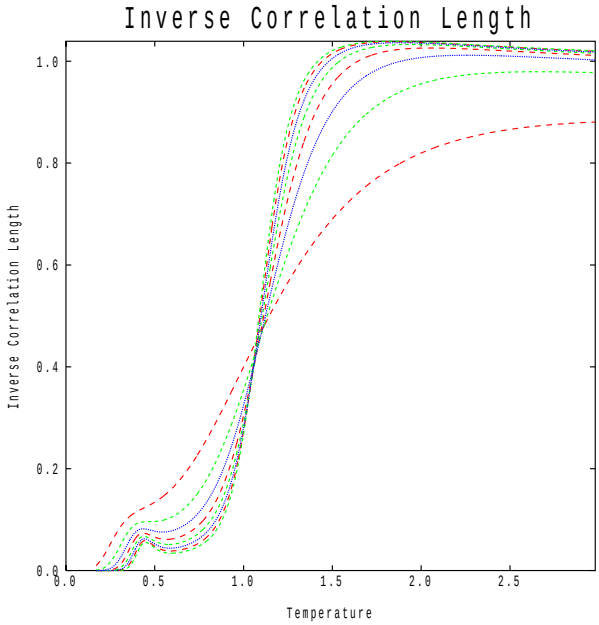

(a)

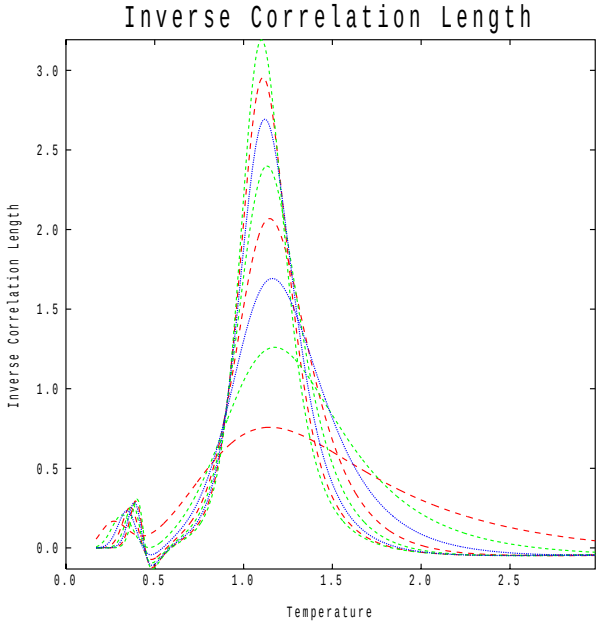

(b)

Figure 3.3: The first two derivatives of the inverse correlation length with respect to temperature for the $p = 7$ model. The curves become convergent with increasing N and the lowest red curve in both graphs is the result for the $J_1 - J_2$ model and they go up to the $J_1 - J_9$ model which is the highest green curve.

3.1.3 Concluding Remarks

Some remarks are required here to emphasize the importance of what we have found from these results. All further results are justified by what is found here; we are able to use this

system to model the 2-D limit.

The correlation length shows that there is no long range interaction that we cannot pick up due to finite N, everything that happens in 2-D that is key to the transition happens to some extent in the smaller system. From the derivatives we find a range for the critical exponent ν.

We will move onto to other well known thermodynamic quantities and see that the anomaly at lower temperature in the correlation length derivatives are seemingly associated with another transition.

3.2 Specific Heat

Anything that exhibits singular behaviour at 2-D should give visible diverging behaviour in our system. We find that the specific heat has two growing peaks with respect to increasing N for clock models with $p > 4$ and its derivatives with respect to temperature show that they are clear divergences. The low temperature transition appears to be associated with the number of clock ticks. We are led to believe from the previous section on correlation length that this is the correct 2-D behaviour.

The partition function established in section 2.2 gives us access to any derivative of the free energy, from these derivatives we wish to determine the number of phase transitions the system exhibits. We look for a quantity that gives unambiguous behaviour in the vicinity of a transition and so we calculate the specific heat as it is singular at critical temperatures. We expect the 2-D behaviour to manifest itself as smooth peaks that diverge with increasing N.

We plot the first three derivatives of the entropy with respect to temperature

$$\left[T\frac{\partial}{\partial T}\right]^n S, \tag{3.2.1}$$

where the case $n = 1$ gives the specific heat. We plot higher derivatives so that the divergence

is emphasised.

The Ising model is used as an example, which is known to have a singularity in the specific heat. We then move onto the $p > 4$ clock model.

3.2.1 Ising Model Results

We plot the results for the Ising model in figure 3.4. A clear peak can be seen at the known transition temperature. It should be seen that though we know that this peak is associated with the singularity in 2-D, it does not appear to diverge with respect to increasing N. Only when we see the derivatives of the specific heat can we be sure that there are divergences. The nature of the logarithmic divergence in the Ising model explains the slow divergence that we see in the specific heat.

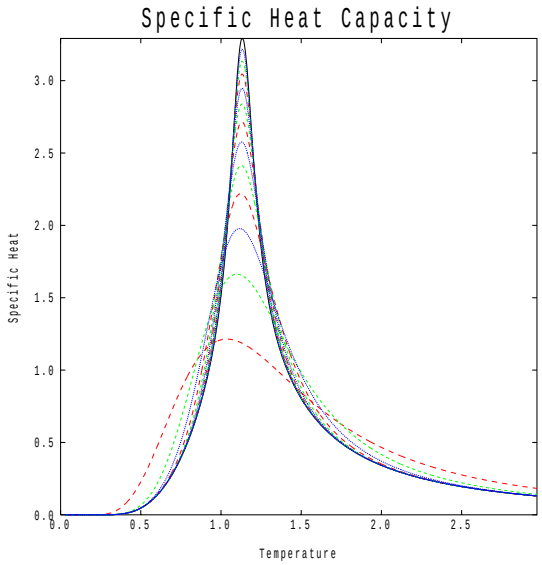

(a) The specific heat of the $p = 4$ model. The lowest red curve is $J_1 - J_2$ and they go up to $J_1 - J_{13}$

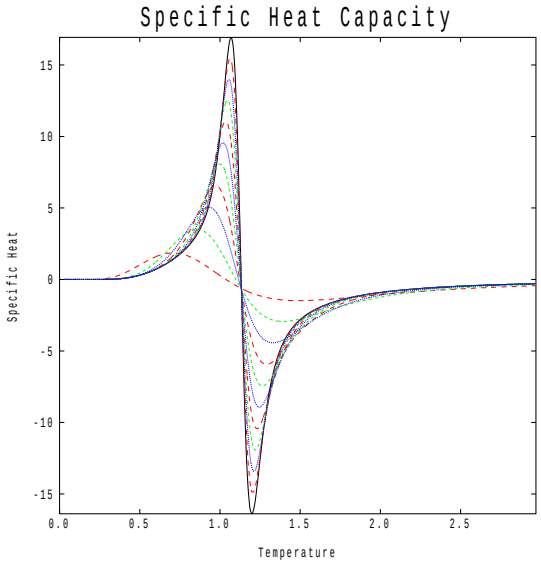

(b) The first derivative with respect to temperature of the specific heat of the $p = 4$ model. The lowest red curve is $J_1 - J_2$ and they go up to $J_1 - J_{11}$

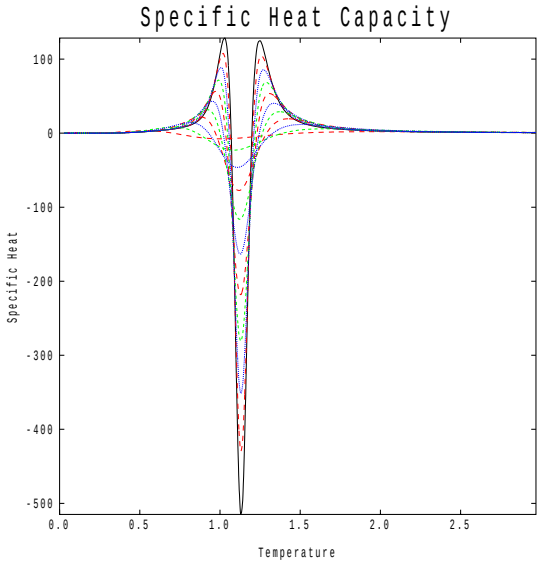

(c) The second derivative with respect to temperature of the specific heat of the $p = 4$ model. The lowest red curve is $J_1 - J_2$ and they go up to $J_1 - J_{11}$.

Figure 3.4: The specific heat and its first two derivatives with respect to temperature with the extrapolation (solid black curve).

3.2.2 Clock Model Results

We plot the clock model specific heat in figure 3.5. We see two peaks that increase in the same fashion to the Ising model peak. The high temperature peak is associated with the critical behaviour in the correlation length, indicating that this peak is indeed a phase transition in the infinite N limit.

Once we plot the derivatives in figures 3.5b and 3.5c , much like the Ising model we can see that the two peaks are diverging into phase transitions. This is the case for all clock models, and we see that the temperature of lower transition decreases with more clock ticks as see in appendix A. This lower transition is clearly associated with the anisotropy of the system, and from the correlation length results must be a transition between two phases that have an infinite correlation length.

We plot also the ratio in the specific heat between the $p = 7$ model and the plane rotator in figure 3.6, where we can see that the high temperature transition exhibited in the clock model is also exhibited in the plane rotator. The two models converge rapidly after the low temperature transition.

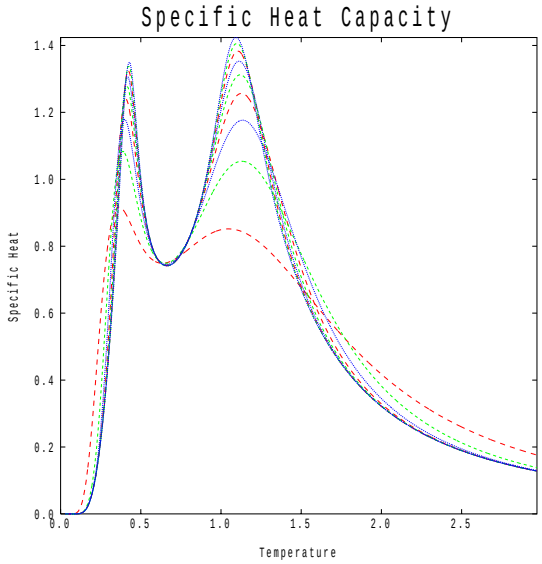

(a) The specific heat of the $p = 7$ model.

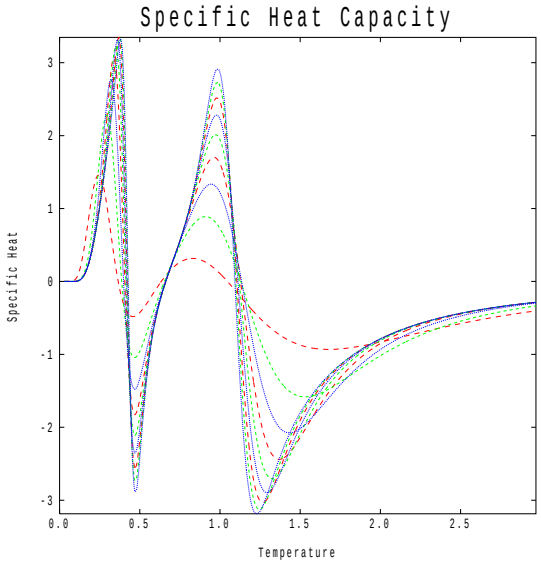

(b) The first derivative of the specific heat with respect to temperature of the $p = 7$ model

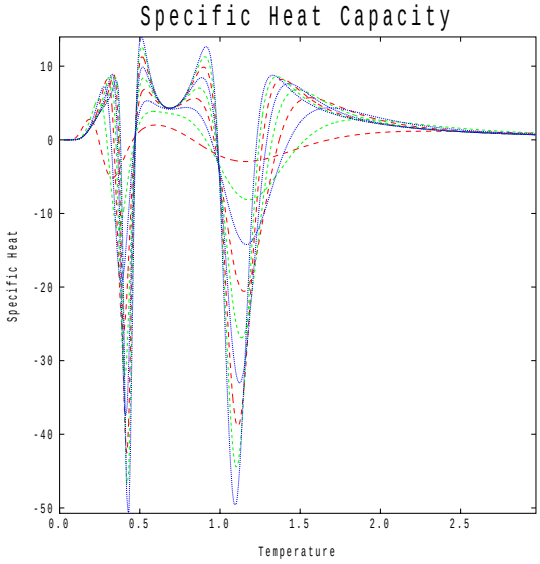

(c) The second derivative of the specific heat with respect to temperature of the $p = 7$ model.

Figure 3.5: The specific heat for the $p = 7$ model with derivatives. The lowest red curve is the $J_1 - J_2$ model and they go up to the $J_1 - J_{10}$ model.

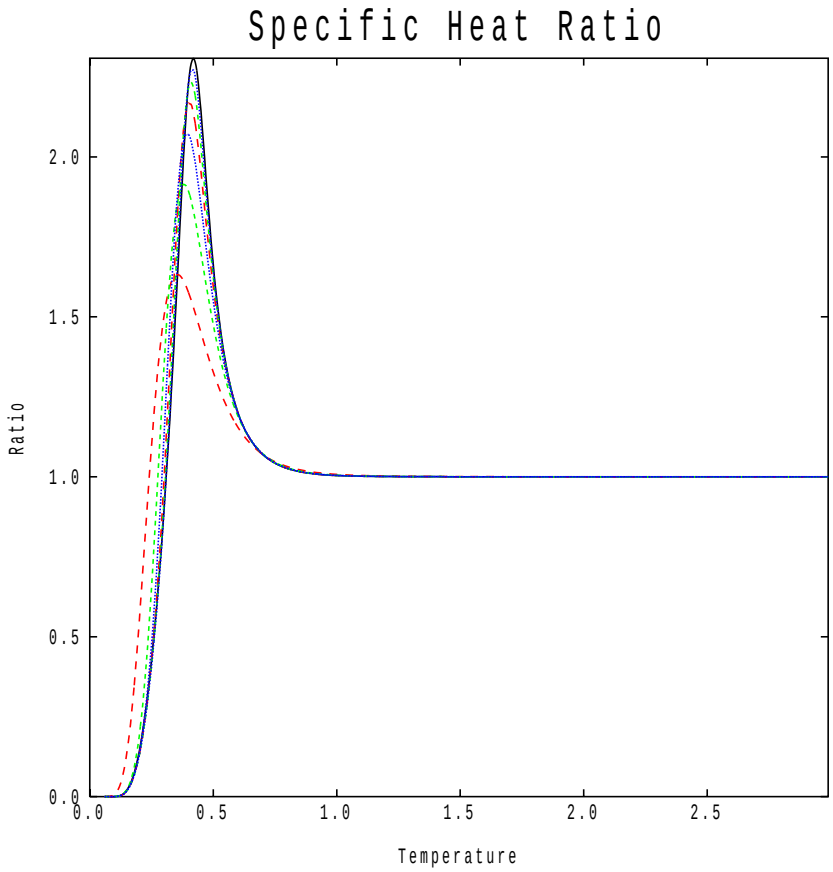

Figure 3.6: The specific heat ratio between the $p = 7$ model and the plane rotator for increasing N with the extrapolation (solid black curve). The lowest red curve is the $J_1 - J_2$ model and the curves go up to $J_1 - J_7$. Plane rotator data has been taken from [58]

3.2.3 Concluding Remarks

The clock model results present two clear transitions. Both anomalies behave much like the Ising model anomaly in our system; they only clearly diverge in the first and second derivatives with respect to temperature. It is also clear that the high temperature result is associated with the critical behaviour of the correlation length, indicating that the low temperature transition is between two phases of different types of order. Results with different clock ticks show that where the low temperature transition is associated with the anisotropy, the high temperature transition is not; it is the same transition in the plane rotator implying that the clock model can be used to probe this system above the lower transition. We will characterise these phases in further sections.

3.3 Conditional Probabilities

The previous sections have focused on determining the existence of phase transitions within the system, we will now turn the focus on characterising the three phases. We find the probabilities of different relative orientations between two sites in both real space and Fourier space. The region of most interest is between the two transitions as it poses quite novel behaviour and the real space and Fourier space result show that the two transitions are complementary. Further sections on the similarities between the clock model and plane rotator will present some insight into this phase, but more investigation is warranted.

We can gain an understanding of the state from the eigenvector of the highest eigenvalue of the transfer matrix by calculating the probability of the relative spin orientations between two sites. In this section we plot the probability of two spins to be $0, 1, 2 \cdots$ clock ticks away from each other with respect to temperature at a fixed N and plot the probabilities of two spins at increasing distance apart. Discussions from the previous section on the correlation length included emphasis on the effect of boundary conditions on correlation functions; at temperatures above the high temperature transition, the correlation length is of the order of the periodicity and the system is not in the 2-D limit in the regions of most interest. Nevertheless we will gain insight into the different phases that occur.

To put the orientational probabilities in context we show that the correlation function between two spins can be split up into these probabilities:

$$\langle \mathbf{S}_0 \cdot \mathbf{S}_i \rangle = \sum_{n,m} P_{0,i}\left(n, m\right) \cos\left(\frac{2\pi\left(n-m\right)}{p}\right). \tag{3.3.1}$$

We look specifically at the critical temperatures highlighted by the specific heat to spot any universal difference in behaviour for all clock ticks. As there is no transition in 1-D it is hard to pick out any sharp behaviour, especially at the high temperature transition which has a broad specific heat peak so that the entropy is spread over a large temperature region. The phase between transitions poses the greater challenge to understanding, both high and low

temperatures are easy to classify as a disordered and long range ordered phase respectively. We look to compare the transitions by performing the same calculations in Fourier spin space, using equation (2.2.18).

The results we show in Fourier space are much like the real spin space representations, we plot with respect to temperature, the probability of each difference in k-value between two sites for fixed N. An important relation between the real space and Fourier space is that localised states in one representation correspond to delocalised states in the other, it should also be noted that the aligned k value, corresponds to the total probability and remains a constant at all temperatures.

The curves we plot are on a single model, for the Ising it is the $J_{19} - J_{20}$ and for $p = 7$ it is the $J_9 - J_{10}$. On the Ising model in both real spin space and Fourier spin space the blue curves represent probabilities between nearest neighbours; the green curves between second nearest neighbours; the black curves between spins that are diametrically opposite on the spiral. For the $p = 7$ model in both spaces the blue curves represent the relative probabilities between sites $i, i + N - 1$ and $i, i + N - 2$ and the green curve between sites i and $i + 1$; the black curve again between spins that are diametrically opposite and the red curves are all sites between i and $i + N$.

3.3.1 Ising Model Results

Our example calculation to illustrate the concept uses the Ising model. We plot the real spin space relative orientation probabilities for fixed $N = 20$ in figure 3.7a and the Fourier space in figure 3.7b. In the real spin space, the top set of curves is the probability of alignment and the bottom, anti-alignment. In the Fourier spin space, the only set of curves show the probability of anti-alignment in k values.

These results show behaviour that is expected of the Ising model. At low temperatures the system is in a long range ordered state, a finite fraction of the system is aligned. It then undergoes a second order phase transition into a disordered phase and the spins are equally

likely to be aligned and anti-aligned. The Fourier space results indicate the duality in the model. At low temperature (high β) both Fourier components are equally likely, and then at high temperature (low β) only the aligned k values are probable.

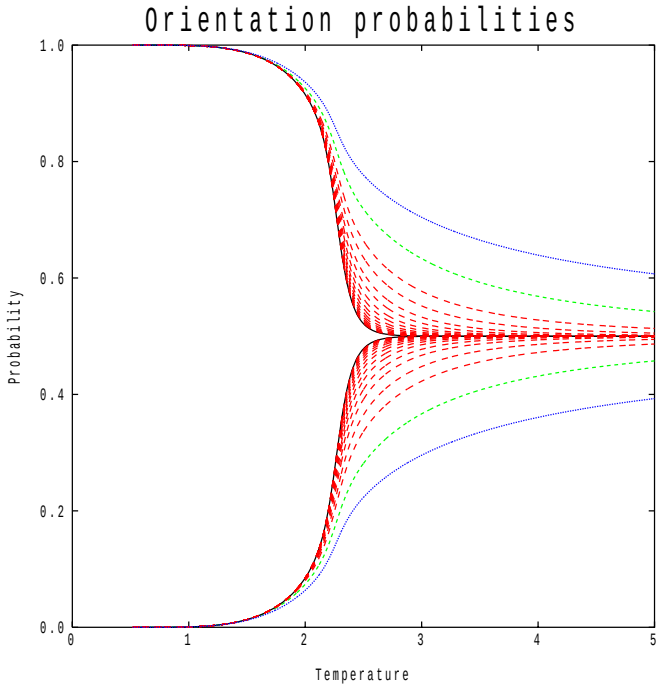

(a)

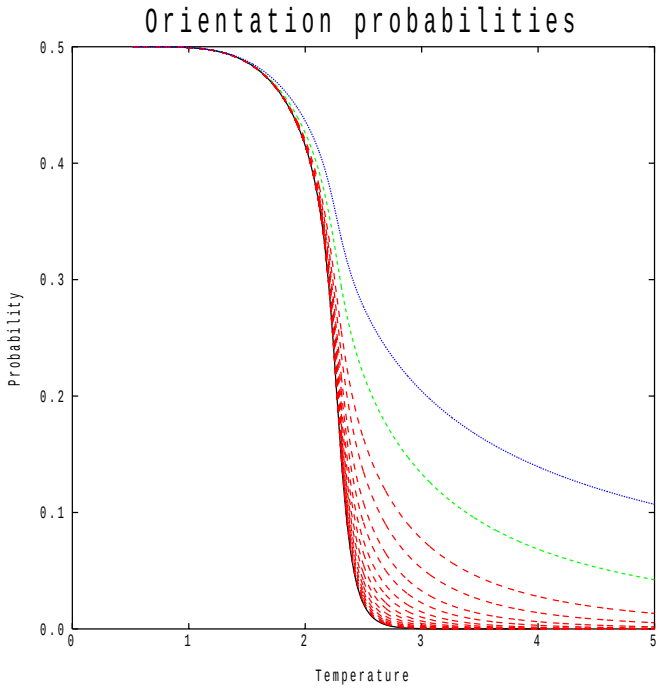

(b)

Figure 3.7: The orientational probabilities for the $p = 2$, $J_{19} - J_{20}$ model in both the real spin space (a) and Fourier spin space (b).

3.3.2 Clock Model Results

We plot the orientational probabilities for $p = 7$, $N = 10$ in figure 3.8a. To find universal behaviour we plot many clock ticks which can be found in appendix C, which will indicate behaviour that is associated with the low temperature transition. The plots in Fourier space are presented similarly. It should be noted that only about half the clock ticks are plotted as the probability is an even function of relative orientation. We have seen plenty of evidence that the system represents the 2-D limit, so there must be indicators in these results to the qualitative behaviour of each temperature region.

The real space probabilities show some universal behaviour in the three different phases. Both the low and high temperature phases are easily categorised. Long range order occurs from discrete models at low temperatures, and we see that at low temperatures there is a sizeable probability of alignment between spins. The lower critical temperature decreases with an increase in clock ticks as the energy barrier to the nearest clock tick decreases. High temperature brings expectations of disorder, and we see that in all models the probability of each clock tick tends to $\frac{1}{p}$; spins are equally likely to point in any direction. The phase between the transitions is the most challenging to grasp. We can see that the behaviour that occurs around the first critical temperature for any model is an increase in the probability of a difference of one clock tick, which is of the same order to alignment between spins. The most surprising part of this result is that at temperatures around the critical region, there is negligible probability of a difference of two clock ticks. This implies that there is a disorder between just two neighbouring clock ticks. Such a state clearly presents more questions than it answers, and though we will discuss this, very little further insight will be gained on the region between transitions.

We turn to the Fourier space probabilities and note the striking similarities between these results and the real spin space results. At low temperature (high β) every relative k orientation is equally likely. At around the first transition all relative k orientations drop off dramatically apart from neighbouring k orientations. After the high temperature transition

and in the low β phase, the only non zero Fourier component is the aligned orientation that corresponds to the total probability. The crucial result from the Fourier space calculation is that in the region between transitions the critical behaviour arises dominantly from nearest k value but not of the second nearest, much like the real space behaviour between nearest clock ticks. Clearly the two transitions have very similar traits.

Calculations in both representations present a very novel phase and complementary transitions. There are points for further investigation into this middle phase: an explanation on the number of clock ticks selected; the symmetry that is broken at the transition and the type of order that is exhibited, appear to be the most puzzling topics, but we are unable to probe questions of such detail. This is simply because that in the systems we use the problem of what to calculate is significantly harder than how to calculate. We can affirm that our calculations represent a 2-D phase as we know from previous results that the system is a good representation of 2-D. The phenomena are also not likely to be due to the finite size of the system; there is no obvious decrease in behaviour with increasing N. It is clear that at both extremes in temperature there exist natural representations to the system, low temperature in real spin space, high temperature in Fourier spin space.

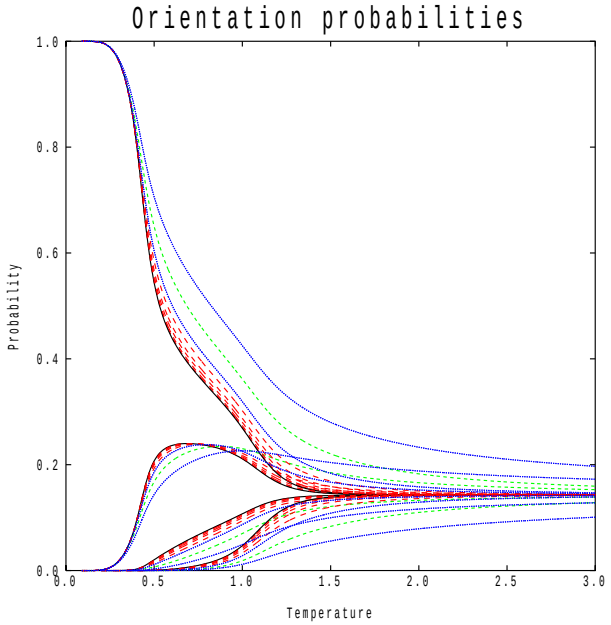

(a) The orientational probabilities for the $p = 7$, $J_9 - J_{10}$ model in real spin space.

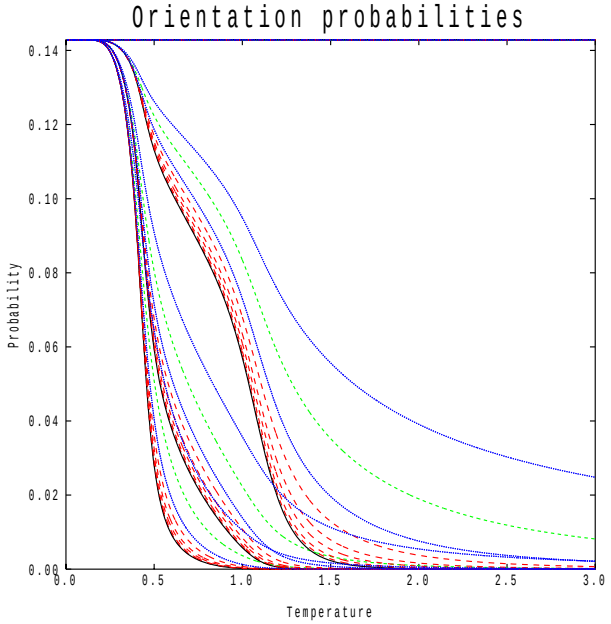

(b) The orientational probabilities for the $p = 7$, $J_9 - J_{10}$ model in Fourier spin space.

Figure 3.8: The orientational probabilities in both real and spin space for the $p = 7$ model. The different set of curves are between different relative clock ticks. The blue curves are relative orientations between i and $i + N - 1$ and i and $i + N - 2$; the green curves between i and $i + 1$, the black curve between two spins diametrically opposite and the red curves every site in between i and $i + N - 1$.

3.3.3 Concluding Remarks

We have found clear qualitative behaviour of the three different phases of the system. The two regions that correspond to the two extremes in temperature are well understood as long range order and disorder; the middle phase is the focus of the results. Above the low critical temperature, the system forms domains of spins disordered between two nearest neighbour clock ticks, above the low critical temperature the system forms domains of nearest neighbour k-points in Fourier spin space and intermediate temperatures must be superpositions of the two. As both transitions are so similar they are perhaps in the same universality class.

The amount of information that we can gain from this novel phase is limited despite that we have access to any correlation function we desire. To shed some light on this we will investigate the similarities between the clock and plane rotator models. Some of the results found will be required to discuss the section on possible order parameters.

3.4 High Temperature Expansion

We have so far highlighted that the high temperature transition that is apparent in the clock model is the same transition that is seen in the plane rotator.

Here in this section we shall see the analytic relationship at high temperature between the clock model and plane rotator. This is done through a high temperature expansion of the partition function, where we are in the regime of small β. We find the free energy as a power law expansion of β and find the leading order difference between the clock model and plane rotator.

We begin with recognising that the partition function can be expanded as a power series:

$$\begin{aligned} \mathcal{Z} =& \text{Tr } e^{-\beta\mathcal{H}} \\ =& \sum_m \frac{1}{m!} \text{Tr } \left[(-\beta\mathcal{H})^m\right], \end{aligned} \tag{3.4.1}$$

where the trace can be understood as the sum over all possible configurations.

We are interested in $F = \frac{-1}{\beta}\log(\mathcal{Z})$ and so shall attempt to obtain a function A such that

$$\begin{aligned}\mathcal{Z} =& e^{A} \\ =& 1 + A + \frac{A^2}{2!} + \cdots\end{aligned}, \tag{3.4.2}$$

where A must depend linearly on the number of atoms in the system N, as it is proportional to the free energy, but will also be a perturbative expansion in β. We will gain an expansion of both plane rotator and clock models where we expect

$$F_{\text{clock}} = F_{\text{PR}} + f(\beta), \tag{3.4.3}$$

where f is some homogeneous function of β.

Our only necessary example is the 1-D chain. We find the free energy using diagrammatic techniques. Consider the Hamiltonian

$$\mathcal{H} = -\frac{1}{2}\sum_i \left[e^{i(\phi_{i+1}-\phi_i)} + e^{-i(\phi_{i+1}-\phi_i)}\right], \tag{3.4.4}$$

where $\phi_i \in [0, 2\pi)$. The trace in this model is explicitly

$$\text{Tr } O = \left(\frac{1}{2\pi}\right)^N \int_{-\pi}^{\pi} \mathrm{d}\phi_1 \cdots \int_{-\pi}^{\pi} \mathrm{d}\phi_N \, O\left(\underline{\phi}\right). \tag{3.4.5}$$

The dot product between nearest neighbour spins has been split up so that they can be represented diagrammatically and to ease the calculation.

i ----➔ $i+1$ $\quad \Rightarrow e^{i(\phi_{i+1}-\phi_i)}$

i ➔---- $i+1$ $\quad \Rightarrow e^{-i(\phi_{i+1}-\phi_i)}$ For ease we drop the indices from the diagrams.

The Hamiltonian raised to any power is a taxing sum of complex exponentials. The

trace tells us that the only contribution to the partition function are those exponentials that cancel to give unity as

$$\frac{1}{2\pi}\int_{-\pi}^{\pi} \mathrm{d}\phi\, e^{i\phi} = 0. \tag{3.4.6}$$

This is only the case if the diagram of the term forms a closed loop. Our task is simply to count the loops at each order. Note that the lattice allows only even powers of $\mathcal{H}$ to contribute.

We will lay out each contributing diagram at each order and collate them in powers of N. From here we will find order by order a power law expansion for A in terms of β

$(\mathcal{H})^2$

 $\frac{1}{2!}\left(\frac{\beta}{2}\right)^2 N2!$

$(\mathcal{H})^4$

 $\frac{1}{4!}\left(\frac{\beta}{2}\right)^4 N\frac{4!}{2!2!}$

 $\frac{1}{4!}\left(\frac{\beta}{2}\right)^4 \frac{N(N-1)}{2!}4!$

$(\mathcal{H})^6$

 $\frac{1}{6!}\left(\frac{\beta}{2}\right)^6 N\frac{6!}{3!3!}$

 $\frac{1}{6!}\left(\frac{\beta}{2}\right)^6 N\left(N-1\right)\frac{6!}{2!2!}$

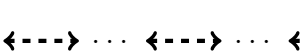 $\frac{1}{6!}\left(\frac{\beta}{2}\right)^6 \frac{N(N-1)(N-2)}{3!}6!$

$(\mathcal{H})^8$

 $\frac{1}{8!}\left(\frac{\beta}{2}\right)^8 N\frac{8!}{4!4!}$

 $\frac{1}{8!}\left(\frac{\beta}{2}\right)^8 N\left(N-1\right)\frac{8!}{3!3!}$

 $\frac{1}{8!}\left(\frac{\beta}{2}\right)^8 \frac{N(N-1)}{2}\frac{8!}{2!2!2!2!}$

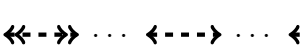 $\frac{1}{8!}\left(\frac{\beta}{2}\right)^8 \frac{N(N-1)(N-2)}{2!}\frac{8!}{2!2!2!}$

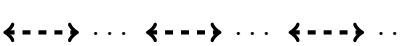 $\frac{1}{8!}\left(\frac{\beta}{2}\right)^8 \frac{N(N-1)(N-2)(N-3)}{4!}8!$

[Note the ellipses imply both joined and separate diagrams.]

Now we collate the terms for increasing powers of β and we gain a power series expansion

for $A = \log \mathcal{Z}$ which will be linear in N. At order β^2

$$\begin{aligned}\mathcal{Z} =& 1 + \frac{1}{2!}\text{Tr } \left[(\beta\mathcal{H})^2\right] \\ \mathcal{Z} =& 1 + N\left(\frac{\beta}{2}\right)^2 \\ \frac{A}{N} =& \left(\frac{\beta}{2}\right)^2;\end{aligned} \tag{3.4.7}$$

at order β^4

$$\begin{aligned}\mathcal{Z} =& 1 + \frac{1}{2!}\text{Tr } \left[(\beta\mathcal{H})^2\right] + \frac{1}{4!}\text{Tr } \left[(\beta\mathcal{H})^4\right] \\ \mathcal{Z} =& 1 + N\left[\left(\frac{\beta}{2}\right)^2 - \frac{1}{4}\left(\frac{\beta}{2}\right)^4\right] + \frac{N^2}{2!}\left[\left(\frac{\beta}{2}\right)^4\right] \\ \frac{A}{N} =& \left(\frac{\beta}{2}\right)^2 - \frac{1}{4}\left(\frac{\beta}{2}\right)^4.\end{aligned} \tag{3.4.8}$$

Note that the term at $O(N^2)$ is equal to the square of the term at $O(N)$ to $O(\beta^4)$. At order β^6

$$\begin{aligned}\mathcal{Z} =& 1 + \frac{1}{2!}\text{Tr } \left[(\beta\mathcal{H})^2\right] + \frac{1}{4!}\text{Tr } \left[(\beta\mathcal{H})^4\right] + \frac{1}{6!}\text{Tr } \left[(\beta\mathcal{H})^6\right] \\ \mathcal{Z} =& 1 + N\left[\left(\frac{\beta}{2}\right)^2 - \frac{1}{4}\left(\frac{\beta}{2}\right)^4 + \frac{1}{9}\left(\frac{\beta}{2}\right)^6\right] + \frac{N^2}{2!}\left[\left(\frac{\beta}{2}\right)^4 - \frac{1}{2}\left(\frac{\beta}{2}\right)^6\right] \\ &+ \frac{N^3}{3!}\left[\left(\frac{\beta}{2}\right)^6\right] \\ \frac{A}{N} =& \left(\frac{\beta}{2}\right)^2 - \frac{1}{4}\left(\frac{\beta}{2}\right)^4 + \frac{1}{9}\left(\frac{\beta}{2}\right)^6.\end{aligned} \tag{3.4.9}$$

We thus have a perturbative expansion for A in terms of β, and by extension the free energy $F = -\frac{A}{\beta}$.

The expansion for the clock model behaves almost exactly the same, the difference is discretisation.

$$\phi_i \in \frac{2\pi n_i}{p}, \text{ s.t. } n_i \in 0, \ldots, p-1, \tag{3.4.10}$$

and the trace is no longer an integral

$$\mathrm{Tr}\ O = \frac{1}{p^N} \sum_{n_1=0}^{p-1} \cdots \sum_{n_N=0}^{p-1} O\left(\mathbf{n}\right). \tag{3.4.11}$$

This trace now implies that the contributing terms to the partition functions satisfy

$$\frac{1}{p} \sum_{n=0}^{p-1} e^{i\frac{2\pi}{p}n} = \sum_{m=-\infty}^{\infty} \delta_{n,mp}, \tag{3.4.12}$$

which includes, but is not restricted to the $m = 0$ terms that contribute in the plane rotator model.

Though this trace is more inclusive than the plane rotator, the expansion is much the same and the first additional diagrams occur at order β^p

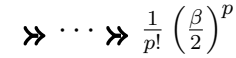
$\frac{1}{p!}\left(\frac{\beta}{2}\right)^p N$

$+$


$\frac{1}{p!}\left(\frac{\beta}{2}\right)^p N$

which implies that the leading order change in $\log \mathcal{Z}$ is

$$\frac{A_{\mathrm{clock}}}{N} = \frac{A_{PR}}{N} + \frac{2}{p!}\left(\frac{\beta}{2}\right)^p, \tag{3.4.13}$$

and so the change in specific heat to leading order is

$$C_{\mathrm{clock}} = -\frac{\partial^2 F}{\partial T \partial \beta} = C_{PR} + \frac{(p-1)(p-2)}{p!}\left(\frac{\beta}{2}\right)^{p-1}. \tag{3.4.14}$$

When we move to 2-D, though the loops are more complicated, the principals are exactly the same and the leading order additional diagrams are


the contributions from the extra diagrams are

$$\Delta Z = \frac{2}{p!}\left(\frac{\beta}{2}\right)^p N + \frac{2}{p!}\left(\frac{\beta}{2}\right)^p N, \tag{3.4.15}$$

and the leading order change to the specific heat is given by

$$C_{\text{clock}} = C_{\text{PR}} + \frac{2\,(p-1)\,(p-2)}{p!}\left(\frac{\beta}{2}\right)^{p-1}. \tag{3.4.16}$$

3.5 Helical Stiffness

There exists thermodynamic quantities that measure the response of the system to some external parameter. These parameters change the Hamiltonian that was initially under investigation, but often the most interesting region is the response to an infinitesimal value of the parameter. The response is measured as the lowest order change to the free energy; one well known example is the magnetic susceptibility, which measures the instantaneous change to the system to a uniform magnetic field, another is the helical stiffness. These parameters can provide insight into the original Hamiltonian around critical temperatures.

The system has been somewhat characterised by the results on conditional probabilities, but we have yet to find order parameters for the transitions. We will be seeking quantities that are non zero only in ordered regions and behave singularly at critical regions in the 2-D limit. This will be an obstacle to discerning the validity of these order parameters, as our results will not behave singularly and nor will their extrapolation. In this section we use the helical stiffness to show that there is a possible order parameter for each of the transitions. This quantity is generally used as an order parameter in Kosterlitz-Thouless type transitions [6],[12].

We will first discuss the helical stiffness at some length; the quantity applied both to 1-D and 2-D with plane rotator and clock models and then its use in the spiral systems. In the context of our Hamiltonian we note a gauge invariance which is crucial to understanding the difference to the two order parameters. It will be shown that with this gauge invariance

and the results on the relationship between clock and plane rotator models that one order parameter is associated solely with the anisotropy lost at the first transition, and the other associated with the order of the plane rotator.

3.5.1 Examples in 1-D and 2-D

We examine the effects on the free energy as a function of the external parameter chi in the Hamiltonian:

$$\mathcal{H} = \sum_{\langle i,j \rangle} \cos\left(\theta_j - \theta_i - \chi\right), \tag{3.5.1}$$

for a finite χ, the spins are encouraged to spiral across the system. The region of most here interest is in the limit $\chi \to 0$

$$F\left(\chi\right) - F\left(0\right) = \frac{\chi^2}{2!}\frac{\partial^2 F}{\partial \chi^2}\bigg|_{\chi=0} + \frac{\chi^4}{4!}\frac{\partial^4 F}{\partial \chi^4}\bigg|_{\chi=0}. \tag{3.5.2}$$

The helical stiffness is the leading order change for an infinitesimal spiral across the system $Y_2 = F_{\chi\chi}\left(0\right)$.

It is important to highlight that the helical stiffness is not associated with the excitations of the original Hamiltonian. This quantity is best understood through simple examples at extreme temperatures; at low temperature we calculate ground state energies and at high temperature we use the diagrammatic technique developed in the previous section.

The first examples that we deal with will be the clock model in 1-D and 2-D. Consider an infinite 1-D chain of spins with the Hamiltonian

$$\mathcal{H} = \sum_i \cos\left(\frac{2\pi\left(n_{i+1} - n_i\right)}{p} - \chi\right), \tag{3.5.3}$$

where $n_i \in \mathbb{Z}$. At low temperature the most relevant contribution to the free energy is the ground state energy of the system. The ground state for such a Hamiltonian is dependant

on the size of the spiralling angle. For $\frac{2\pi n}{p} < \chi < \frac{2\pi(n+1)}{p}$, the ground state is a spin spiral with a pitch of $\frac{p}{n}$ and an energy of

$$F \sim E = -\cos\left(\chi - \frac{2\pi n}{p}\right), \tag{3.5.4}$$

and so the helical stiffness is

$$Y_2 \sim \cos\left(\frac{2\pi n}{p}\right). \tag{3.5.5}$$

This solution also includes the ferromagnetic ground state for $n = 0$.

At high temperatures, we use the expansion developed in the previous section and re-represent each diagram as :

$$\mathcal{H} = \frac{1}{2}\sum_i \exp\left[i\left(\frac{2\pi\left(n_{i+1} - n_i\right)}{p} - \chi\right)\right] + \exp\left[-i\left(\frac{2\pi\left(n_{i+1} - n_i\right)}{p} - \chi\right)\right], \tag{3.5.6}$$

which implies that the diagrams introduced in the previous section have slightly altered

 $= \exp\left[i\left(\phi_{i+1} - \phi_i - \chi\right)\right]$ Again the diagrams that contribute to the partition function are closed loops, those that do not contribute now include the diagrams that differentiate the clock model from the plane rotator.

 $\Rightarrow \sum \exp\left[ip\chi\right] = 0$ the difference between the free energy is already known from the previous section

$$\begin{aligned} \Delta F =& \frac{\chi^2}{2}\frac{\partial^2 F}{\partial F^2} + O\left(\chi^4\right) \\ \sim& \frac{1}{T^p}. \end{aligned} \tag{3.5.7}$$

For small χ ΔF is the helical stiffness to leading order.

This example shows that anisotropic models can have a finite response to an infinitesimal spin spiral at low temperature and at high temperature tends to zero.

Another important example is with the isotropic spin model: the plane rotator. This is

key as we know that the intermediate phase in the clock model behaves as the low temperature phase of the plane rotator:

$$\mathcal{H} = \sum_n \cos\left(\phi_{n+1} - \phi_n - \chi\right). \tag{3.5.8}$$

If we change the basis to

$$\phi_n => \phi_n + n\chi, \tag{3.5.9}$$

then we are left with the original Hamiltonian. This is a gauge transformation of the original Hamiltonian leaving the thermodynamics unchanged, implying that the helical stiffness is zero for the infinite plane rotator chain at all temperatures. The result extends to the two dimensional model.

This quantity appears to be able to pick out behaviour in 1-D that extends to long range order in 2-D. At a quantitative level it measures the difficulty of inducing a spin spiral. For models that extend to quasi long range order in 2-D the effect of a spin spiral is not apparent on the infinite system scale. When we calculate for the systems that we use, we see that due to the geometry, the helical stiffness is finite for quasi long range ordered regions.

3.5.2 Helical Stiffness in the Spiral Geometry

After simple examples of helical stiffness for both clock and plane rotator models, we shall calculate the helical stiffness in the two temperature extremes for the spiral system that we use. It is worth exploring this before presenting the results as there are complexities associated with the helical stiffness in these models that should be addressed so that the full implication of the results are understood. We shall see that there are two helical stiffnesses, one that can be associated with those calculated above, and another which occurs from the boundary conditions.

We consider first the low temperature results of the Hamiltonian

$$\mathcal{H} = \sum_i \cos\left(\theta_{i+1} - \theta_i - \chi_\parallel\right) + \cos\left(\theta_{i+N+1} - \theta_i - \chi_\perp\right), \tag{3.5.10}$$

and calculate its ground state for both the clock and plane rotator models. For both cases, we only consider small χ, where $\chi << \frac{2\pi}{p}$. In further sections we shall see the ground state for the clock model for the case $0 < \chi < 2\pi$.

In the region of interest of the clock model the ground state is a ferromagnet with no spin spiral. It has the energy

$$\begin{aligned} E^\parallel &= \cos\left(\chi_\parallel\right) \\ E^\perp &= \cos\left(\chi_\perp\right), \end{aligned} \tag{3.5.11}$$

where the first is with $\chi_\perp = 0$ and the second with $\chi_\parallel = 0$. The helical stiffness for both is

$$Y_2 = 1, \tag{3.5.12}$$

and just as in the above examples, there is a finite result for zero temperature for the clock model.

The plane rotator model behaves markedly differently to the clock model. In the 2-D limit we expect the above gauge transformation for the plane rotator, but there is one even for the 1-D spiral geometry.

We expect from the above example that in the 2-D limit that there is a gauge transformation that implies a zero helical stiffness, but we note that even in the 1-D spiral system, with specific boundary conditions, there still is a gauge transformation.

Consider the change of variables $\phi_i \to \phi_i + i\chi_\parallel$, which leads to a Hamiltonian

$$\mathcal{H} = \sum_i \cos\left(\phi_{i+1} - \phi_i\right) + \cos\left(\phi_{i+N} - \phi_i + N\chi_\parallel - \chi_\perp\right). \tag{3.5.13}$$

This gauge invariance does not exist for the clock model

3.5.3 High Temperature Expansion

At high temperature we use the diagrammatic technique to show that the helical stiffness in both clock and plane rotator models go to zero. We will then plot the difference in free energy between models with and without the induced spiral and see that each helical stiffness is associated with the different transitions, providing an order parameter for each.

The leading order difference in the clock model is that the diagram

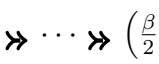
$\left(\frac{\beta}{2}\right)^p N$

does not contribute. Which means that the leading order difference is

$$4\left(\frac{\beta}{2}\right)^p N. \tag{3.5.14}$$

In the plane rotator model the leading order diagram that does not contribute is the diagram that loops around the spiral

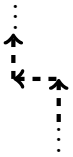
$2\left(\frac{\beta}{2}\right)^{m+1} N$

Where in this case we have used m to refer to the size of the spiral. This is again another power law tail at high temperature.

3.5.4 Results

There are two clearly different helical stiffnesses, one associated with the clock model and the other with the plane rotator. As they are also possible measures of order in a system, they are clear choices as possible order parameters. The helical stiffness has been proposed before as an order parameter, and found experimentally, in the form of the superfluid density of helium; an analgous quantity [13].We find the helical stiffnesses numerically.

We plot the helical stiffness associated with $\chi_{\parallel}$ and $\chi_{\perp}$ in figure 3.9 respectively for different values of N. There are clear changes in behaviour at critical temperatures; $\chi_{\perp}$ appears to tend to critical behaviour at the upper transition; $\chi_{\parallel}$ appears to tend to critical behaviour at the lower transition. This is exactly as we outlined above, that one helical stiffness is associated with the decrease in the effect of the anisotropy of the clock model to the thermodynamics, which from results in the previous section we know is at the lower transition. We also know that the other helical stiffness is the loss of order associated with the plane rotator model.

We also plot the high temperature expansion in figure 3.10.

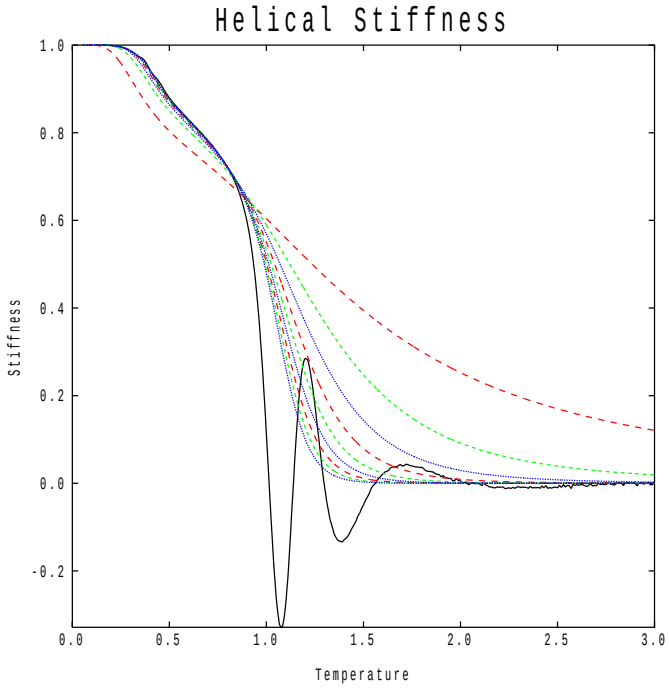

(a) The helical stiffness with $\chi_\perp = 0$

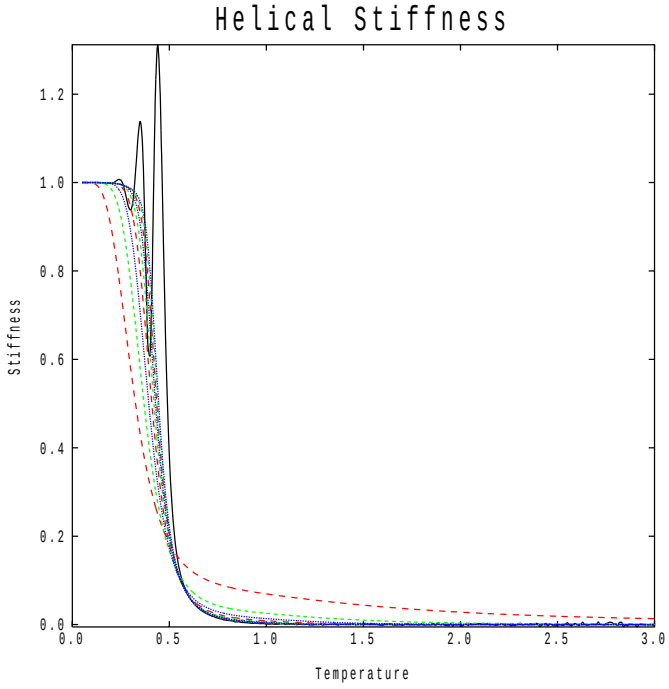

(b) The helical stiffness with $\chi_\parallel = 0$

Figure 3.9: The helical stiffness for $p = 7$ along both directions, plotted with the extrapolation (solid black curve). The red curve furthest away from the extrapolation is $J_1 - J_2$ and they go up to $J_1 - J_{10}$.

Pure N black, pure P red (blue), n+p green (blue)

3.5.5 Concluding Remarks

The helical stiffness in our system provides two distinct quantities that are each associated with each phase transition, and provide possible order parameters for the critical regions. Like all calculations we have performed on the 1-D systems, we cannot draw explicit conclusions about the 2-D limit; the helical stiffness can only appear to tend towards critical behaviour at the transitions.

One of these quantities is associated with the helical stiffness that is often calculated in the 2-D limit, which behaves accordingly; it highlights long range ordered states, and due to a gauge transformation is zero for isotropic systems. The second quantity highlights both long range and quasi long range order that is witnessed in the plane rotator model.

We have seen in the previous section which explicitly shows the relationship between the clock and plane rotator models, that the clock model becomes the plane rotator after the first transition. We are able to measure the extent to which the anisotropy of the clock model is relevant to the thermodynamics. Once the clock model becomes the plane rotator, the free energy becomes a function of only one parameter.

The two transitions have now been characterised as much as the technique allows. The existence of singular behaviour at two critical temperatures have been established, and we have gained insight into the nature of the three temperature regions. The focus of our results shall turn away from the characterisation of the transitions and we deal with a complementary investigation of the clock model with a finite χ within the context of an extension of Fisher Zeros.

3.6 Vortices through the spiral

In this section we will attempt to show that there are phase changes at points of degeneracy in eigenvalues of the transfer matrix. We do this using the Hamiltonian in the previous section and calculate the free energy as a function of the external parameter χ. A comparison between analytic results of the ground state and the free energy of our system at low temperature will show that there are crossing points of the highest eigenvalue and the free energy follows them.

We introduced the notion of a generalisation of Fisher Zeros in section 2.4.2 where in our 1-D to 2-D crossover technique the idea is that a phase transition occurs when the highest eigenvalues are degenerate. It is worth calculating the highest lying eigenvalues as a function of temperature to see if there is any degeneracy that occurs around the presumed phase transitions. Work has been performed in this area which suggests degeneracy in the limit $N \to \infty$ but this work was not included in this investigation.

Instead we find as a function of $\chi_\perp$ the free energy of the Hamiltonian we used in the previous section at select temperatures.

$$\mathcal{H} = -\sum_i \cos\left(\phi_{i+1} - \phi_i\right) + \cos\left(\phi_{i+N} - \phi_i - \chi_\perp\right), \tag{3.6.1}$$

where in this case $0 < \chi_\perp < 2\pi$. The idea is that vortices are induced through the middle of the spiral, which correspond to discretised ground states and quantised flow. At low temperature we shall see that the structure of the free energy is very much dependant on the value of p, where the structure has a periodicity of π. In the intermediate phase we shall see that regardless of clock tick, the free energy is periodic in $\frac{2\pi}{N}$, resembling the exact results we achieve for the plane rotator. At very high energy, the amplitude of this periodicity tends to zero as the cost to put any number of vortices into the system tends to zero.

3.6.1 Results

We plot the low temperature solution for the $p = 7$, $N = 8$ with the zero energy solution which has been found analytically in figure 3.11a. Each lowest energy state corresponds to an increase in the number of vortices placed through the system. As expected these agree with each other very well; the free energy is dominated by the energy at low temperature.

We plot the results for the intermediate phase in figure 3.11b and notice that the system no longer notices the anisotropy inherent in the clock model. In this intermediate phase the free energy is still sharp but now has a periodicity of $\frac{2\pi}{N}$. We see this behaviour in most clock models when the power law convergence between the plane rotator and clock model is sufficiently large. This indicates that the spins at this temperature are behaving isotropically.

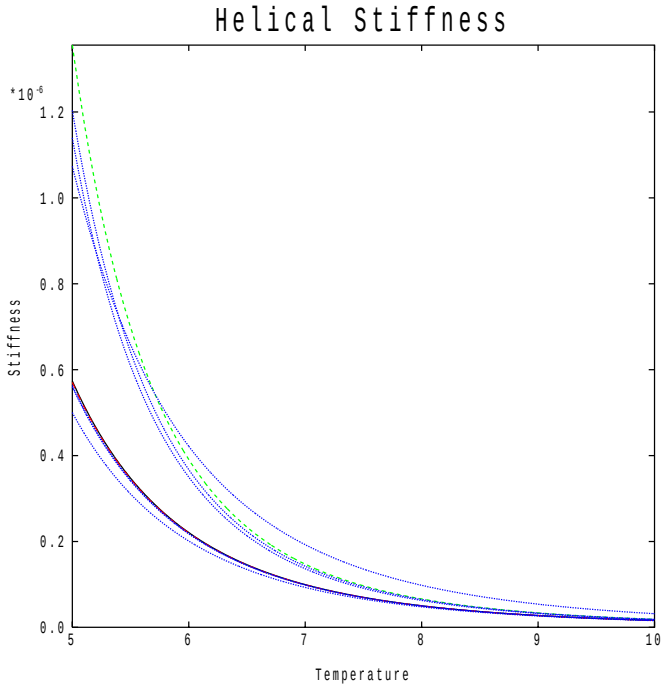

(a) The high temperature expansion between $T = 5 - 10$ for the $p = 6$, $n = 8$ model. The blue curves are the calculated expansion at higher orders, the lower set is considers the contribution from p only and the higher set are both p and N contributions. The green and red curve are the extrapolated helicity moduli. The black curve is simply the contribution from N.

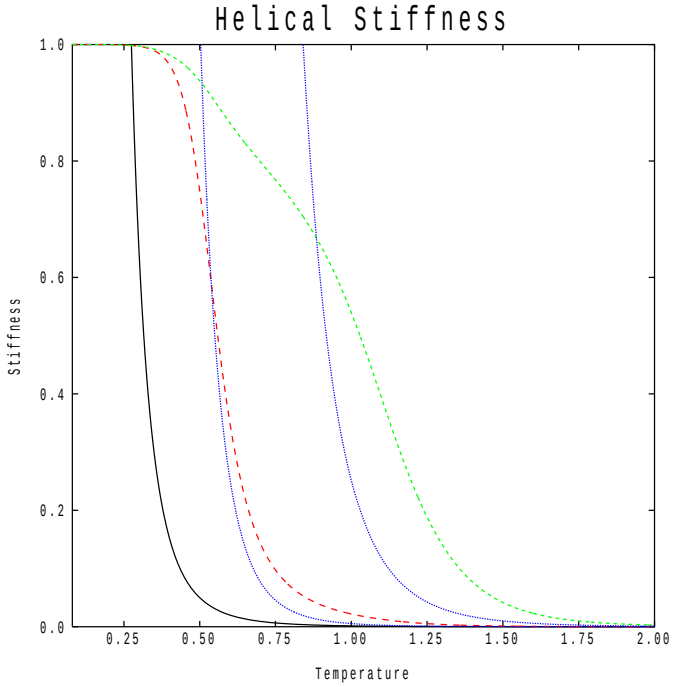

(b) The same graph taken at temperatures between $T = 0 - 2$.

Figure 3.10: The high temperature expansion of the helical stiffness for the $p = 6$, $n = 8$ model.

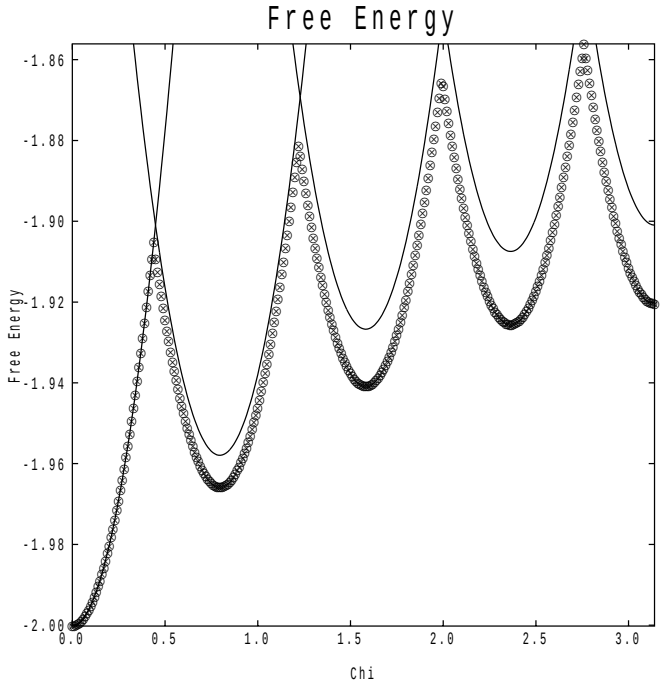

(a)

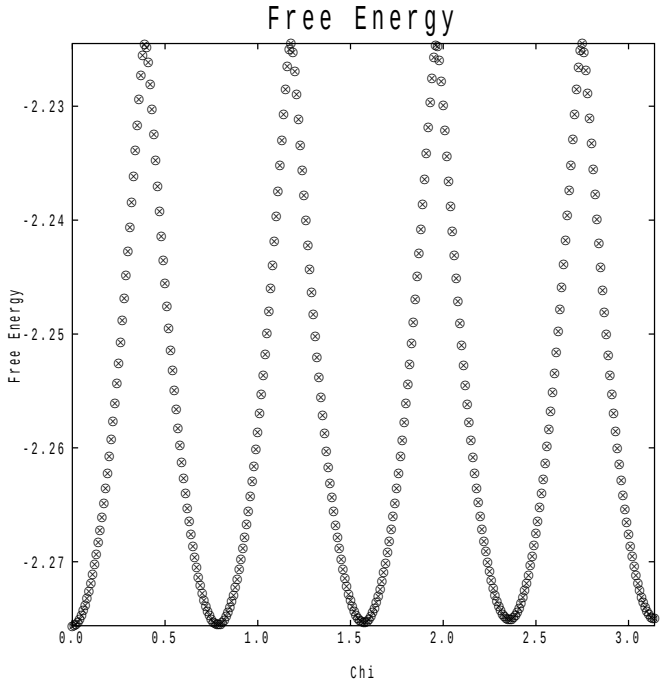

(b)

Figure 3.11: The free energy as a function of $\chi_{\|}$ for the $p = 7$, $N = 9$ model at temperatures $T = 0.2$ (a) and $T = 0.75$ (b)

Chapter 4

CONCLUSIONS

We have developed a novel technique for probing 2-D thermodynamic systems. It is conceptually easy to understand as it is an extension of the well known transfer matrix method of solving the Ising model in 1-D. The power in the technique relies on the ability to use it on models that tend towards a 2-D lattice model limit, which we see in the spiral geometry. Unlike other statistical techniques, macroscopic quantities are known exactly for the models that we calculate and the calculations are made in the 1-D thermodynamic limit where the total number of sites is infinite. The technique is not restricted to clock models, there is work to be published by *Robson et al* [58] that relies on this technique for the plane rotator model and further work has begun on clock model analogues to spins with 2 degrees of freedom.

Our results allow us to draw two main conclusions about the square lattice clock model. From results mainly on the specific heat, figures 3.5 we can conclude that there are indeed two second order phase transitions in clock models with $p > 4$. Our second conclusion dictates that above the low temperature transition there is a power law convergence between the clock model and the plane rotator in the free energy, implying that the high temperature transition that is seen in the clock model is exactly the same transition in the plane rotator. This is seen in figure 3.6. This implies that clock systems can be used to model the plane rotator, which can ease calculations. Both conclusions are in direct contrast with a lot of

literature results, and we shall place them in context here, addressing results on both clock and plane rotator calculations.

It has been generally accepted that the method of transition for both plane rotator and clock models on the square lattice are Kosterlitz-Thouless in type [1], [2]. This is based on continuum results of the plane rotator, which is best represented in helium-4 films [13]-[16] rather than on discrete lattices where the effect of the lattice has been ignored.

Nevertheless there is plenty of numerical data that conclude Kosterlitz-Thouless type transitions for the $p > 4$ clock models but there appears to be a general acceptance within the literature that they are not thermodynamically the same model.

Our data on specific heat provides clear divergent behaviour for the 2-D limit, and coupled with correlation length results, figures 3.1b and 3.3 we see that in the $N \to \infty$ limit our system provides a plausible 2-D limit. The specific heat scales with the size of our system and the derivatives which we calculate essentially exactly show that it is diverging. Though we only deal with a small system size we pick up no long range behaviour such as a unbinding of vortices which would be characteristic of a Kosterlitz Thouless transition. In fact our data is self consistent in the idea that their extrapolated behaviour present a physical realisation of a 2-D limit.

This is in contrast to the literature. Monte Carlo results which fit using a Monte Carlo Renormalisation Group technique or fit to the magnetic susceptibility or correlation length that exhibit essential singularities conclude Kosterlitz Thouless type transitions [29], [28], [24], [26], [59], [25], [60], amongst many others. However many of these investigations numerically calculate the specific heat and find the same two peaks that are seen in this investigation. We plot examples of these in figure 4.1. Currently there is no general acceptance of the behaviour associated with these peaks in either numerical or analytical investigations. In fact our investigation is more in line with conclusions drawn by *Lapilli et al* [25] and *Hwang* [30]. *Lapilli* concludes that $p < 7$ models do not exhibit Kosterlitz Thouless transitions and *Hwang* concludes that the $p = 6$ model, using a numerical Fisher Zero approach exhibits a

normal continuous phase transition.

We see from the correlation length that we have plausible 2-D behaviour and now that we see that we have continuous phase transitions, we use its derivative to gain a range for the critical exponent and an idea of the universality class. We get Ising like transitions but we see from a lot of the literature that the correlation length experiences an essential singularity [1], [2] and does not have critical exponents in the normal sense. The only critical exponent that can be found is the one associated with correlation function η, which is associated with the long range decay of the correlation function. According to the literature [1], [2] and [10] the Kosterlitz Thouless transition occurs when $\eta = \frac{1}{4}$ and at the lower transition $\eta \sim \frac{1}{p^2}$. This has not been confirmed by the literature [19], [29], [24], [26].

The relative orientational probabilities that we plot in figure 3.8a and 3.8b attempt to characterise the three phases, and we see a novel intermediate phase that exists in the critical region. We can conclude from the Fourier and real spin space probabilities that both are very similar transitions, in both spaces the intermediate regime can be characterised similarly; disorder between neighbouring clock ticks and the high and low temperature phase can be characterised by a single orientation presenting a possible duality between transitions. This is in fact in line with the arguments presented by *Ortiz et al* [50] and *Elitzur et al* [61], but their conclusions are based on the idea that both transitions are Kosterlitz Thouless in type rather than a second order transition.

We have used the helicity modulus in figure 3.9 as the order parameter for both transitions, much like the literature on Kosterlitz Thouless transitions, but we do not expect, yet cannot conclude that our calculated results exhibit a discontinuous jump at the phase transition, rather it is more likely that it behaves singularly.

Our second main conclusion draws again upon our specific heat results, the high temperature expansion and vortex inducing Hamiltonian but also on similar data found by *Robson et al* [58] on the plane rotator. We see that comparisons between specific heat on any clock model and plane rotator results show that the high temperature transition is the same in

both models. The two models are thermodynamically equivalent at the second transition and from our high temperature expansions the free energy converges as a power law after the low temperature transition. As we force a vortex in the spiral we see again the same results, that the free energy as a function of the induced spiral ignores the effect of the symmetry breaking field after the low temperature transition.

This again is in contrast to much of the literature. There is a lot of discussion about the clock model exhibiting plane rotator like behaviour and it is generally believed that both models undergo the same type of transitions. However, transition temperature results place the two models at different temperatures, general consensus with the literature place the plane rotator transition temperature at ~ 0.89, [21], [62], [18], but there have been some recent results that place it at ~ 0.70 [63], [64], [65]. The literature for the clock model, place what we are claiming to be the same transition at a different temperatures. There is no general consensus for the high temperature transition, whether it is a universal temperature or not, and for a variety of clock ticks the transition is between 0.9[26]-1.3[29]. There exists some results by *Lapilli* [25] that equate the two models above $p = 6$ and conclude much like we do that they are equivalent. Our results have more agreement with this investigation than with the rest of the literature and we conclude that studying the $p > 4$ clock model above the low temperature transition is equivalent to studying the plane rotator model.

Overall our new technique has prescribed an exact method of extracting critical information about two dimensional systems through exactly solvable 1-D models. We hope that with this new technique the key information regarding the nature of the transitions in both the clock and plane rotator systems is illuminating as singular behaviour in thermodynamic quantities.

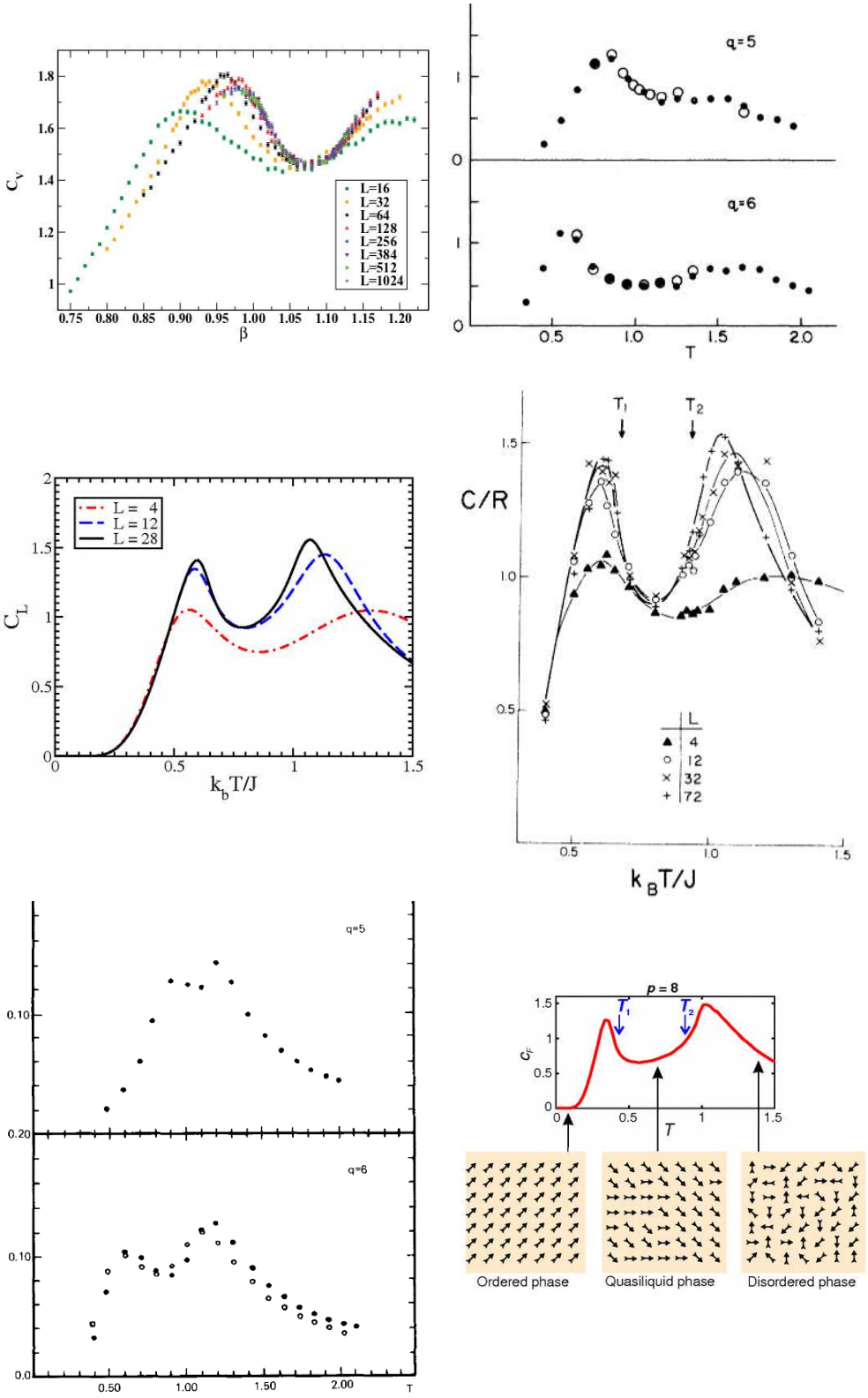

Figure 4.1: Investigations that show the same specific heat peaks that are seen in this investigation. Figures taken from [60], [29], [30], [24], [59], [25]

Appendix A

SPECIFIC HEAT RESULTS

Here we present the specific heat results and their first two derivatives along with the its ratio with the specific heat of the plane rotator model on our $J_{N-1} - J_N$, $p = 5, 6, 8, 9$ clock models.

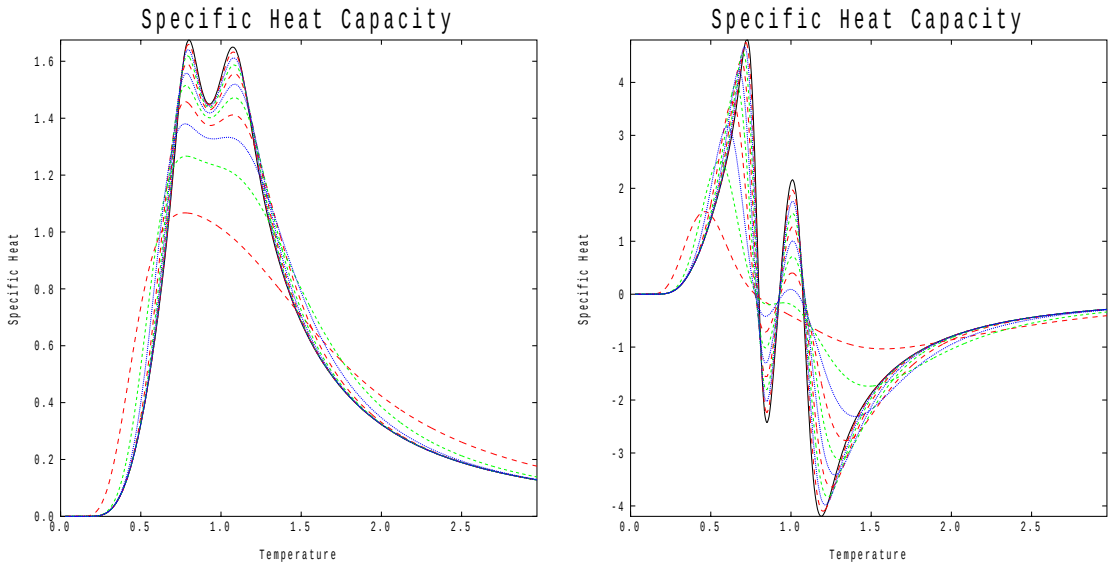

(a) (b)

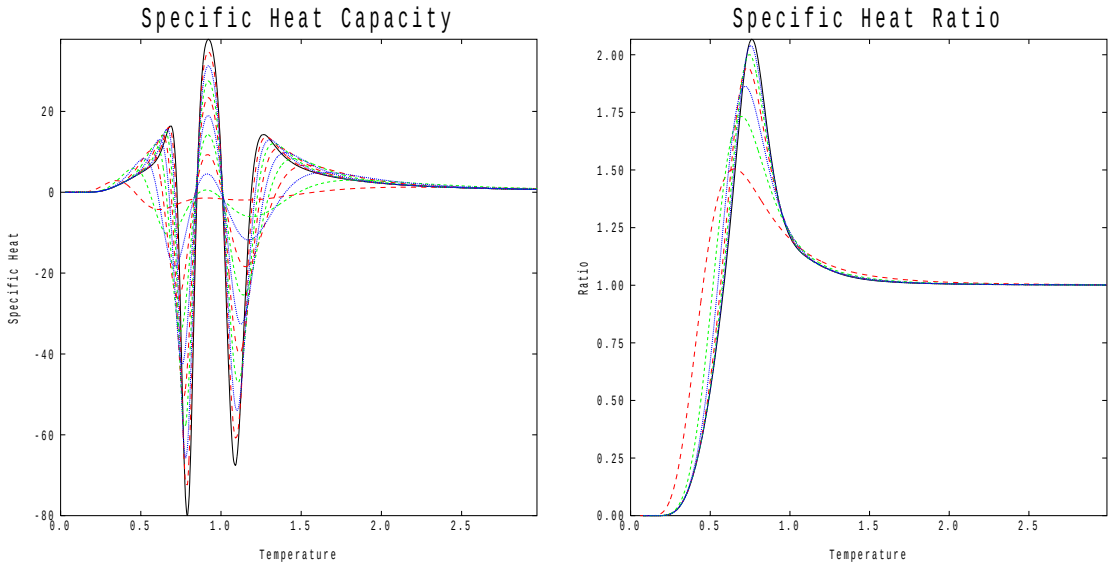

(c) (d)

Figure A.1: The specific heat and first two deriviatives and the specific heat ratio with the plane rotator model for the $p = 5$ clock model. The extrapolation is plotted in each (solid black curve). The spcific heat and its dreivatives go from $J_1 - J_2$ which is the lowest red curve up to $J_{10} - J_{11}$. The specific heat ratio goes up to $J_6 - J_7$.

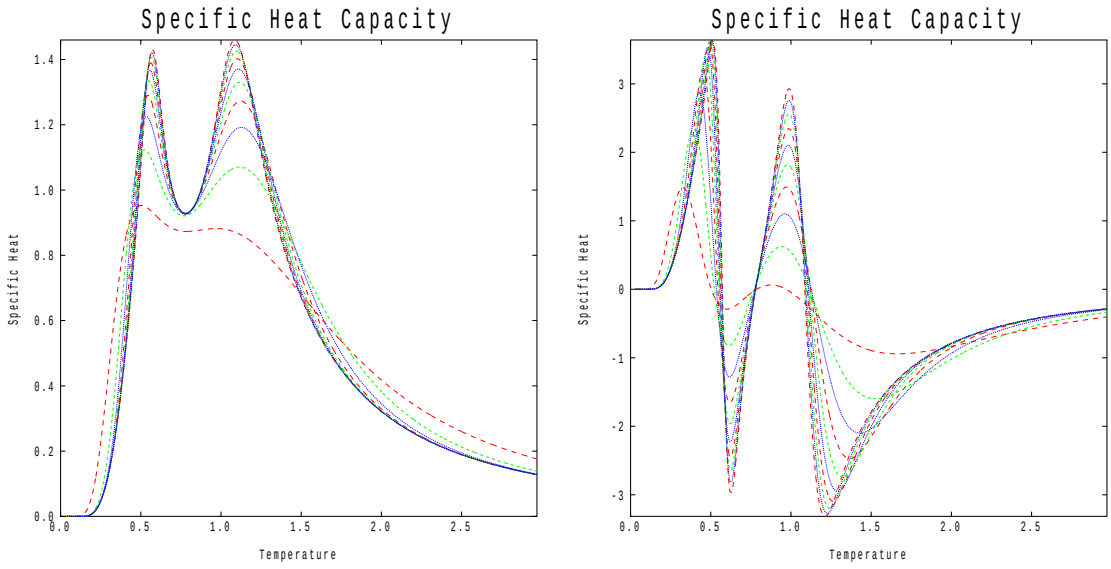

(a) (b)

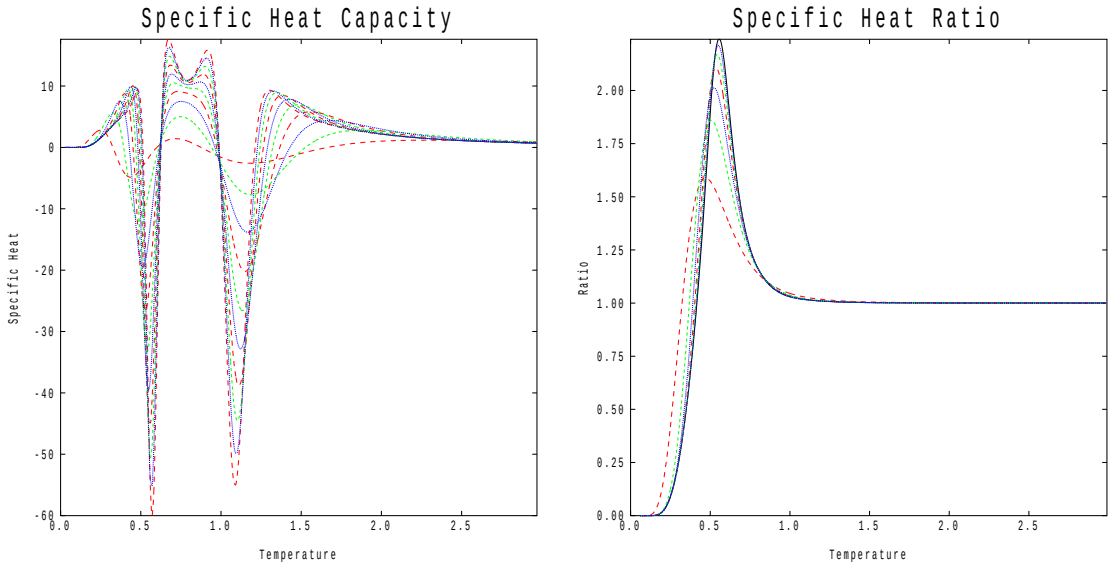

(c) (d)

Figure A.2: The specific heat and first two deriviatives and the specific heat ratio with the plane rotator model for the $p = 6$ clock model. The spcific heat and its derivatives go from $J_1 - J_2$ which is the lowest red curve up to $J_{10} - J_{11}$. The specific heat ratio goes up to $J_6 - J_7$, which is plotted with the extrapolation (solid black curve).

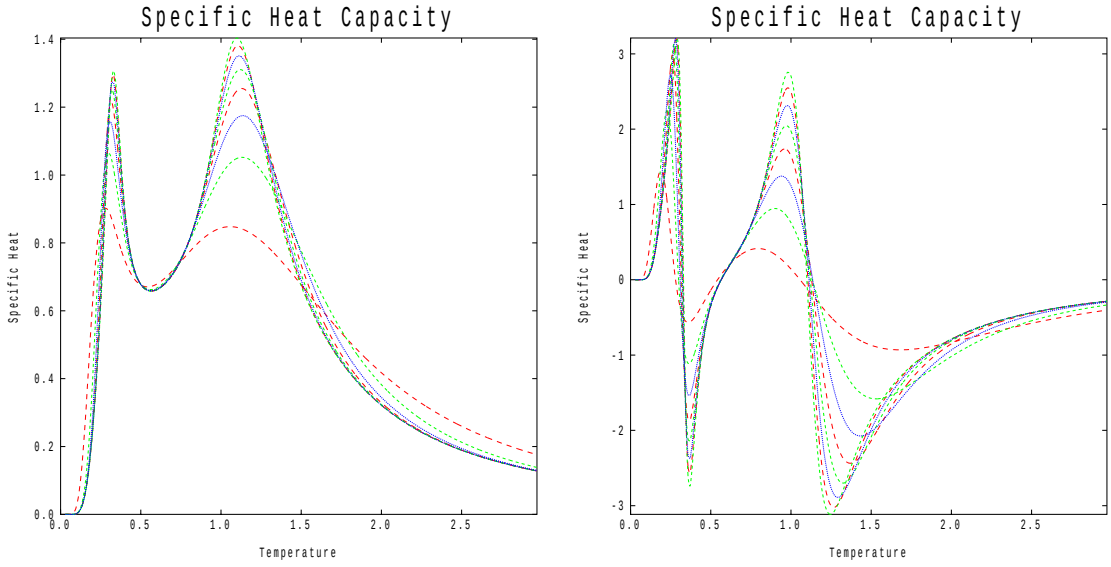

(a) (b)

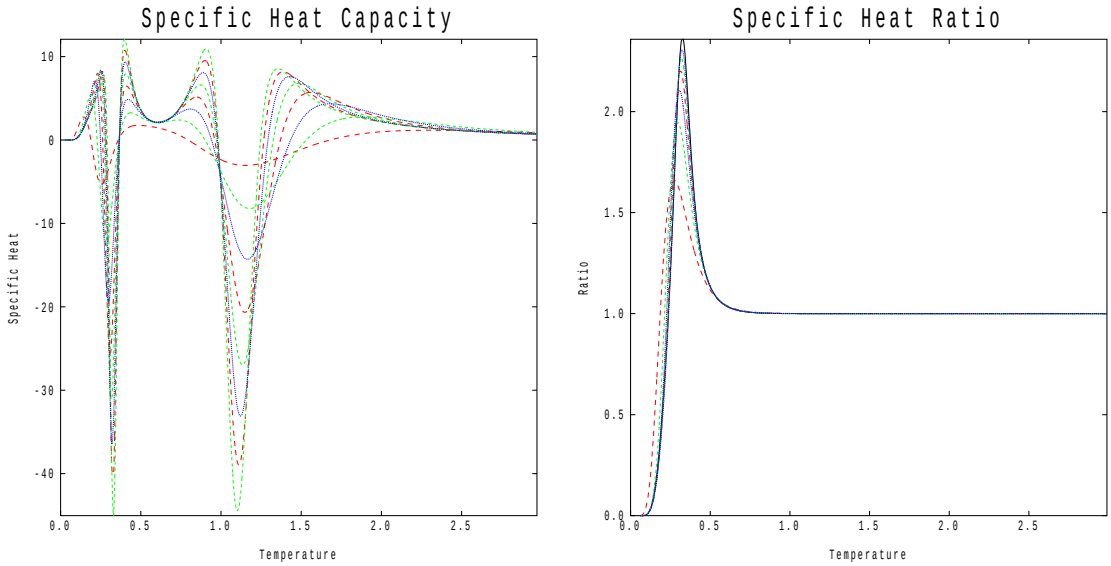

(c) (d)

Figure A.3: The specific heat and first two deriviatives and the specific heat ratio with the plane rotator model for the $p = 8$ clock model. The spcific heat and its derivatives go from $J_1 - J_2$ which is the lowest red curve up to $J_8 - J_9$. The specific heat ratio goes up to $J_6 - J_7$, which is plotted with the extrapolation (solid black curve).

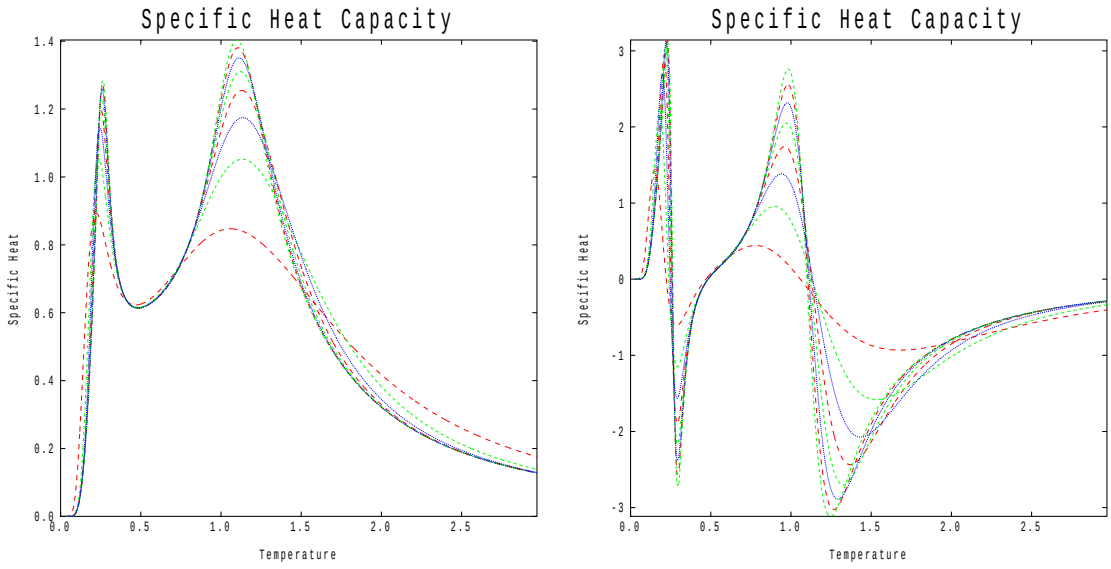

(a) (b)

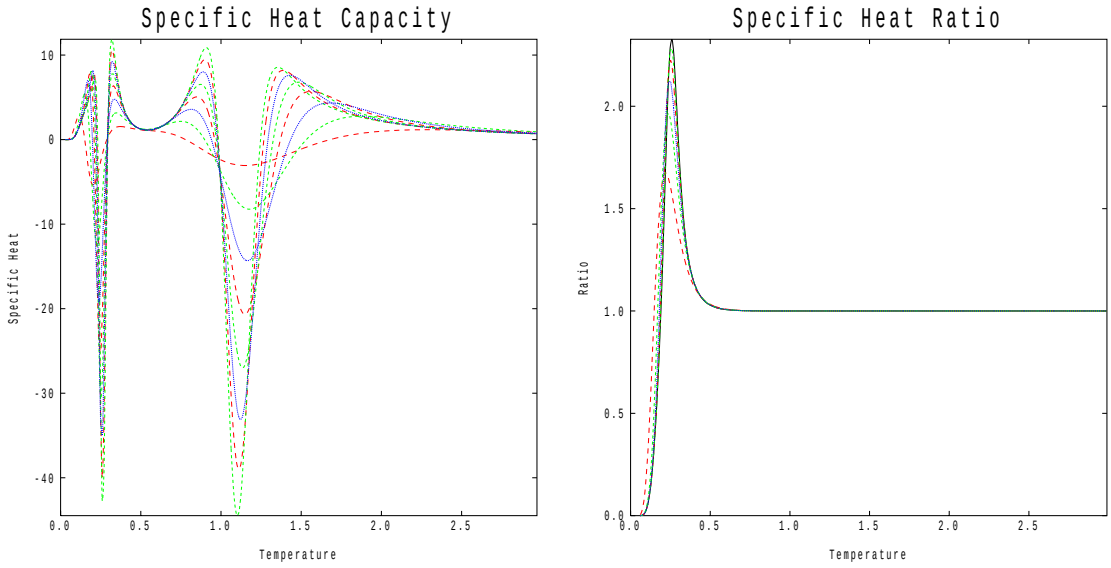

(c) (d)

Figure A.4: The specific heat and first two deriviatives and the specific heat ratio with the plane rotator model for the $p = 9$ clock model. The spcific heat and its derivatives go from $J_1 - J_2$ which is the lowest red curve up to $J_8 - J_9$. The specific heat ratio goes up to $J_5 - J_6$, which is plotted with the extrapolation (solid black curve).

Appendix B

CORRELATION LENGTH RESULTS

We present the correlation length results and their first two derivatives on our $J_{N-1} - J_N$, $p = 5, 6, 8, 9$ clock models.

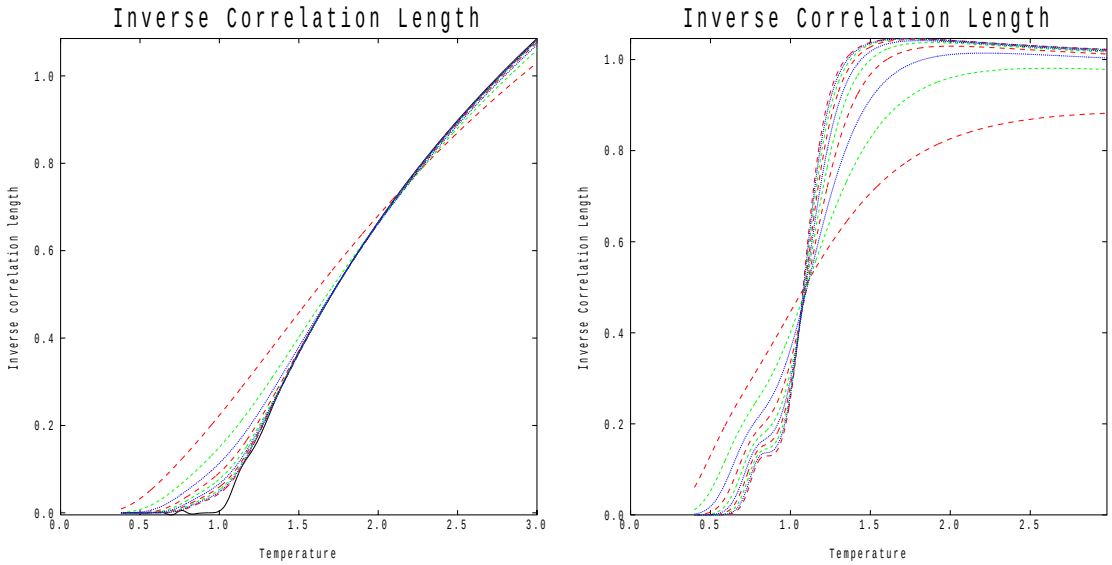

(a)

(b)

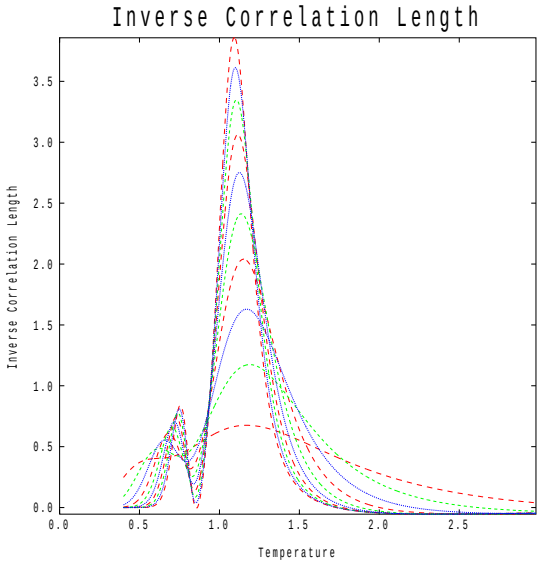

(c)

Figure B.1: The correlation length (a) and first two deriviatives (b) and (c) for the $p = 5$ clock model. Plotted is the $J_1 - J_2$ model up to the $J_{10} - J_{11}$ model

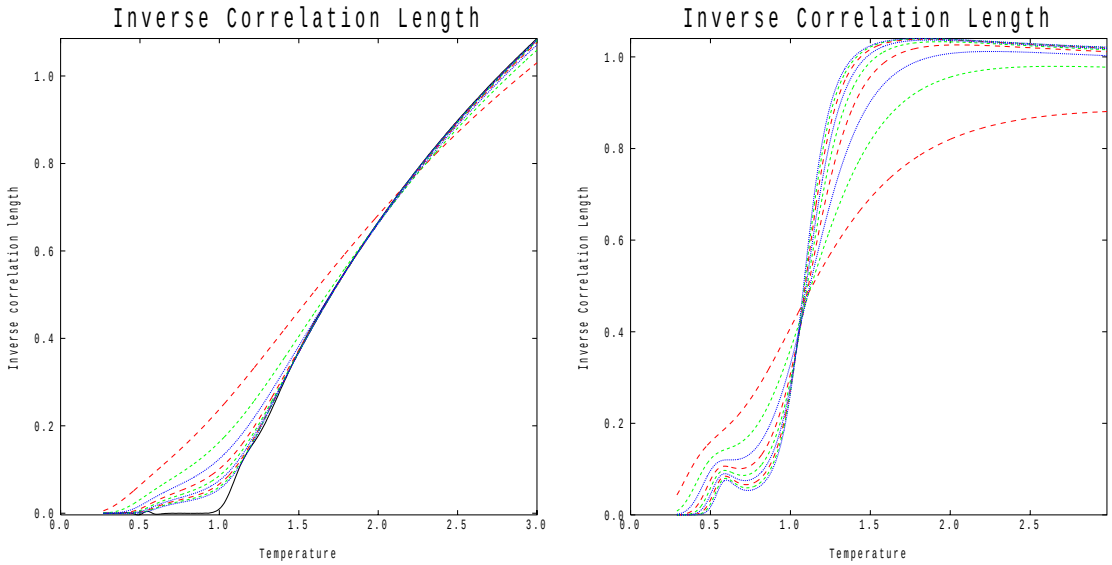

(a)

(b)

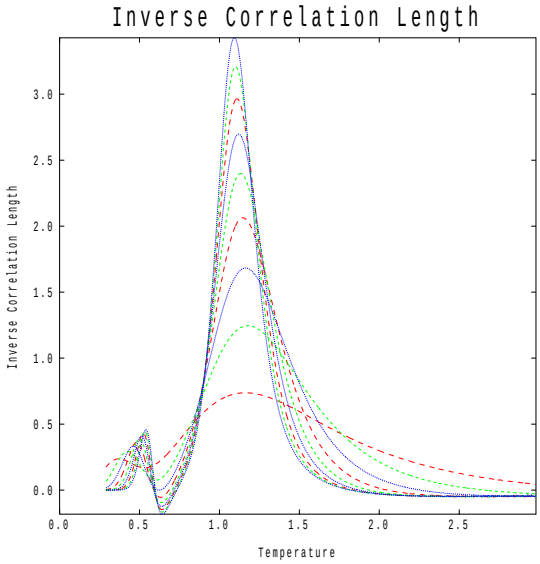

(c)

Figure B.2: The correlation length (a) and first two deriviatives (b) and (c) for the $p = 6$ clock model. Plotted is the $J_1 - J_2$ model up to the $J_9 - J_{10}$ model.

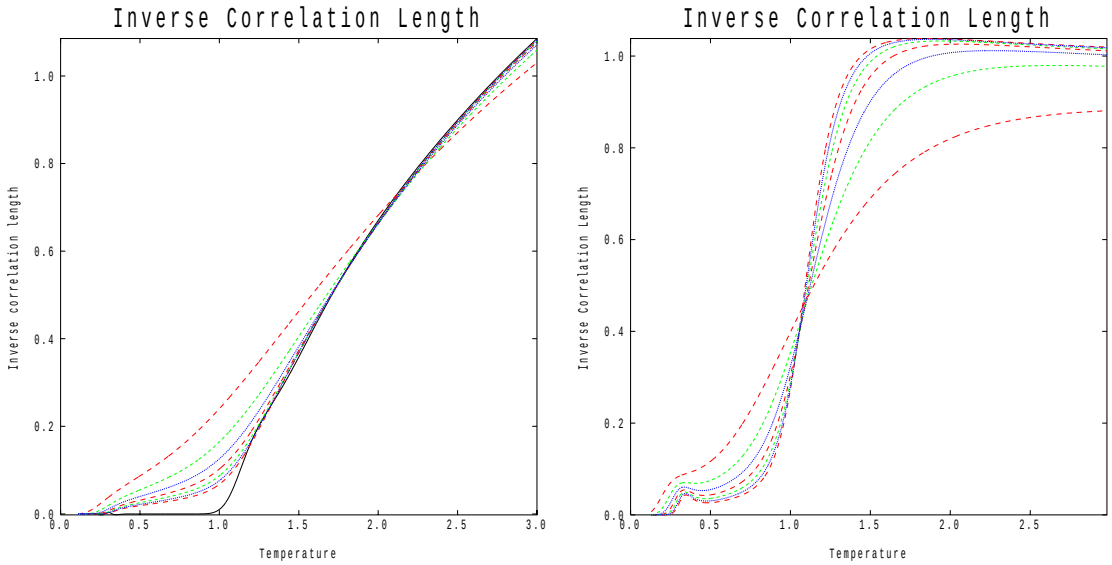

(a)

(b)

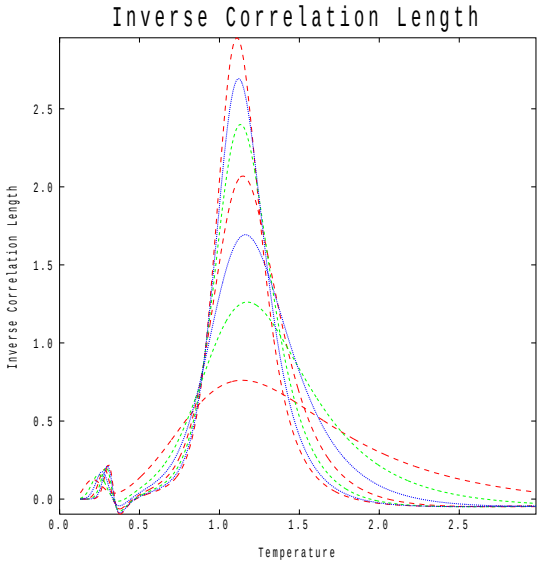

(c)

Figure B.3: The correlation length (a) and first two deriviatives (b) and (c) for the $p = 8$ clock model. Plotted is the $J_1 - J_2$ model up to the $J_7 - J_8$ model.

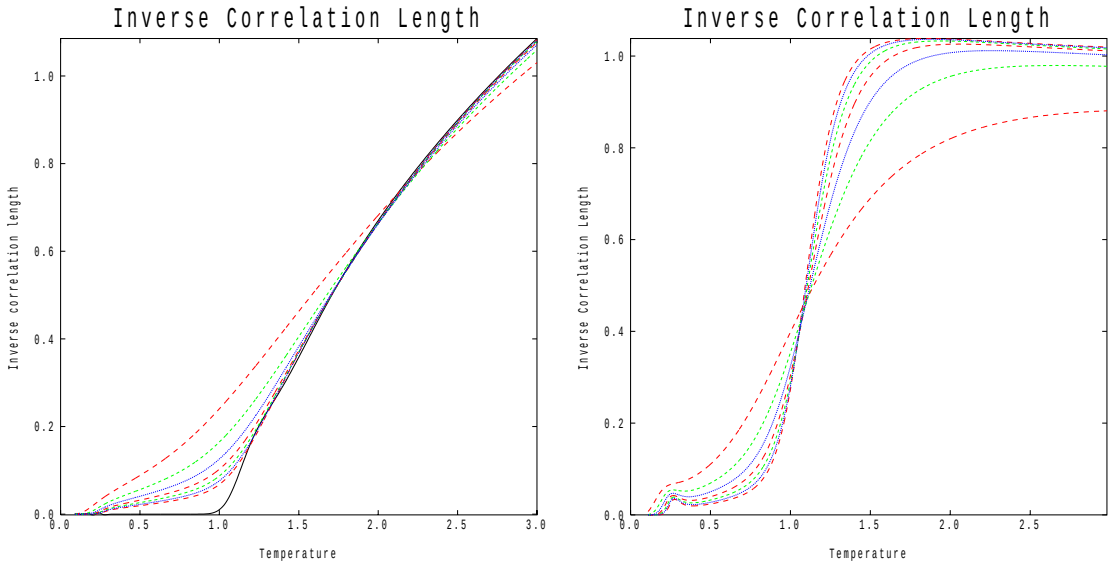

(a)

(b)

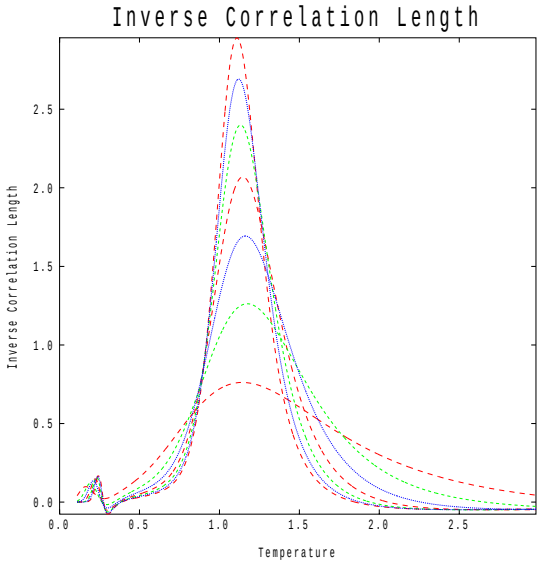

(c)

Figure B.4: The correlation length and first two deriviatives for the $p = 9$ clock model. Plotted is the $J_1 - J_2$ model up to the $J_7 - J_8$ model.

Appendix C

ORIENTATIONAL PROBABILITY RESULTS

We present here the orientational probability results for both real and fourier spin space for $p = 5, 6, 8, 9$ for the $J_{N-1} - J_N$. The blue curves are between sites i and $i + N - 1$ and i and $i + N - 2$; the green curve between sites i and $i + 1$; the black curves are between sites that are diametrically opposite and the red curves are between all sites from $i + 2$ to $i + N - 3$.

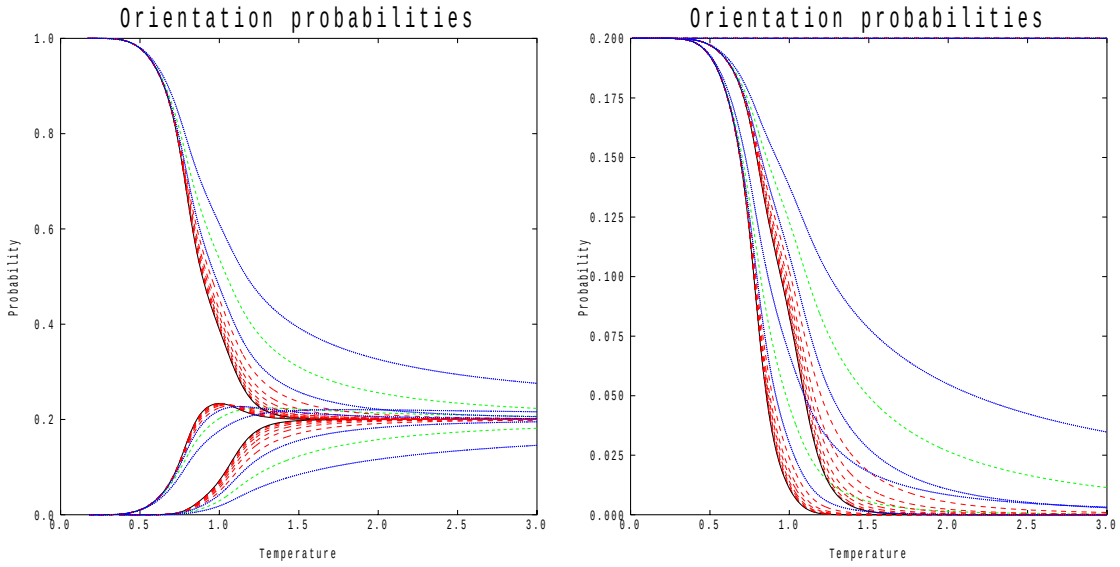

(a) (b)

Figure C.1: The relative orientational probabilities for both real and fourier spin space for the $p = 5$, $J_{11} - J_{12}$ clock model

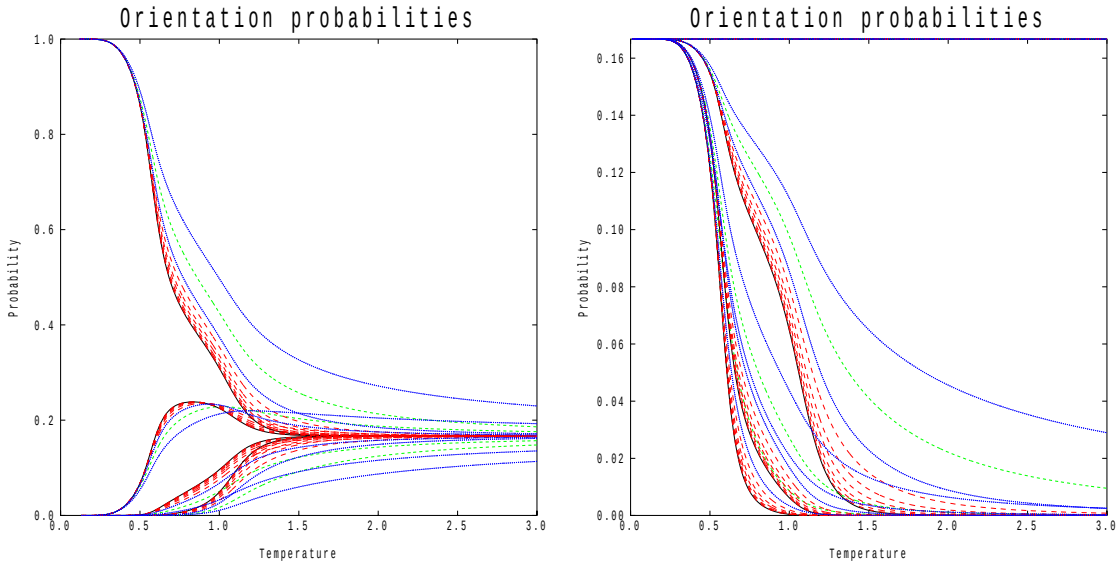

(a) (b)

Figure C.2: The relative orientational probabilities for both real and fourier spin space for the $p = 6$, $J_{10} - J_{11}$ clock model

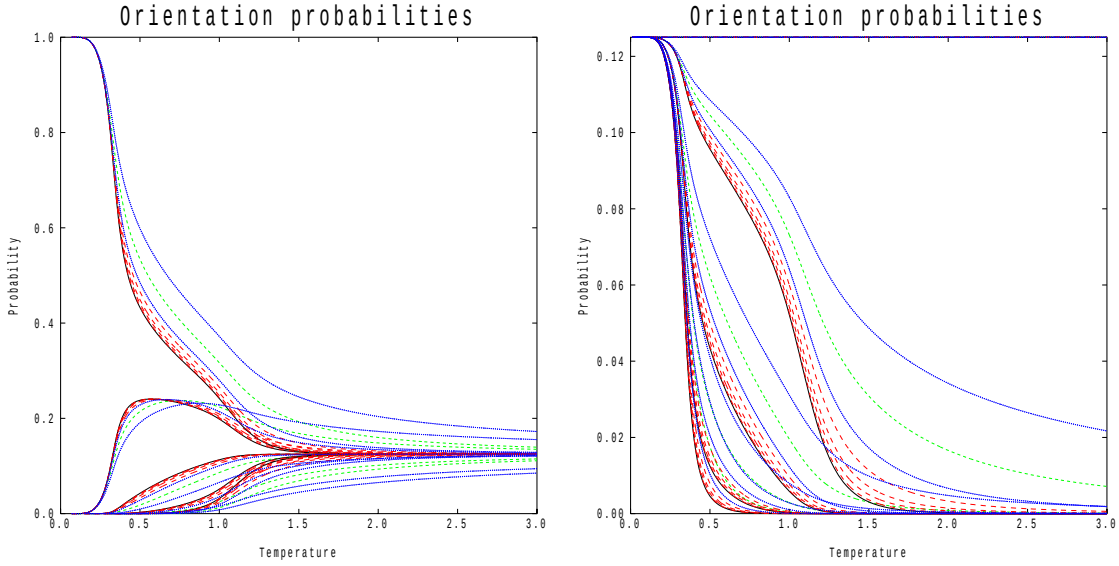

(a) (b)

Figure C.3: The relative orientational probabilities for both real and fourier spin space for the $p = 8$, $J_8 - J_9$ clock model

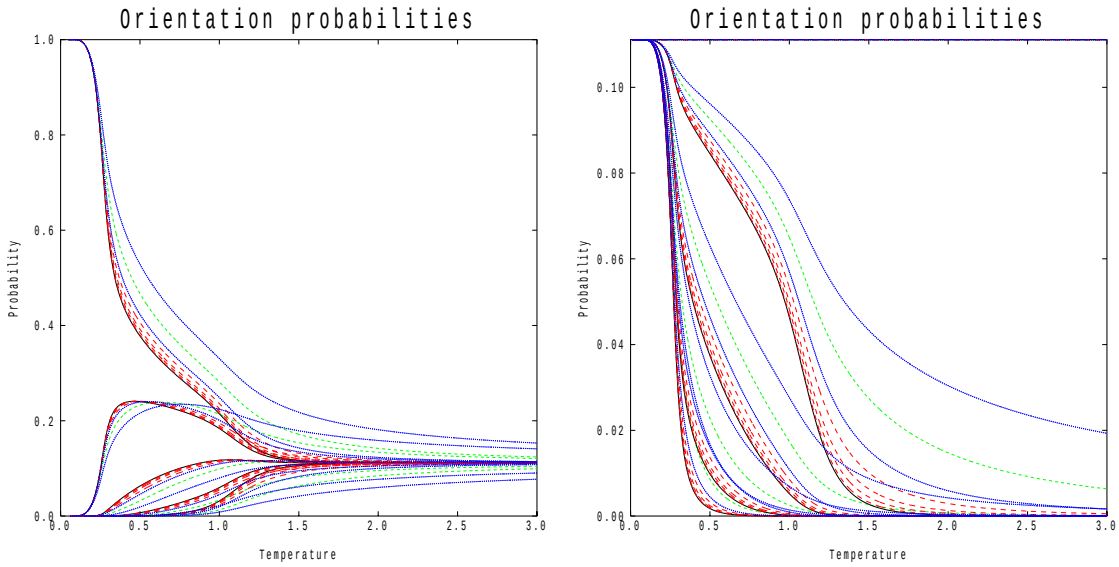

(a) (b)

Figure C.4: The relative orientational probabilities for both real and fourier spin space for the $p = 9$, $J_8 - J_9$ clock model.

Appendix D

HELICAL STIFFNESS RESULTS

We present the helical stiffness results for $J_1 - J_N$, $p = 5, 6, 8, 9$ models for both cases where $\chi_\parallel = 0$ and $\chi_\perp = 0$ from the Hamiltonian (3.5.10)

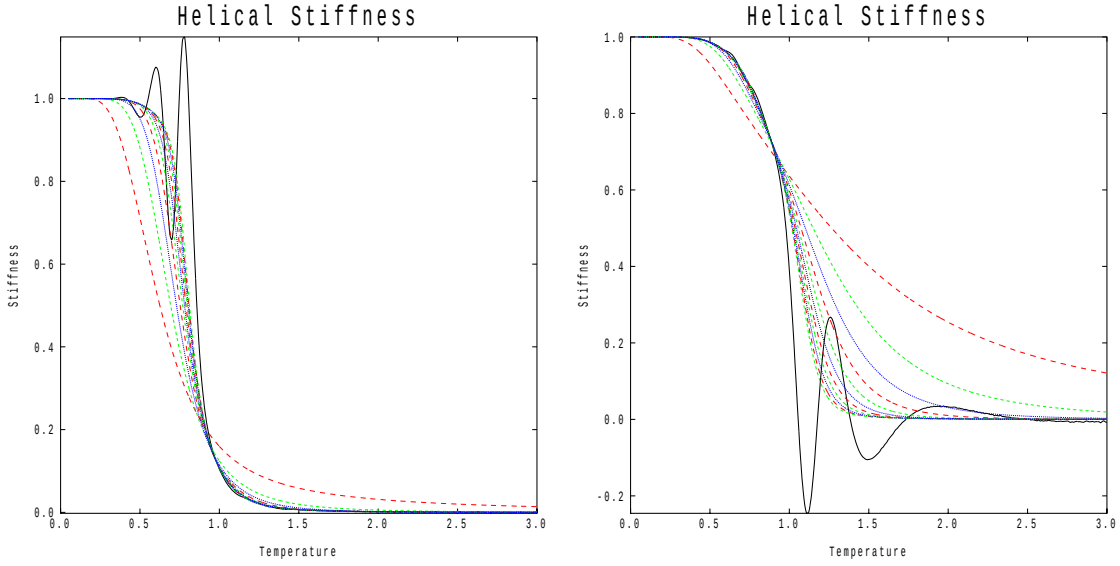

(a) (b)

Figure D.1: The helical stiffness for the $p = 5$ model for $\chi_\perp = 0$ and $\chi_\parallel = 0$ respectively with their extrapolation. The curves plotted are for the $J_1 - J_2$ model up to the $J_1 - J_{12}$ as they become more convergent.

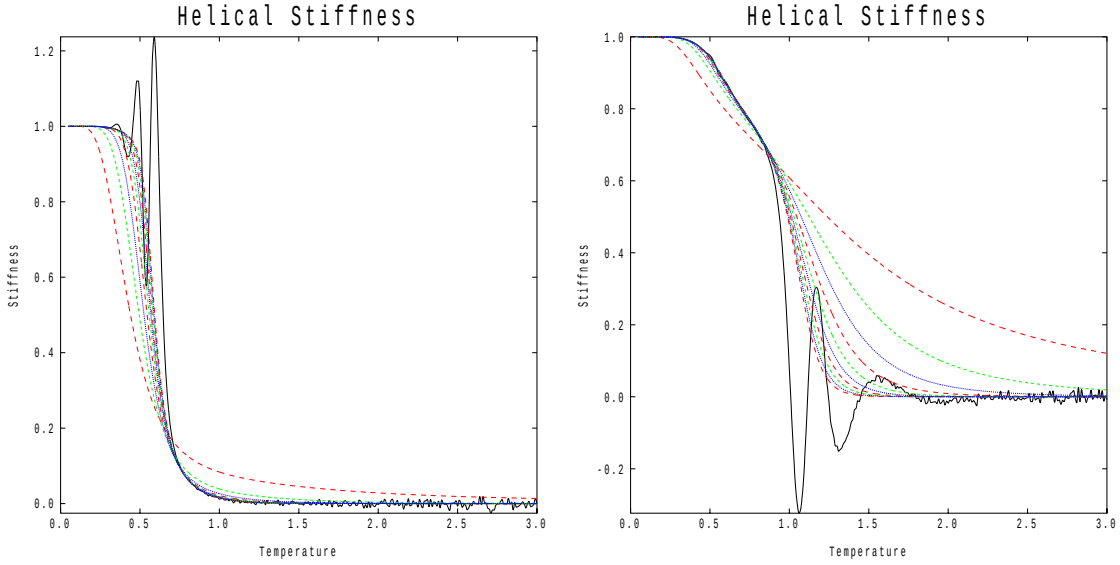

(a) (b)

Figure D.2: The helical stiffness for the $p = 6$ model for $\chi_\perp = 0$ and $\chi_\parallel = 0$ respectively with their extrapolation. The curves plotted are for the $J_1 - J_2$ model up to the $J_1 - J_{11}$ as they become more convergent.

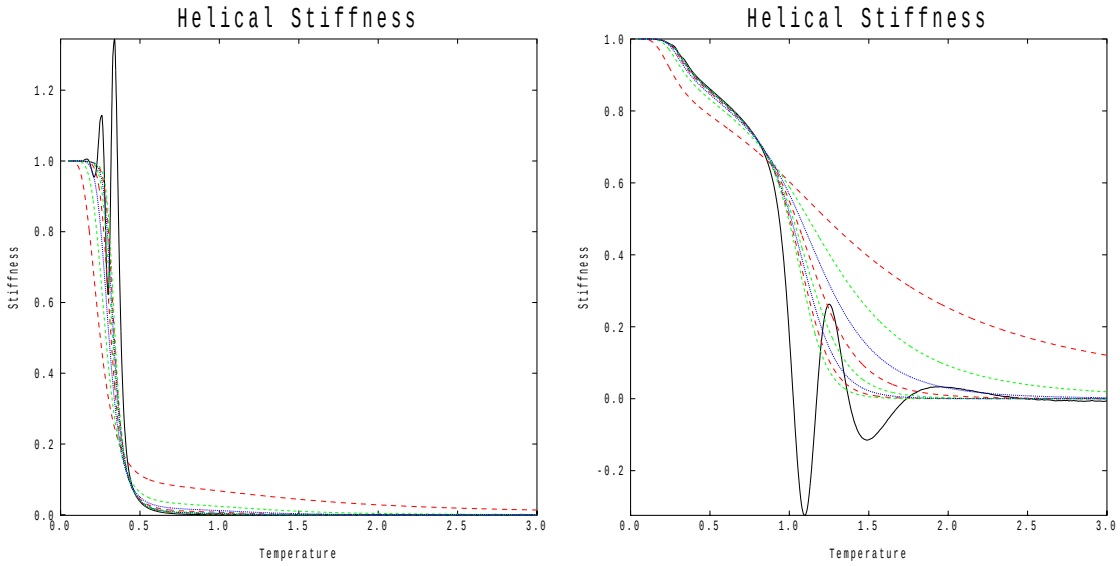

(a) (b)

Figure D.3: The helical stiffness for the $p = 8$ model for $\chi_\perp = 0$ and $\chi_\parallel = 0$ respectively with their extrapolation. The curves plotted are for the $J_1 - J_2$ model up to the $J_1 - J_9$ as they become more convergent.

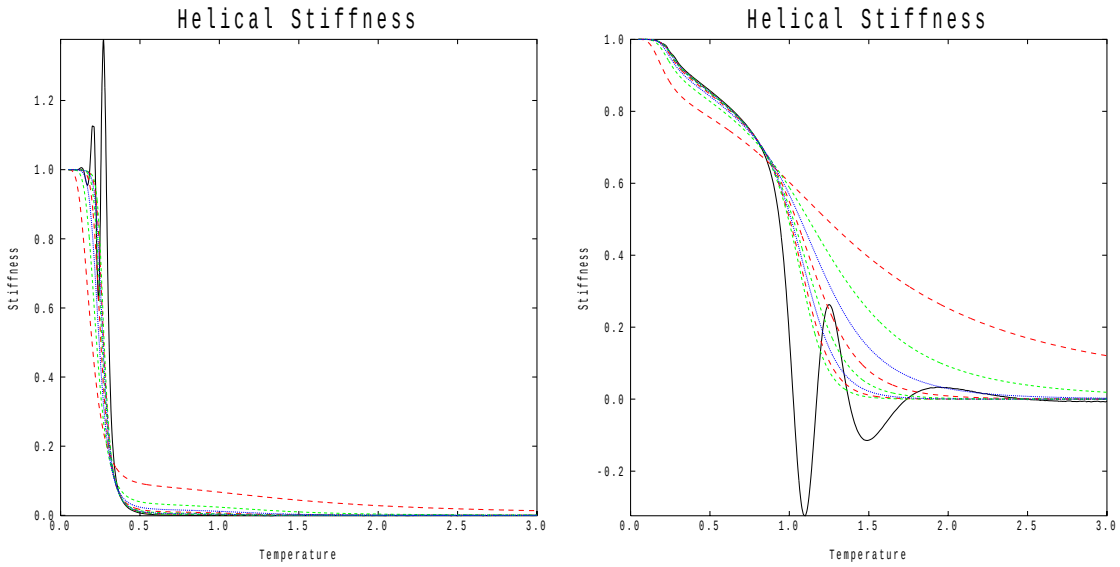

(a) (b)

Figure D.4: The helical stiffness for the $p = 9$ model for $\chi_\perp = 0$ and $\chi_\parallel = 0$ respectively with their extrapolation. The curves plotted are for the $J_1 - J_2$ model up to the $J_1 - J_9$ as they become more convergent.

Appendix E

INDUCED VORTICITY RESULTS

Here we present vortices through the spiral data for the $p = 5$ model.

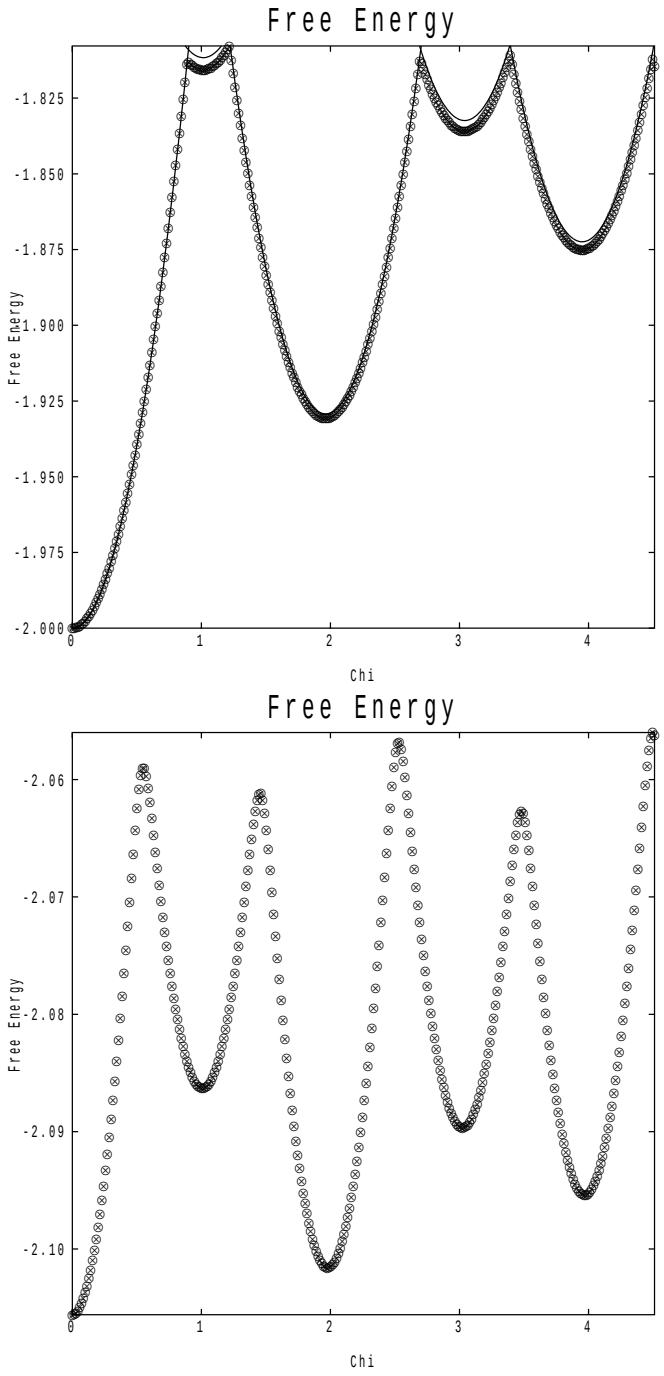

Figure E.1: Free energy calculations for induced vorticity for $p = 5$, $J_1 - J_9$ model at $T = 0.2$ and $T = 0.85$ respectively. The low temperature has the exact energy calculations overlaid.

List of references

[1] J. M. Kosterlitz and D. J. Thouless, J. Phys. C, **6**, 1181 (1973)

[2] J. M. Kosterlitz and D. J. Thouless, J. Phys. C, **5**, L124 (1972)

[3] V. L. Berezinskii, Sov. Phys. JETP-USSR, **32**, 493 (1971)

[4] V. L. Berezinskii, Sov. Phys. JETP, **59**, 907 (1970)

[5] J. M. Kosterlitz, J. Phys. C, **7**, 1046 (1974)

[6] D. R. Nelson, J. M. Kosterlitz, Phys. Rev. Lett, **39**, 1201 (1977)

[7] N. D. Mermin and H. Wagner, Phys. Rev. Lett, **22**, 1133 (1966)

[8] J. Fröhlich and T. Spencer, Commun. Math. Phys **81**, 527, (1981)

[9] J. Fröhlich and T. Spencer, Commun. Math. Phys **83**, 411 (1982)

[10] J. V. José, L. P. Kadanoff, et al, Phys. Rev. B, **16**, 1217 (1977)

[11] P. Minnhagen, Reviews of Modern Physics, **59**, 1001 (1987)

[12] P. Minnhagen, Phys. Rev. B, **24**, 2526 (1981)

[13] D. J. Bishop and J. D. Reppy, Phys. Rev. Lett, **40**, 1727 (1978)

[14] J. E. Berthold, D. J. Bishop and J. D. Reppy, Phys. Rev. Lett, **39**, 348 (1977)

[15] D. J. Bishop and J. D. Reppy, Phys. Rev. B, **22**, 5171 (1980)

[16] D. J. Bishop and J. E. Berthold and J. M. Parpia, Phys. Rev. B, **24**, 2844 (1981)

[17] D. McQueency, G. Agnolet and J. D. Reppy, Phys. Rev. Lett, **52**, 1325 (1984)

[18] J. Tobochnik and G. V. Chester, Phys. Rev. B, **20**, 3761 (1979)

[19] R. Gupta, J. Delapp, et al, Phys. Rev. Lett, **61**, 1996 (1988)

[20] R. Gupta, C. F. Baillie, Phys. Rev. B, **45**, 2883 (1992)

[21] H. Weber, P. Minnhagen, Phys. Rev. B, **37**, 5986 (1988)

[22] J. E. Van Himbergen and S. Chakravarty, Phys. Rev. B **23**, 359 (1981)

[23] R. Ben-Av and Sorin Solomon, Phys. Rev. B, **37**, 9817 (1988)

[24] C. S. S. Murty and D. P. Landau, Phys. Rev. B, **33**, 437 (1986)

[25] C. M. Lapilli, P. Pfeifer and C. Wexler, Phys. Rev. Lett, **96**, 140603 (2006)

[26] Y. Tomita and Y. Okabe, Phys. Rev. B, **65**, 184405 (2002)

[27] S. Fujiki, T.Horiguchi, J. Phys. Soc. Jpn, **64**, 1293 (1993)

[28] A. Yamagata and I. Ono, J. Phys. A.: Math and Gen, **24**, 265 (1991)

[29] J. Tobochnik, Phys. Rev. B, **26**, 6201 (1982)

[30] C. Hwang Phys. Rev. E, **80**, 042103 (2009)

[31] S. S. Zumdahl, D. J. DeCoste, *Chemical Principles*, 7th Ed, Cengage Learning (2013)

[32] P. Misra, *Physics of Condensed Matter*, Academic Press (2012)

[33] M. P. Marder, *Condensed Matter Physics* 2nd Ed, John Wiley & Sons (2010)

[34] N. W. Ashcroft and N. D. Mermin *Solid State Physics*, Holt, Rinehart and Winston (1976)

[35] P. Kopietz et al *Introduction to the Functional Renormalisation Group*, Springer (2010)

[36] L. P. Kadanoff, *Statistical Physics: Statics, Dynamics and Renormalization*, World Scientific (2000)

[37] C. Rebbi, *Lattice Gauge theories and Monte Carlo simulations*, World Scientific (1983)

[38] P. M. Chaikin and T. C. Lumbensky, *Principles of Condensed Matter Pysics*, Cambridge University Press (1995)

[39] E. Ising Zeits. für. Physik, **31**, 253 (1925)

[40] R. Peierls, Math. Proc. Camb. Phil. Soc, **32**, 471 (1936)

[41] H. A. Kramers and G. H. Wannier, Phys. Rev, **60**, 252 (1941)

[42] L. Onsager, Phys. Rev, **65**, 117 (1944)

[43] B. Kaufman, Phys. Rev, **76**, 1232 (1949)

[44] C. N. Yang, Phys. Rev, **85**, 808 (1952)

[45] T.D. Schultz, D.C. Mattis and E.H. Lieb, Rev. Mod. Phys. **36**, 856 (1964)

[46] K. Wilson, Rev. Mod. Phys, **47**, 733 (1975)

[47] L. P. Kadanoff, Annals of Phys, **100**, 359 (1976)

[48] A. A. Migdal, Sov. Phys. JETP, **42**, 413 (1975)

[49] A. A. Migdal, Sov. Phys. JETP, **42**, 743 (1975)

[50] G. Ortiz, E. Cobanera and Z. Nussinov, Nuc. Phys. B, **854**, 780 (2012)

[51] T. D. Lee and C. N. Yang, Phys. Rev, **87**, 410 (1952)

[52] M. E. Fisher, Rep. Prog. Phys, **30**, 615

[53] M. E. Fisher, *Lectures in Theoretical Physics* Volume 7c, University of Colorado Press (1965)

[54] L. Landau, Zh. Eksp. Teor. Fiz, **7**, 19 (1937)

[55] J. Cardy, *Scaling and Renormalization in Statistical Physics*, Cambridge University Press (1996)

[56] W. Heisenberg, Zeits. für. Physik, **49**, 619 (1928)

[57] C. S. S. Murty and D. P. Landau J. Appl. Phys **55** 2429 (1984)

[58] M. R. Robson et al, to be published

[59] J. Zhang and D. Ji, Phys. Lett. A **151** 469 (1990)

[60] O. Borisenko et al, Phys. Rev. E, **83** 041120 (2011)

[61] S. Elitzur, R. B. Pearson and J. Shigemitsu, Phys. Rev. D, **19**, 3698

[62] D. C. Mattis, Phys. Lett. A, **104**, 357 (1984)

[63] J. C. S. Rocha et al arXiv:1507.02231v2 (2015)

[64] J. C. S. Rocha et al, Physics Procedia **57** 94 (2014)

[65] B. V. Costa et al Phys. Lett. A, **377** 1239 (2013)

[66] R. Martin *Electronic Structure: Basic Theory and Practical Methods*, Cambridge University Press (2004)

[67] T. Holstein and H. Primakoff Phys. Rev. **58**, 1098 (1940)